Evaluation of Hybrid Electrically Conductive Adhesives

by

Ephraim Trinidad

A thesis

presented to the University of Waterloo

in fulfillment of the

thesis requirement for the degree of

Master of Applied Science

in

Chemical Engineering (Nanotechnology)

Waterloo, Ontario, Canada, 2016

AUTHOR'S DECLARATION

I hereby declare that I am the sole author of this thesis. This is a true copy of the thesis, including any required final revisions, as accepted by my examiners.

I understand that my thesis may be made electronically available to the public.

Abstract

An electrically conductive adhesive (ECA) is a composite material acting as a conductive paste, which consists of a thermoset loaded with conductive fillers (typically silver (Ag)). Many works that focus on this line of research were successful at making strides to improve its main weakness of low electrical conductivity. Most research focused on developing better silver fillers and co-fillers, or utilizing conductive polymers to improve its electrical conductivity, however, most of these works are carried out on small scale. In this work, we aim to produce larger quantities of hybrid ECA to successfully test its properties.

Industry is interested in materials with superior physical properties. As such, rheological behavior and mechanical strength were explored as it has been theoretically hinted that incorporation of exfoliated graphene within the composite could impact those factors listed in a positive manner.

In the first step of this project, pre-treated sodium dodecyl sulfate (SDS)-decorated graphene's rheological properties were examined. An epoxy resin diglycidylether of bisphenol-A (DGEBA) was the main polymer used for this study: a well-known material that can behave either as a shear-thinning or shear-thickening material depending on the supplier. We showed how composites that contain graphene (Gr) had higher viscosities than ones that contained SDS decorated graphene Gr(s). Not only did we confirm that surfactant was a key factor in the decrease of viscosity, but we also report how Gr and Gr(s) had a special effect that suppresses the intrinsic shear thickening behavior of epoxy resin at weight concentrations (wt%) higher than 0.5 wt%. The results showed that Gr(s) is not only beneficial in terms of improving the conductivity of conventional ECAs, but it also acts as a solid lubricant that decreases the viscosity of the composite paste at higher weight concentrations.

In the second step of the project, pre-treated SDS decorated graphene's mechanical properties were examined. In specific, its lap-shear strength (LSS) as well as the effect of residual solvent when present in our hybrid ECA system were studied in order to follow up on the thermal results obtained from a previous study. We showed that our initial

suspicion was correct as the LSS did decrease for all of the solvent-assisted formulations that contained Gr(s) ranging from 66 to 84%, however, we were not able to tell whether or not that decrease was caused by lower crosslinking density. Instead, we uncovered another reason for this decrease: bubble formation during the curing step. This suspicion was confirmed qualitatively through light microscopy and quantitatively through optical profilometry, where we present an increase in surface roughness for the solvent-assisted samples. Furthermore, by using SEM, we also confirmed that this bubble formation extends throughout the entire bulk material rather than just at the interface. Lastly, we investigated whether the use of solvent to assist in the mixing process significantly improves the electrical conductivity at a lower weight loading of Ag, and compared the electrical conductivity with that of the products prepared under the same higher weight loading of Ag using a solvent-free mixing method from previous work.

Thirdly, we investigated another mechanical property of our hybrid ECAs through indentation tests, where we use Hertizan equations to characterize elastic modulus. Since we learned that the addition of Ag flakes is detrimental to the mechanical strength, we focused on the difference between the elastic moduli for Gr and Gr(s) in a solvent-free environment.

In the last step of this project, we explored the use of a liquid-suspended co-filler (instead of carbon filler-based materials) in Poly(3,4-ethylenedioxythiophene) polystyrene sulfonate (PEDOT:PSS): a conductive polymer that is frequently in conductive thin-films. We report that by using PEDOT:PSS as a conductive co-filler into the conventional ECA with 60 wt% of Ag, we observed higher conductivity equivalent to adding an extra 20 wt% of Ag into the system. Furthermore, we report that an increase of PEDOT:PSS in the composite appears to decrease the LSS of the material by 20%.

Acknowledgements

I want to firstly express my deepest gratitude to my supervisor, Professor Boxin Zhao, for his guidance, support, constructive criticism, advice and encouragement. Thanks to him, my graduate study experience became rich with challenges and opportunities, as I was consistently encouraged to be surrounded by experts in my field of research, and was provided with many opportunities to learn, network and build my reputation within my field of study. His support and understanding as I wrote this thesis allowed me to have a writing process that is less frustrating and difficult than it could have been.

Secondly, I want to express my deepest gratitude to Dr. Behnam Meschi Amoli for mentoring me from scratch. Without you, I would not have been able to learn as much as I was able to, and my graduate studies would not be as successful as it is. From literature knowledge to paper writing, to fundamental training in the laboratory and even as far as brainstorming novel ideas for my work, Dr. Amoli has given great dedication, one-on-one attention and countless hours to ensure that I grew professionally, academically and personally throughout my graduate studies and I cannot stress enough how much I value all that he has done.

Thirdly, I want to thank Dr. Wei Zhang for teaching me a variety of details that I would otherwise have not learned on my own, improving both my ability to present, package reports, create vibrant figures and images and overall adapt a scientific mindset in all my work.

Besides my research supervisor and two mentors, I would like to thank all of my lab mates: Zihe Pan, Kelvin Liew, Fatemah Ferdosian, Alek Cholewinski, Kuo Yang, Jeremy Vandenberg and Hamed Shasavan for all of their contributions, educational discussions and assistance to my work and ideas that helped me solve all kinds of problems.
I also want to give a special mention to Mr. Geoff Rivers, who although is not in our immediate research group has given me plenty of ideas, advice and support on both my academic graduate studies and ongoing projects.

Lastly, wish to acknowledge financial support from both the Natural Sciences and Engineering Research Council (NSERC) as well as ReMAP for helping fund my projects.

Dedication

I dedicate this to my beloved parents, Grace and Raymund Trinidad and the love of my life Anna Tsao. With this, I hope that you are all truly proud that I am not only exerting the potential you all see in me, but also, I hope you realize that thanks to the sacrifices, encouragement and support that you provided me throughout this pursuit, I now have the capacity to go beyond the limits I had when I graduated from BASc.

Table of Contents

List of Figures

List of Tables

Chapter 1 Introduction

Today is an age of unprecedented technological growth as the semiconductor electronics industry continues to make advancements, spanning over the past few decades [1–3]. With it comes the constant demand for improving interconnection technology: an essential requirement that supports the components necessary for the electronic systems to function [1]. However, one of the consequences that comes with the rapid growth of technology is that mass produced electronic devices suffer from a short product life cycle [2,4,5], leading to many of these Printed Circuit Boards (PCBs) to be thrown out into landfills to become what is known as e-waste [2]. Most interconnection technologies responsible for creating a continuous bridge between the PCB and electrical components traditionally utilize a material known as eutectic Lead/Tin (Pb/Sb) solder [2,3,5–11]. First of all, it is important to state that Pb is a toxic material [2,3,5,11,12]. The primary reason why Pb/Sn solder is a concern stems from the fact that as of 2006, 90% of e-waste was deposited into landfills without pre-treatment or prior action taken to remove such hazardous chemicals before being incinerated [4]. When incinerated, the Pb/Sn liquefies and finds its way into groundwater or rivers, causing massive damage as an environmental contamination risk. In response to this, legislative bodies in EU [2–4,6,13,14] and Japan [1,3,6,14] have made laws that ban the use of hazardous substances within their electronic packaging and component interconnections. In order to meet these laws, both electronics producing companies and researchers have begun looking into alternative electronic packaging materials that can completely replace Pb/Sn [3,5,11,12]. Among these alternatives, two options proved promising: lead-free metal alloy-based solutions (Sn/Ag/Cu or SAC representing the first letter of each element, is an alloy series that are the most dominant) [1,2,6,15] and a polymer composite-based material known as electrically conductive adhesives [1,3–7,9,10,13,14,16]. Although the SAC series are already commercial and a popular alternative to Pb/Sn solders, they suffer from thermal cycling issues, high temperature requirements that risk device damage during reflow, as well as a low drop performance [1,15] making it a temporary solution for the time being. As such, great focus is placed onto ECAs as the next alternative electronic packaging material, owing to many desirable properties such as high shear strength, low

temperature requirements, fewer processing steps, finer pitch capabilities and environmental friendliness [1,3,5,6,9,10,16]. ECAs are primarily comprised of a polymeric binder resin (typically in the form of a thermoset (e.g. epoxy)) and conductive fillers (typically in the form of silver flakes) [4,6], which is depicted below in Figure 1-1[13].

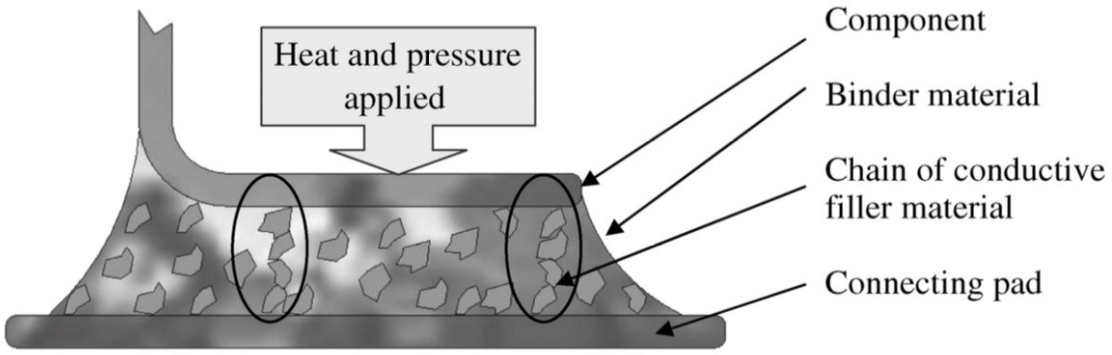

Figure 1-1: Schematic example of an electrically conductive adhesive bonded to an electrical component and connecting pad (printed circuit board) (Reproduced with permission Copyright 2008, Taylor & Francis) [13]

Although there are many disadvantages, drawbacks and issues that are attributed to ECAs (that will be discussed later in this thesis), the major drawback of low electrical conductivity [8,10,17–20] has been heavily researched and to some degrees, been overcome. However, there is much work to be done before the new generation high conductivity ECAs are commercialized for a wider variety of applications, as many other important characteristics (especially on the physical mechanical side) have yet to be explored nor optimized. Furthermore, the goal of achieving both high electrical conductivity and mechanical strength is not a simple task, as simply increasing the weight concentration of silver in the composite will result in the electrical conductivity hitting a plateau as described in the "percolation threshold theory" (which will be discussed in further sections), and at the same time, weaken the physical properties of the composite [20,21] and overall increase the cost of the material. Instead of adding higher concentrations of Ag, we intend to add a nanoparticle known as graphene (depicted in

Figure 1-2), a co-filler that has recently proven useful for improving the electrical conductivity of conventional ECAs.

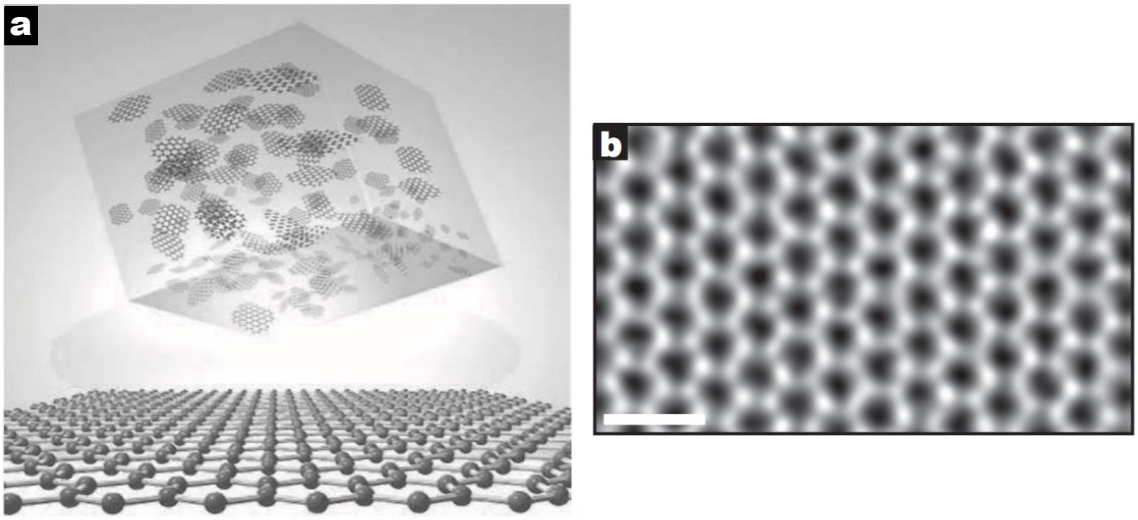

Figure 1-2: a) Graphene in polymer composites (Reproduced with permission Copyright 2012, Wiley) [22]; b) Atomic resolution of graphene from annular dark-field scanning transmission electron microscopy (ADF-STEM) (Reproduced with permission Copyright 2011, Nature) [23]

It is important to note, however, that graphene on its own will not be successful in this effort because of the difficulty in handling. For example, it suffers from poor dispersion in many common solvents, having a tendency to aggregate/agglomerate [22,24–26]. One work intending to use graphene as a co-filler in ECAs reports the use of Ag nanoparticles grown on graphene to covalently stabilize the carbon-based nanoparticles, however, this resulted in the disruption of its pi-bond resonance and overall decrease of its conductivity [17]. Another work reports the use of a non-covalent stabilization method, where surfactant SDS was used to decorate the graphene so as to prevent further aggregation without disrupting the resonance of the graphene [18]. This SDS-decorated graphene (Gr(s)) is the main co-filler that is chosen for this study, as it was shown to have provided a significant increase in electrical conductivity and overall and great promise as co-filler for hybrid ECAs. It must be noted that the procedure involved with making this lab-grade

conductive hybrid ECA is complex and difficult (when attempting to make larger amounts), thus preventing us from conducting further physical tests.

As such, this study changed the synthesis method of Gr(s) in such a way that it is easier to produce in large quantities. In order to produce larger volumes of the composite, we used what is known as a planetary shear mixer (PSM). After this was achieved, the next step of this study was to produce this Gr(s)-filled ECA at varying parameters so that its physical properties could be characterized.

The purpose of this thesis is to present the results of the physical properties found when preparing hybrid ECAs, as well as the usefulness and impact that Gr(s) provides to the composite. Since graphene is known to have excellent mechanical properties, it would be very useful to know whether or not these benefits could act to reinforce the composite's mechanical properties, besides just improving the electrical conductivity of the material, while at the same time, reducing the need to use higher Ag concentrations thereby negating the negative aspects associated with the addition of Ag flakes.

This thesis contains seven chapters. The first two chapters act to inform the reader of the field of study, as well as particular literature information intended to explain mechanisms, theories and useful knowledge surrounding the topic of conductive adhesives. Chapter three outlines the work on characterizing the rheological properties of epoxy-based composites that use graphene (Gr) and SDS decorated graphene (Gr(s)) as fillers. Chapter four outlines the work on characterizing one of the practical mechanical properties of interest to this field describing the adhesive strength between the PCB boards and the conductive paste: Lap shear strength (LSS). Furthermore, this chapter will discuss how the use of solvent in certain formulations affects the LSS of the composite, as well as potential factors that could elucidate the results. Chapter five outlines the work on characterizing the elastic modulus of the epoxy-based composites using Gr and Gr(s) to further understand any potential reinforcing effects that these nanoparticles offer the composite. Chapter six outlines the possibility of using PEDOT:PSS as a co-filler for ECAs, in hopes that we could find further alternatives for making ECAs with higher

electrical conductivities even at low weight loadings of Ag. Finally, the last chapter concludes the entire scope of this thesis, and closes off with future work, recommendations and ideas that should be further pursued to gain even higher levels of understanding for the field of conductive adhesives. The work described in chapter three was formatted for publication in the journal – *Journal of Materials Science: Materials in Electronics,* and cited as reference [27] in this thesis. The work described in chapter four was formatted for publication in the journal – International *Journal of Adhesion and Adhesives*; the manuscript is currently in preparation for submission and cited as reference [21] in this thesis. The work described in chapter five was submitted to Thermoset Resin Formulators Association (TRFA 2015) for a conference contest cited as reference [3] in this thesis. The work described in chapter six was submitted to Surface Mount Technology Association (SMTA 2016) as a technical paper cited as reference [5] in this thesis.

Chapter 2 Literature Background and Review

2.1 Interconnection Materials: Electronic Packaging for ICs

Electronic packaging is a field of electrical engineering that studies ways to attach, enclose and protect electronic components on devices, where soldering is currently the most cost-effective method for both small and large-scale assembly/manufacturing [28,29]. The main principle behind electronic packaging lies with the task of joining two components together: a) the electrical devices, for example, integrated circuit chips, resistors, capacitors etc. that are needed to create the circuit; b) the circuit board known as a printed circuit board (PCB) that acts as a substrate to hold these electrical devices in place [29]. Figure 2-1 shows an illustration to summarize the above statement, including an example of a fully assembled circuit board using what is known as surface mount technology: a method that has recently begun to replace pin through hole technology [28,30,31].

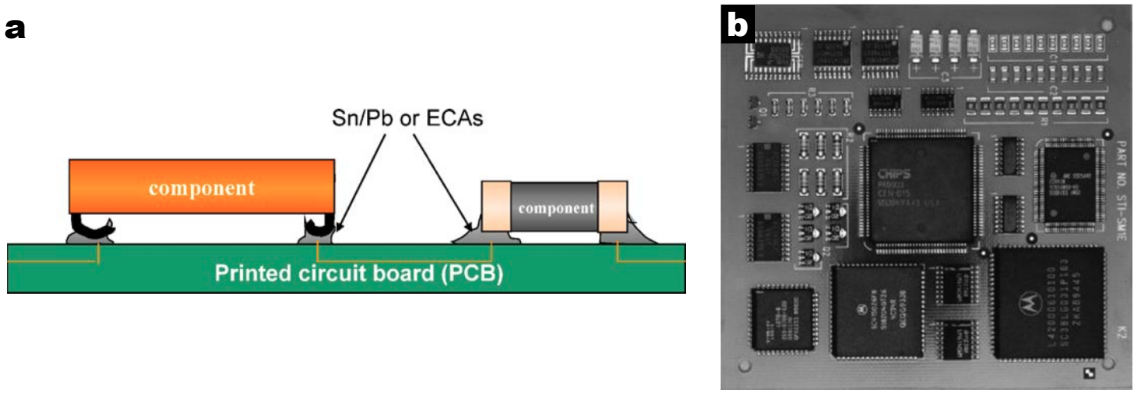

Figure 2-1: a) Schematic illustration of how an interconnect material joins a functional component onto a PCB (Reproduced with permission Copyright 2006, Elsevier) [1]; b) Example of fully-assembled circuit board that used surface mount technology to join the component to the PCB (Reproduced with permission Copyright 2016, Elsevier) [28].

Both of these components must be connected in such a way where the circuit has access to power, signal transmissions (i.e. data) and ground in order to function [1]. Besides

simply joining the electrical device onto the PCB, the interconnecting material is tasked with providing the following: a) electrical connectivity between the device and the board; b) thermal conductivity for heat dissipation; c) mechanical continuity so as to ensure that the components have intimate contact between one another even through physical agitation [12]. In order to bridge these two components, interconnection materials and technologies were engineered through techniques such as pin through hole (PTH), surface mount technology (SMT), ball grid array (BGA), chip scale packaging (CSP), and finally, flip-chip technology [1].

2.2 Three Interconnecting Materials: Pb/Sn, SAC305 and ECAs

As was mentioned in the previous section, interconnection materials are tasked with providing continuity on various levels between the PCB and electronic device. It was also mentioned that soldering is the most common method, however, the material that is responsible for creating this continuity is also important. Figure 2-2 summarizes these materials by classification [32].

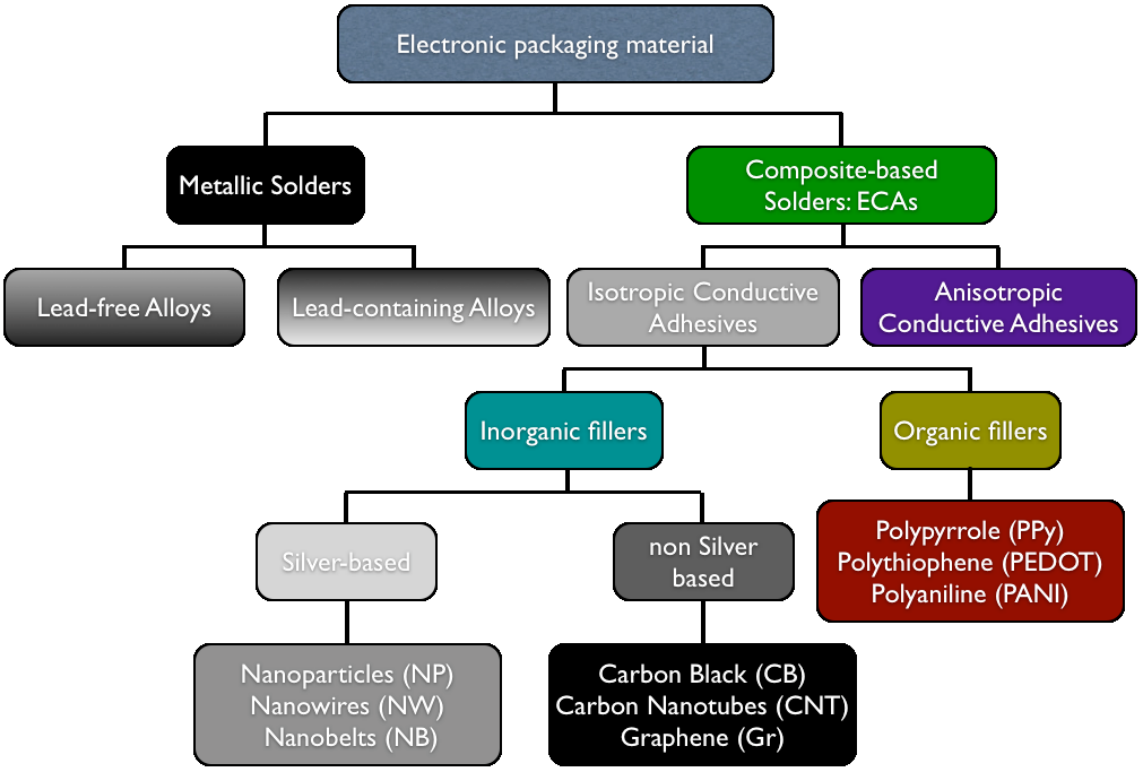

Figure 2-2: Summary of different materials used to create electrical interconnections (inspired by I. Mir [32])

The first group, also the most commercially available and the most commonly used, is metallic-based solders. Traditional lead-based solders (Pb/Sn) for decades, acted as the go-to material for electronic packaging [11,12,29,31]. Due to the health and environmental concerns mentioned earlier, lead-free alloys have taken over as the more popular choices in today's market [12]. The second group of interconnecting materials is a composite-based material known as electrically conductive adhesives (ECAs). Although it brings interesting properties that are useful as interconnecting materials, more research is needed in order for ECAs to fully mature and realize its full potential before becoming a major commercial interconnecting material. Each material will be expanded upon in the upcoming sections.

2.2.1 Traditional Lead-based Solder (Pb/Sn)

Traditional lead-based solder (Pb/Sn) has for decades been the dominant material chosen to join devices onto PCBs at large scale and low cost in industrial manufacturing [29] as

well as for smaller scale electronic processes such as in laboratories or small shops. In specific, Pb/Sn solders are comprised of two elements-lead and tin as an alloy typically in a ratio that allows it to be considered a eutectic system: a system containing two elements with a specific compositional ratio in equilibrium with each other. This means that, a specific ratio of material A and B (according to their phase diagrams) experiences infinite diffusivity in the liquid state at a certain temperature [33]. In the case of eutectic Pb/Sn, the melting temperature is 183ºC[2,15,29], and the eutectic system ratio for the Pb/Sn alloy in specific is 63% Sn and 37% Pb, however, a near-eutectic formulation of 60% Sn and 40% Pb is also widely used for most PCB assemblies [29]. The material properties of eutectic Pb/Sn is summarized below in Table 2-1.

Table 2-1: A summary outlining the material properties of eutectic Pb/Sn [1]

Material Properties	
Volume/Bulk Resistivity (Ω cm)	1.5×10^{-5}
Typical Junction R (mΩ)	10-15
Thermal Conductivity (W/m K)	30
Shear Strength (psi)	2200
Finest pitch (mil)	12
Minimum processing temperature (ºC)	215
Environmental impact	Negative
Thermal Fatigue	Yes

The traditional eutectic Pb/Sn solder is still the best electronic packaging material in terms of fulfilling its purpose. However, due to the negative environmental and health impact it possesses, alternate solutions need to take over as the primary electronic packaging material. The Pb "impurity" provides the traditional soldering material with a few advantages [2,12,29]:

- Pb impurity acts as a surface tension reducing agent for pure tin (550 mN/m at 232ºC, which in turn improves solderability through easy wetting of the material (giving access to small crevices, holes and gaps on the PCB)
- Pb impurity prevents unwanted transformation of tin upon cooling (transformation that leads to a volume increase and loss of structural integrity in the joint)
- Pb impurity acts as a solvent metal, diffusing rapidly in the liquid state as intermetallic bonds are formed

- Pb provides ductility to Pb/Sn solders
- Pb impurity forms an oxide layer that protects the pure tin from forming its own oxide layer
- Pb is an overall inexpensive material

It is important to note that it is unlikely for eutectic Pb/Sn solder to be fully replaced by an alternate material until a suitable replacement is found; mainly due to the continued demand of certain specific electronic applications that require high reliability and long lifespan (i.e. military equipment, aerospace and automotive applications [15,31]).

2.2.2 The current Lead-free alternative: SAC305 (Sn/Ag/Cu)

Lead-free solders have already begun its emergence in the market as another major electronic packaging material, owing to the recent laws passed in the European Union (EU) in 2006, as well as in Japan that have banned the use of lead-containing substances. Similar to its predecessor, the lead-free alternatives are also alloys comprised primarily of tin followed by other metals incorporated into its matrix (e.g. bismuth, indium, zinc, copper, silver, and antimony) [2,12,15]. There are many combinations that have been proposed and studied [2,12,15], however, there has been no successful formulation that can be considered a replacement for all applications. Instead, researchers identified a core group of elements comprised of Sn-Ag-Cu also known as SAC to be the base alloy to work with [2,12,15]. Unlike the well-known eutectic ratio for Pb/Sn that is widely used, industrial consortiums have proposed differing ratios depending on the country. For example, the USA uses 95.5 Sn – 3.9 Ag – 0.6 Cu (SAC396), while the EU uses 95.5 Sn – 3.8 Ag – 0.7 Cu (SAC387), and Japan uses 95.5 Sn – 3.0 Ag – 0.5 Cu (SAC305 [2]). An example of a different formulation that is application specific would be for a process known as ball-grid array (BGA) that uses 95.5 Sn – 4.0 Ag – 0.5 Cu (SAC405) for the BGA solder joints [2]. The SAC series is not without drawbacks despite being accepted as the lead-free alternative material for electronic packaging. One major problem of the SAC series when compared to eutectic Pb/Sn is the operating and melting temperature (with SAC series sitting at 217ºC and eutectic Pb/Sn sitting at 183ºC), which leads to higher reflow temperature and thermal reliability issues with the components [2,15]. Another issue that plagues the SAC series is its solder joint reliability in that it has weak

drop strength, a major problem especially for both portable and handheld devices [2,15]. Furthermore, the SAC series faces issues with uneven distribution, which leads to lower elastic modulus and impact strength [34]. Lastly, issues in the overall cost of SAC alloys contribute to its inability to truly replace eutectic Pb/Sn. Examples of the issues that lead-free SAC series faces can be seen below in Figure 2-3.

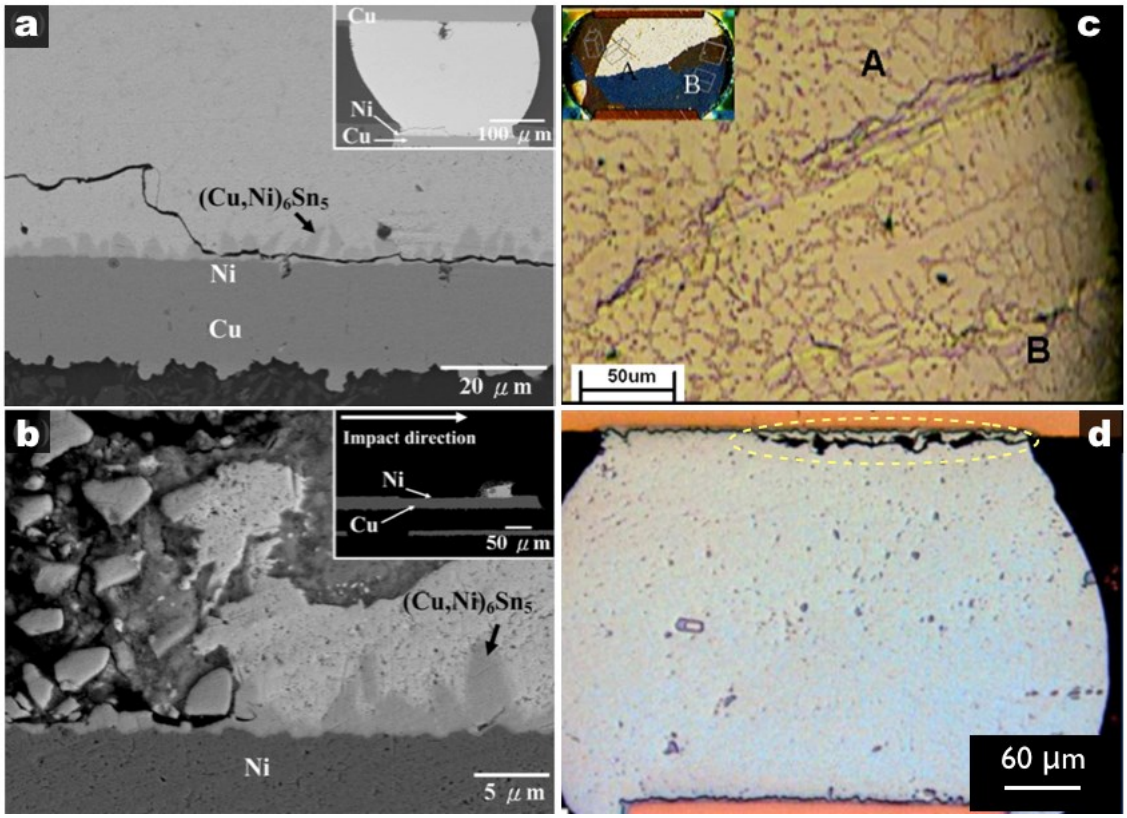

Figure 2-3: a) Fracture behavior of SAC105 during drop test; b) Fracture behavior of SAC105 during impact test PCB (Reproduced with permission Copyright 2012, Elsevier) [34]; c) Plastic deformation near the grain boundaries due to thermal cycling; d) Fatigue cracking at interface PCB (Reproduced with permission Copyright 2011, Elsevier) [15]

2.2.3 Electrically Conductive Adhesives (ECAs)

Another alternative to traditional eutectic Pb/Sn solder is a composite material known as electrically conductive adhesives (ECAs [6,9,11,13,16,17,19,35–42]). The emergence of the first ECAs dates back to 1950s especially with Henry Wolfson et al earning a patent

on “electrically conducting cements containing epoxy and silver [43].” This composite would then become the foundation from which present-day ECAs would be based upon. ECAs are composed of two main components: a polymer matrix (usually a thermoset such as epoxy) and conductive filler material (usually silver based [6,8,10,11,13,19,40–42]) as seen in Figure 2-4.

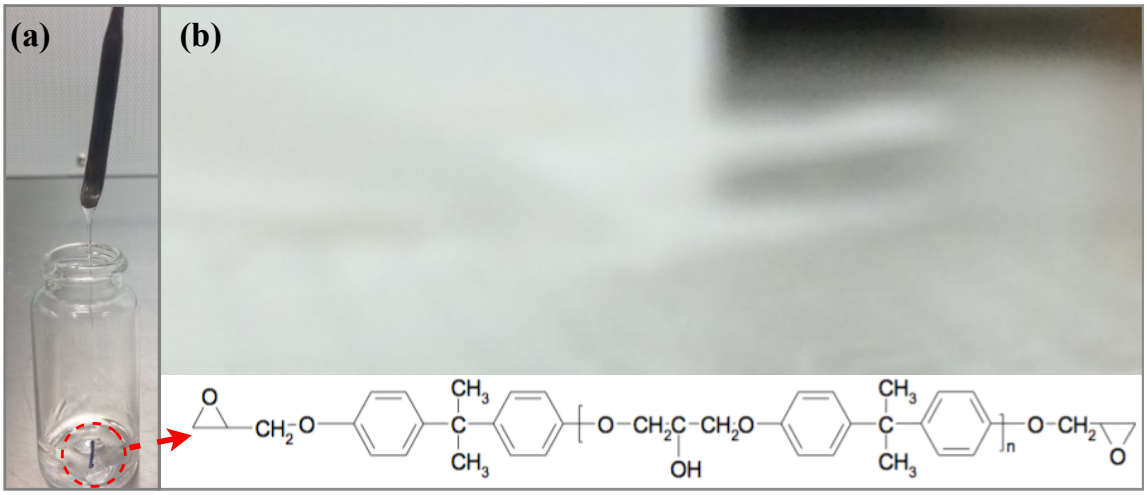

Figure 2-4: a) Polymeric binder: Epoxy resin (DGEBA); b) Conductive filler: Silver Flakes

ECAs can be further divided into two types of materials: anisotropic conductive adhesives (ACAs) and isotropic conductive adhesives (ICAs) [13,32,36,37]. Anisotropic conductive adhesives usually refer to ECAs that exhibit unidirectional conductivity (or in one direction only) and can take either paste form or film form. A schematic of all three forms (including the non-conductive variant can be seen in Figure 2-5 letter a to c. Anisotropic conductive adhesives have characteristically low conductive filler concentrations as can be seen in Figure 2-5 letter d, as it is in the lower region of the percolation curve (a topic that will be further explained in another section).

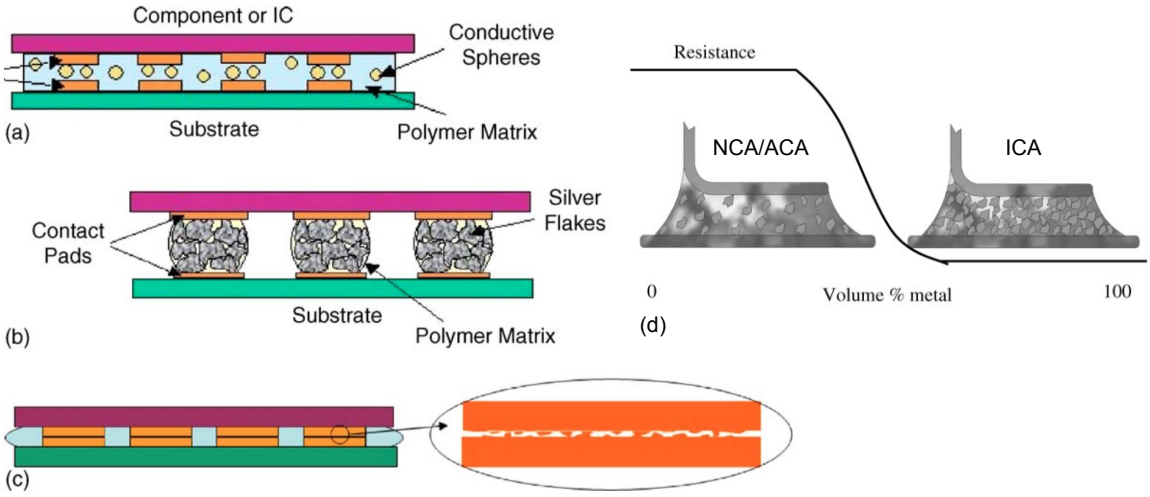

Figure 2-5: a) Schematic of ACA; b) Schematic of ICA; c) Schematic of NCA (Reproduced with permission Copyright 2006, Elsevier) [1]; d) Schematic of the percolation curve of conductive adhesives that determine the classification of the ECA as either ACA or ICA (Reproduced with permission Copyright 2008, Taylor & Francis) [13]

As the concentration of conductive filler content increases in the polymer matrix, a shift in the direction of conductivity begins to form, as it goes from 1-dimensions to 3-dimensions. ECAs that exhibit conductivity in 3 dimensions are known as isotropic conductive adhesives [11,13,41] and will primarily be the ECA this thesis will focus on and refer to throughout the subsequent sections. The advantages and challenges of ECAs are summarized in Table 2-2 below [4,7–11,16,17,19,35–40,44].

Table 2-2: A summary outlining the advantages and limitations of ECAs

Advantages	Disadvantages
Low processing Temperatures	Low Bulk Electrical Conductivity
Fine-Pitch Capabilities	Unstable Contact Resistances
Excellent Adhesion to Numerous Surfaces	Hard to Remove After Cured
Directional Conductivity Possible	Adhesion Strength Needs Improvement
Environmentally Friendly Alternative	Joint Resistance from Oxidation/Corrosion
Minimal Thermal Fatigue & Stress Cracks	High Ag Content is Expensive
Low Dielectric Constant	Limited Impact Resistance
Works with Non-Solder Components	Environmental Reliability Unconfirmed
Less Processing Steps & Operation Cost	Longer Curing Times
Higher Flexibility	Silver Migration Issue
No Flux or Secondary Underfill Needed	Incorrect Spreading from High Viscosity

Before a new type of ECA is considered commercially available for a variety of applications, it is important to gain a better understanding of the material properties, processability and mechanisms before further progressing. Doing so will give researchers and industry a chance at improving the understanding of these challenges, or using external agents that will alleviate or protect the performance of the composite. For the sake of communication, this thesis will from here on refer to the basic epoxy and silver flake-filled composite mentioned above as conventional conductive adhesives (CCAs). The next sections will discuss recent works and progress regarding the improvement of CCAs.

2.3 Conventional ECAs and Recent Progresses

This section will focus on some of the recent progresses that have been made to address the main challenge that ECAs must overcome to be applicable to more fields: low (bulk) electrical conductivity. All of these topics will be only briefly explained with limited explanations on the mechanism, as the purpose of this section is to share the current discoveries related to the improvement of ECAs.

Researchers have taken three different kinds of approaches to improve the electrical conductivity of the composite (some of which deal with using high-aspect ratio/surface-to-volume ratio materials, many of which are linked to the improvement of composites) [45,46]. The first approach deals with modifying the most utilized conductive filler: silver. By changing shape, size and other factors such as surface functionalization of the Ag flakes, researchers are able to improve the bulk electrical conductivity of ECAs. The second approach researchers take to overcome the low bulk conductivity of ECAs reports the use of non-metallic carbon-based solid materials that act as co-fillers with the purpose of working together with the Ag flakes within CCAs so as to create more metallurgical connections between the Ag flakes without excess weight loadings of Ag. The third method researchers report is the incorporation of conductive polymers within the CCA composite again acting as a co-filler material, in hopes of providing more metallurgical ions that will assist in the increase in bulk conductivity within the system.

2.3.1 Conductive metallic filler materials: silver in various forms

One method that researchers have attempted in order to improve electrical conductivity is to change the size and geometry of the conductive filler so as to increase the metallurgical connections between each individual silver flake.

It is known that nanoparticles behave differently and even show different material properties when compared to its bulk counterpart [47] and silver is no different. The size of the silver fillers uniquely impacts the electrical conductivity of ECAs as it offers interesting possibilities (e.g. sintering) that are not possible in the micron level [6,47–51]. As a simple explanation, sintering is a process upon which a metallic particle is heated, and as a result, the atoms within the metallic particles begin to diffuse across its surface to create a different shape, or even potentially join together with separate particles of the same element [52,53]. This joining process under heat results in the formation of a three dimensional network among Ag flakes that are otherwise not joined together, creating new metallurgic connections that will decrease the bulk resistance of the material (or increase the conductivity of the material).

The geometry of the silver fillers also plays a significant role in improving the conductivity of CCAs. As explained above, there are Ag nanoparticles (0 dimensional), and there are other geometries that silver can adapt such as silver nanowires and silver nanobelts (1 dimensional). Figure 2-6 shows the three different geometries under TEM that can be adapted by Ag and used to improve the electrical conductivity of CCAs by increasing the metallurgical connections between silver flakes.

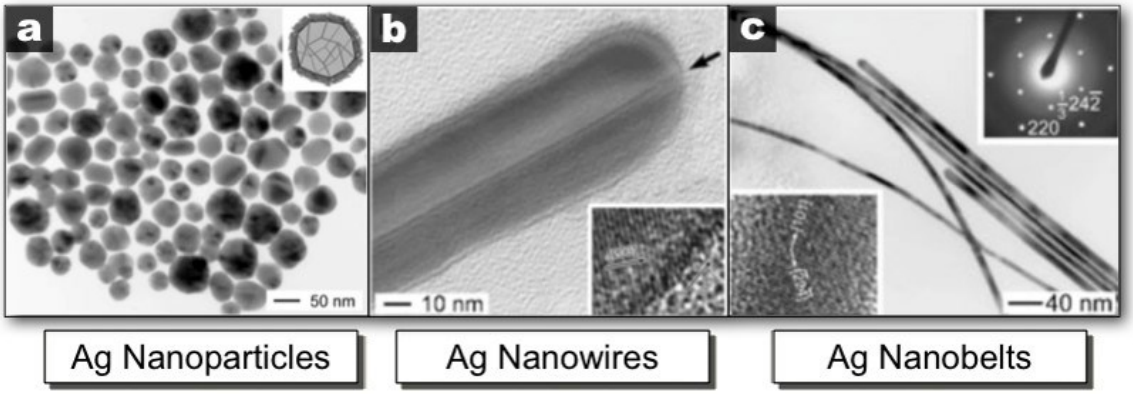

Figure 2-6: a) Example of Ag nanoparticles (0-D); b) Example of Ag nanowires (1-D); c) Example of Ag nanobelts (1-D) (Reproduced with permission Copyright 2005, Wiley) [54]

It is interesting to note that one potential drawback of using these silver nanoparticles would be the introduction of more contact points. Literature reports that although multiple contact points are made, there is little evidence pointing to an increase in continuous linkages made as more nanoparticles are added into the composite [55]. An excess amount of nanoparticles in the composite may even cause a decrease in conductivity in some instances [19,51].

The incorporation of one-dimensional Ag nanowires into CCAs has been reported to improve the electrical conductivity by D. Chen et al [56]. This group also performed an interesting experiment where a CCA was loaded with both Ag nanowires and Ag nanoparticles. They found that the electrical conductivity of the system is better than that with either one of the two co-fillers [56]. Similarly, Z. Zhang et al reported the use of Ag nanowires in CCAs, except that they used high temperatures to cure and sinter the hybrid ECA [57]. As a result of the high sintering temperature, they were able to achieve bulk conductivity values that were 1000x higher than what D. Chen et al reported [56,57]. However, operating temperatures in the 300ºC range is far too high for practical use, therefore making their material unsuitable as a potential replacement for eutectic Pb/Sn solder.

Literature also reports the use of another promising co-filler, a one-dimensional Ag nanoparticle known as Ag nanobelts [19]. The Ag nanobelts have three distinct advantages over Ag nanowires: a) Ag nanobelts are synthesized using a high yield self-assembly method at room temperature; b) Ag nanobelts have a low weight-to-length ratio meaning that the total mass of this co-filler is very small compared to that of other co-fillers; c) Ag nanobelts possess the ability to form a percolated network at low concentrations, meaning it can improve the electrical conductivity of the composite at low weight loadings [19]. It is important to note that using excess amount of Ag nanobelts also yielded similar results as excess amounts of Ag nanoparticles in CCA as again, an increase in contact points leads to a decrease in electrical conductivity [19].

Lastly, researchers have attempted to change the surface functionalization of Ag flakes. Ag flakes are made from mechanical milling and the product is coated with a thin layer of lubricant: a non-conductive chemical that is intended to prevent the flakes from aggregating, thus improve the dispersibility of the metal fillers (which in turn also improves the rheological properties) [1,10,14,42,58–61]. Daoqiang Lu et al as well as Fatang Tan et al have conducted extensive research in this field, and were able to determine that the lubricant on the surface of Ag was a salt of the lubricant and silver. Literature also suggests that replacing the carbon chain with shorter dicarboxylic acids or even removing the organic lubricants off the surface of the Ag flakes will improve its electrical conductivity [1,10,14,58,60], thanks to easier tunneling and electron transport among flakes upon complete removal (removing the lubricant increases intimate contact between flakes).

2.3.2 Conductive Non-metallic Co-fillers: Carbon based nanoparticles and the potential of Graphene

Researchers have also approached the conductivity problem of CCAs using non-metallic co-fillers. In specific, they use inorganic carbon-based nanoparticles such as carbon black (CB) [62–71], carbon nanotubes (CNT) [20,68,71–76], graphene (Gr) [8,17,18,22,25,27,77–81], and even a combination of both known as graphene nanoribbon (GNR) [82,83] as co-fillers in the polymer matrices that either do or do not

contain silver flakes together with it. Figure 2-7 below shows TEM examples of these four types of carbon-based co-fillers.

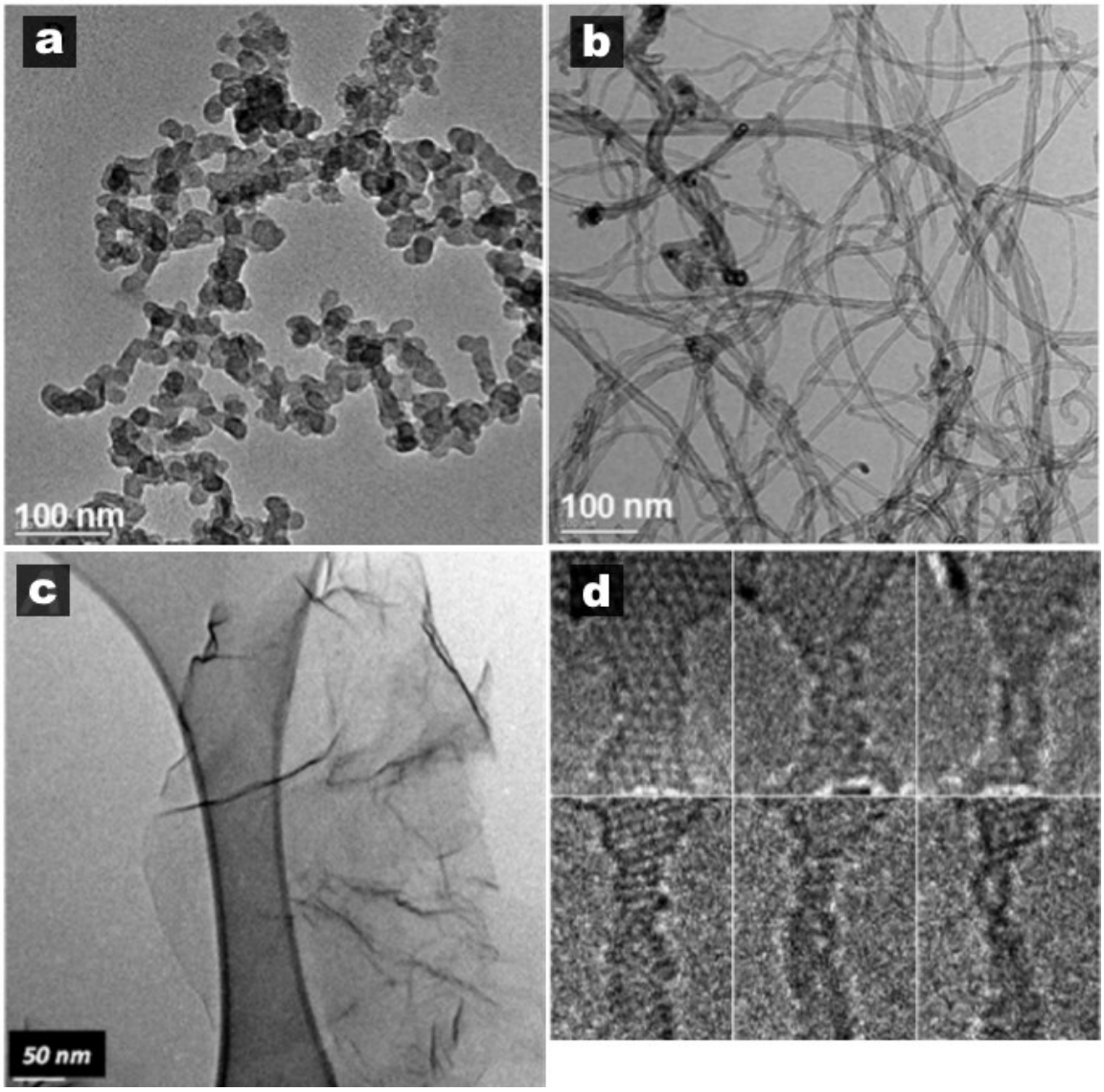

Figure 2-7: a) TEM image of CB; b) TEM image of CNT (Reproduced with permission Copyright 2009, ACS) [71]; c) TEM image of Gr (Reproduced with permission Copyright 2015, Elsevier) [18]; d) TEM image of GNR [83]

These particles help improve the electrical conductivity of the system (CB and other carbon-based particles can decrease electron tunneling resistance when added as a filler) [8,17,52,62,78], or behave like metallic nanoparticles, owing to intrinsic material properties such as high electrical and thermal conductivity [8,17,18,20,22,27,62–

66,68,71–74,77,79,80]. As such, the inclusion of these carbon-based co-fillers proves to be useful as it offers the possibility of shifting the required amount of conductive fillers within ECAs to lower concentrations.

Although carbon-based co-fillers offer plenty of attractive properties that can be utilized by composite materials, there are a few challenges that must be first addressed before being able to take full advantage of what carbon-based fillers (e.g. CB/CNT/Gr/GNR). The most common problem is the agglomeration issue of carbon-based fillers that occurs when incorporated within the polymer matrix [6,17,22,25,27,70,74,80,84,85]. This problem leads to other issues, for example, increase in viscosity and poor dispersion, which cause many of the beneficial properties to be suppressed, resulting in the composite exhibiting minimal performance improvement [17,18,22,27,71,75,76,86]. Researchers have responded to this problem in two ways [17,18,25,75,87]: a) by attempting to use methods that involve the surface functionalization/modification of the carbon filler to allow for better chemical interactions between liquid media (either the polymer itself or solvent) and the carbon filler; b) and using high shear mixing techniques as a physical method of dispersing the carbon filler [76]. The first method of chemically modifying the carbon filler (in this specific case, (Gr)) has been reported to prevent aggregation, but also results in disappointing improvements to electrical conductivity especially for graphene (this is because the pi-electron delocalization is disturbed when covalent bonds are formed) [18]. The second method of using surfactants on carbon fillers as a means to non-covalently exfoliate the carbon fillers was successful at improving electrical conductivity and will be a central topic in this thesis [3,18,21,27].

2.3.3 Conductive Non-metallic Co-fillers: Conductive Polymers and PEDOT:PSS as an Alternative

Another approach that researchers are taking to improve the electrical conductivity of CCAs involves mixing the composite with inherently conductive polymers such as polyaniline (PANI) [88–90], polypyrrole (PPy) [91–93] or a polythiophene based chemical known as poly(3,4-ethylenedioxythiophene) polystyrene-sulfonate (PEDOT:PSS) [5]. An image depicting all known inherently conducting polymers is shown below in Figure 2-8.

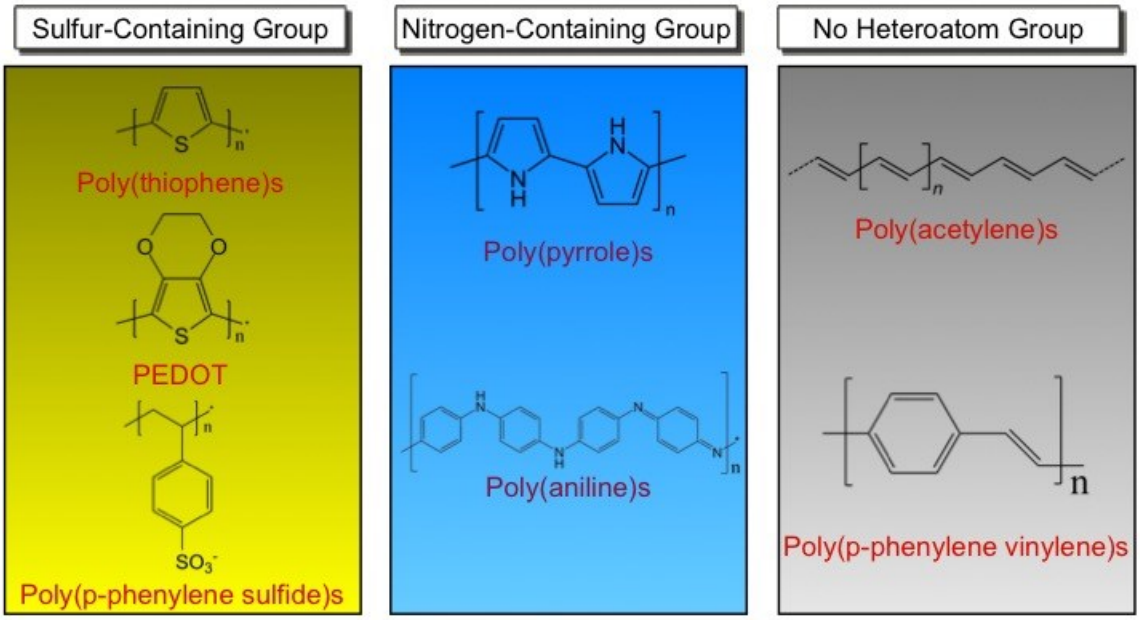

Figure 2-8: Schematic of electrically conducting polymers divided into groups.

While the first conductive polymer suggested (PANI) offers benefits such as easy processability, low bulk cost [94] and has been proven useful as a co-filler that can improve the properties of CCAs [88,90], researchers have also determined that PANI's benzidine moieties present on its backbone could yield carcinogenic products upon degradation, which is counter-productive to the attempts of ECAs acting as greener solutions [94].

PPy on the other hand has shown greater promise, owing to its biocompatibility, ease of synthesis, stability, and low cost [91,95]. Interestingly enough, PPy is already enjoying commercial use today as it offers other benefits such as corrosion inhibition, good electrical conductivity, electroactivity, and electrocromism to applications including rechargeable batteries, electrochromic displays, ion-exchangers, pH sensors, etc. [91]. Researchers, however, soon discovered the drawbacks of this conductive polymer: insolubility in water and most organic solvents making it difficult to process/functionalize, and poor mechanical/adhesion properties such as self-delamination off common substrates such as glass [91,95]. To alleviate this problem, PPy has been modified with other polymers to form a composite and mitigate its weaknesses while at

the same time, even provide newer strengths such as smoother percolation curves in the context of electrical conductivity [91]. However, sometimes, the modifications use harsh post-treatments that are detrimental to the overall products that result in the decrease of PPy's biocompatibility [95]. Reports of using PPy-epoxy have been made and demonstrated to function as ICAs, showing great promise as a potential alternative to eutectic Pb/Sn that can be used in industry [91,92]. There is also a report that uses dopamine (DA) as the modification to PPy to form a functionalized PPy composite that adapts a tunable fibrous morphology capable of exhibiting enhanced water dispersibility, adhesion properties, and electrical conductivity [92]. Both of these reported modified PPy composites were used in CCAs and were shown to improve both mechanical and electrical conductivity, and overall displays excellent potential as a commercial ECA.

Finally, the incorporation of thiophene derivative PEDOT:PSS into CCAs will be shown in this thesis to see whether or not it also had the potential to become the next commercial ECAs in the market [5]. To the best of our knowledge, no work has been published regarding the use of PEDOT:PSS as a bulk material acting as a co-filler for improving the electrical conductivity of CCAs.

2.4 The Material Properties of ECAs

2.4.1 The Mechanism behind Conductivity in ECAs: The Percolation Theory

This section will concentrate on explaining a frequently used term throughout this thesis that details the conduction mechanism responsible for making conductive adhesives exhibit electrical conductivity upon loading the polymer matrix with conductive filler: the percolation theory. The word percolation means *to spread gradually through an area or group* according to various dictionaries, and is even explained in chemical/mathematical terms by S.R. Broadbent and J.M. Hammersley [96]. However, if described in the context of ECAs, this theory specifically refers to the gradual spreading of conductive filler content within the insulating polymer matrix [32,40,52,61,97].

What the percolation theory tries to explain when it comes to ECAs is the critical volume fraction (i.e. V_{perc}) of the conducting substance necessary to illicit electrical conductivity

within a medium presumed to be completely insulating. We call the point at which we reach/exceed the V_{perc} as the percolation threshold (where the insulating material begins to express electrical conductivity as a result of the conductive particles forming a network throughout the entire composite) [32,40,52,61,97].

To simplify, we can divide this theory into three sections. Conductive filler is gradually added into an insulating matrix, and as a result, will elicit a gradual electrical conductivity increase within the insulating matrix (denote this as section I) owing to the increasing amount of metallurgical connections being made as the polymer network is saturated with conductive filler. After reaching and exceeding V_{perc}, the conductivity increase will experience a sharp rise where the composite material transitions from a bulk insulator into a bulk conductor (denote this as section II with the dotted line). Conductive filler is added after the sharp rise, but once again experiences only a gradual increase in electrical conductivity (denote this as section III). A schematic of this phenomenon can be seen in Figure 2-9 where the increasing number of the section represents more silver filler added (with different color to show particles overlapping).

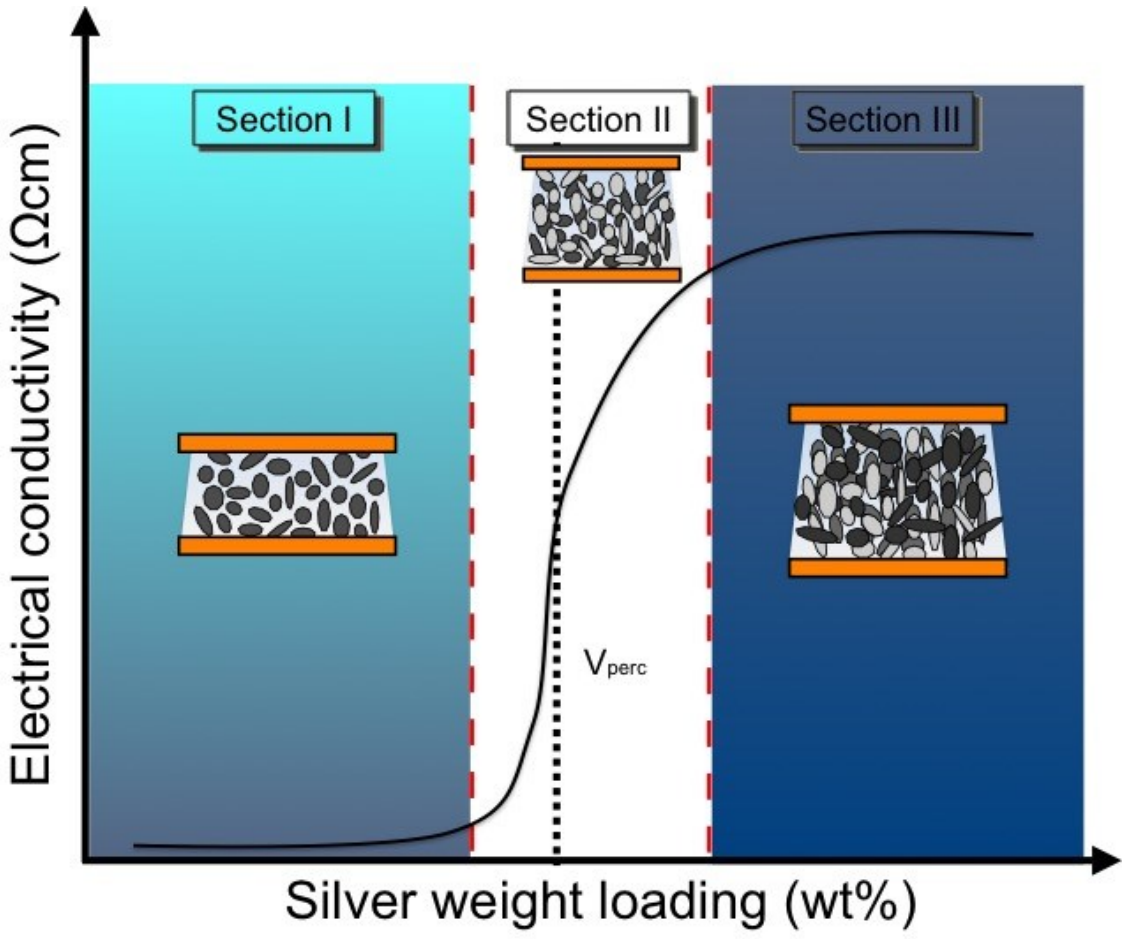

Figure 2-9: Schematic of Percolation curve to explain percolation theory. As the polymer network is slowly saturated with conductive filler, more metallurgical connections are made between filler particles resulting in an increase in conductivity.

We can also describe this phenomenon in mathematical terms based on equations stated by N. Lebovka et al. Electrical conductivity $\sigma(V)$ is dependent on volume fraction of conductive filler (V) and the area near section I (that approaches the dotted line and begins to transition to section II), and can be summarized using equation 1 below:

$$\textbf{while } V > V_{perc}\text{:} \quad \sigma(V) = a\left(V - V_{perc}\right)^{t} \qquad \textbf{Eq. 1}$$

whereas area near section III (that passes the dotted line and begins to plateau) can be summarized using equation 2 below:

$$\textbf{while } V < V_{perc}\text{:} \quad \sigma(V) = b\left(V_{perc} - V\right)^{-s} \qquad \textbf{Eq. 2}$$

where s & t denote the electrical conductivity exponents and a & b denote coefficients for different materials [98]. N. Lebovka et al further explained that for random percolation, variables s & t are expected to be $s = t \approx 4/3$ for 2 Dimensional systems, whereas $s \approx 0.75,\ t \approx 2$ for 3 Dimensional systems [98]. It is important to remember that the t value can change depending on a variety of factors, for example, B. Kilbride et al noticed that charge transport through a 2 Dimensional object was unlikely when $t \approx 4/3$ for their CNT system as the exact same values were observed for bulk structures as well as films, indicating that such a phenomenon is possible only through electron transport/tunneling of some sort within the bulk composite [99]. Other observations for CNT systems have also mentioned the possibility of CNT aggregation as the cause of the shift, as the above equations break down if random distribution is not achieved [100], which is a large possibility for carbon-based fillers that tend to suffer from agglomeration issues as mentioned earlier.

Some important remarks must be made to further clarify why this conductivity-shifting phenomenon is possible. In order for electrical conductivity to occur, these conductive particles must be properly distributed throughout the matrix such that the filler material establishes particle-to-particle contacts (in this thesis, we denote this intimate contact between particles as metallurgical connections). It is in this regard that we are able to form a network of conductive particles that are in contact with each other, giving room for electrons to travel through and as a result, express electrical conductivity.

Also, because this network of conductive particles must be in contact with each other to make metallurgical connections (or close proximity between each other), various parameters such as particle geometry, size, aspect ratio, nature and distribution are important to consider [52]. It is precisely because of this fact that many of the recent progresses mentioned earlier in this thesis were possible, as researchers modified particle geometry (nanowires/nanobelts or CNT → GNR), size (Ag nanoparticles and CB), aspect

ratio (exfoliated Gr and Ag nanobelts), nature (presence of lubricant on Ag), and distribution (solvent effects that will be mentioned in later sections).

Furthermore, the idea of the conductive particles requiring intimate contact is easily observed in the case of ECAs, as uncured composites despite being loaded with high weight concentrations of Ag flakes will only exhibit conductivity after the curing process, where the epoxy shrinks and compresses the flakes together [32,52], implying that higher shrinkage leads to better conductivity as more conductive pathways are formed.

As supplementary information, Mikrajuddin et al referred to a model called effective medium approximation (EMA) that incorporates this shrinkage concept into the explanation as to how ECAs conduct electricity (similar to what was proposed by N. Lebovka et al). EMA considers the volume fraction of filler particles to be small cubes that make up the volume of the composite, and was established in order to solidify the relationship between volume fraction of conductive filler, particle size, pressure, as well as the possibility of having two percolation thresholds [97].

2.4.2 The Mechanism behind Conductivity in ECAs: Contact Resistance for a Bulk Composite

Building from what was mentioned from the previous section, this thesis will also touch upon the concepts responsible for creating resistances within a composite system. Amoli et al and other researchers explained that the overall resistivity value measured from ECAs is a summation of a series of resistivities R as seen below in equation 3 [6,52,101]:

$$\boldsymbol{R = R_b + R_{f-f}} \qquad \textbf{Eq. 3}$$

where R_b is the bulk resistance of the conductive filler and R_{f-f} is the filler-filler contact resistance. Moreover, the filler-filler contact resistance can be further broken down into two specific types of resistivity values as seen below in equation 4:

$$\boldsymbol{R_{f-f} = R_{cons} + R_{tunnel}} \qquad \textbf{Eq. 4}$$

where R_{cons} is the constriction resistance that is responsible for restricting the free-electron flow through sharp contact points, while R_{tunnel} is the tunneling resistance, which is formed across two fillers that are not completely in contact with each other, yet still close enough for the electron to tunnel through [52].

It was mentioned in previous sections that Ag nanoparticles begin to exhibit higher resistivity values if the concentration loaded into the polymer matrix is too high. This phenomenon is directly attributed to constriction resistance, since more contact points lead to more bottlenecked electron pathways rather than one large continuous highway. Figure 2-10a shows a cartoon as an example that explains how constriction resistance reduces the current by separating the electrons into multiple roads; half of which do not even reach the end of the material. This drop in current felt originates from the electrons that become stuck among the many contact points within the composite (because the smaller branches have smaller contact area) and is known as constriction resistance. Figure 2-10b on the other hand shows a cartoon of how tunneling resistance requires the electron to overcome an energy barrier (akin to uphill travelling needing more energy) to pass through the gap. When an electron tries to go through this small gap, majority of the signal (in our case current) is not 100% transferred since the probability of the successful electron tunneling is low. This inefficiency known as the tunneling resistance or a drop in current originates from the electron's attempt to overcome the energy barrier at a very low success rate.

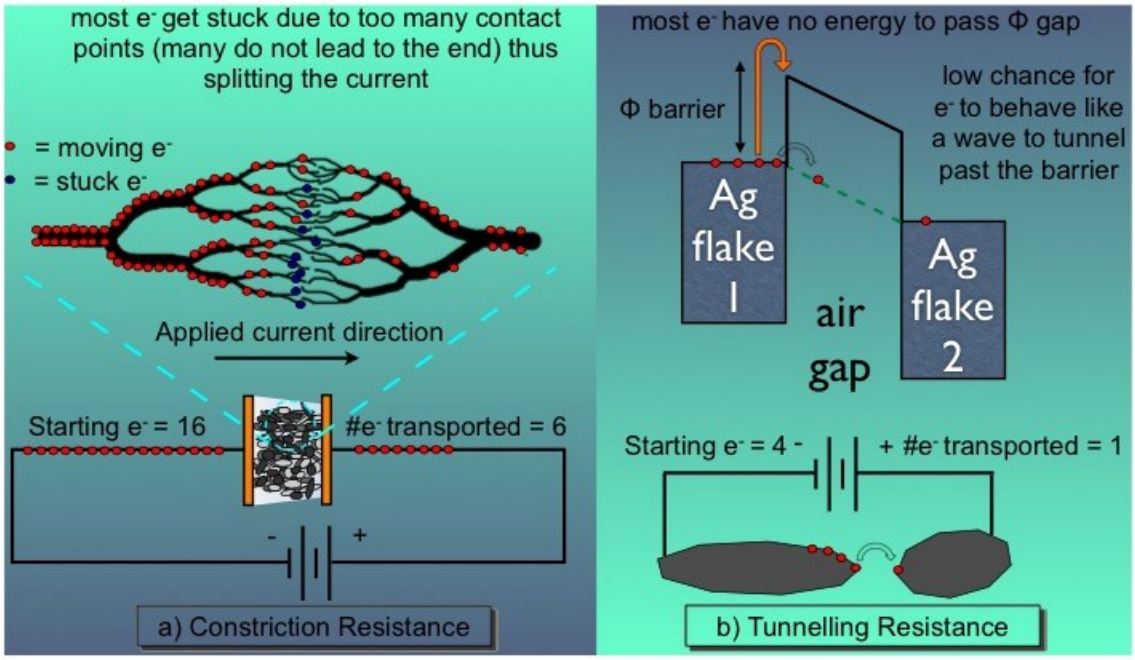

Figure 2-10: a) Image for explaining constriction resistance where electrons attempt to travel from one end of the composite to the other, but only few succeed resulting in a drop in current; b) Image for explaining tunneling resistance where only very few electrons succeed in conquering the Φ barrier, resulting in a drop in current.

2.4.3 Epoxy Resin: A Better Understanding of the Polymer Matrix and its Role in ECAs

Epoxy is a thermoset that has been preferred as polymer matrix for ECAs as well as many other composite materials, as it possesses many attractive characteristics such as excellent environmental and dimensional stabilities, good strength, modulus, hardness and adhesion to a wide variety of filler materials [13,35,60,76,102–105]. But before delving further into how to improve ECAs, it would be prudent to first explore the role of epoxy: the ECA's often overshadowed component.

Plastics, or synthetic polymers are a class of material that is used in all areas of life today, and can be traced back to as early as 1830 when the first sticky latex from natural rubber was used for tires [106]. Since then, synthetic polymers have increasingly grown in production (especially after World War II) in order to mitigate the lack of trade for naturally occurring materials [106]. Eventually, plastics began to compete with the use of

traditional materials such as metal for various mechanical applications especially during the 1960s-1970s. Plastics can be divided into two categories according its behavior during thermal processing: Thermoplastics and Thermosets [106]. Thermoplastics by definition are polymers that are molded by applying heat as its primary means of processing, possessing a special feature of being recoverable and re-fabricated through the use of heat and pressure. Examples of thermoplastics include polyolefins, polyvinyl chloride, polycarbonates, polyacrylics, nylons, etc.

On the other hand, thermoset resins are a class of polymers that account for about 10-20% of the entire polymer market, where they are used as key components for composites, adhesives, and coating technologies [76,106]. Examples of thermosets include epoxy resins, phenol-formaldehyde resins, un-saturated polyesters such as fiberglass and finally synthetic rubbers [106]. In specific, thermosets are polymers that are typically pre-polymerized and then "crosslinked" through chemical or thermal treatment to form chemically linked covalent bonds between individual polymeric chains during fabrication [76,106]. After "setting," the crosslinked networks are able to resist many forms of stimuli (such as heat softening, mechanical deformation and solvent attack) [106], virtually unable to further modify its physical state or chemical structure [107]. Although traditional thermosets are excellent candidates for applications requiring dimensional stability and environmental resistance [107], many shortcomings are encountered because of the same behavior. Examples include the inability to exhibit reusability, post-polymerization manipulation and decomposition [107].

From a chemical point of view, it was first synthesized in 1891 and was not commercialized until 50 years after [105,108]. A prime example of a thermoset is epoxy: a material that is useful in a variety of fields as it offers excellent properties. The chemical structure of commercial epoxy resin and crosslinkers is shown below in Figure 2-11.

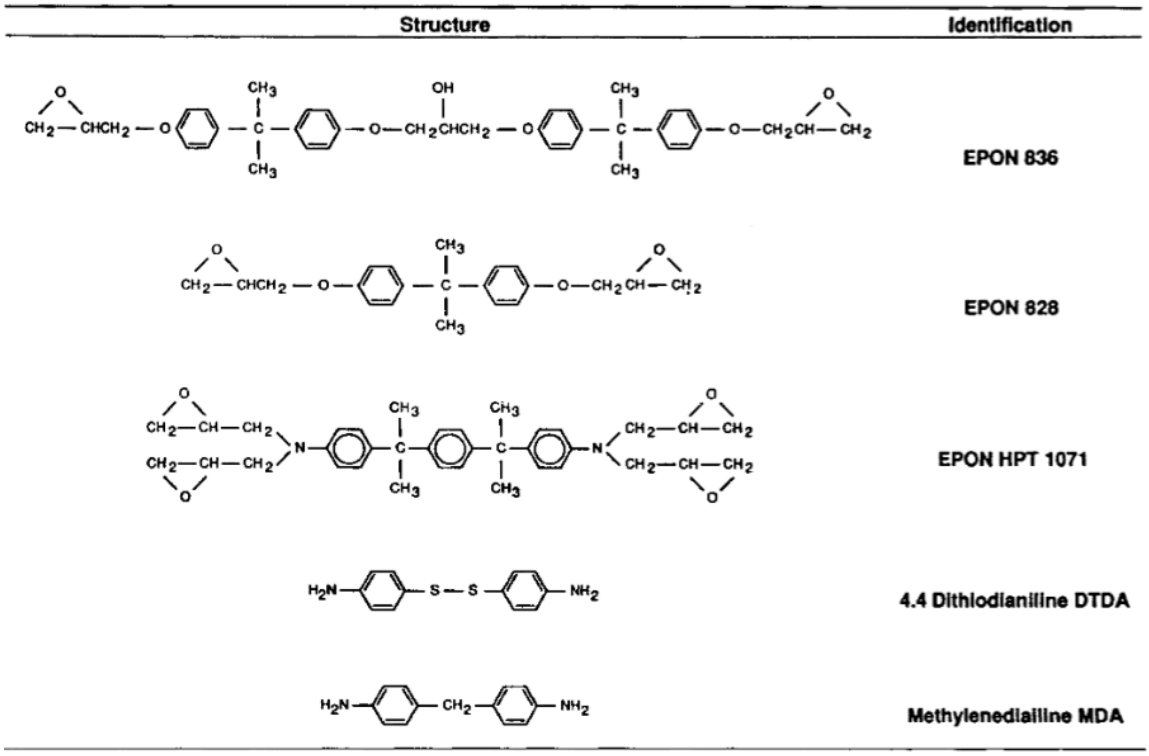

Figure 2-11: Schematic representation of epoxy resin and curing agent chemical structure (Reproduced with permission Copyright 1990, Wiley) [109]

A few examples of these properties are as follows: adhesion (on a variety of surfaces), high mechanical strength (tensile, compressive and flexural), resistance to chemical attack and fatigue, as well as electrical resistance [102,103,105,108,110]. Furthermore, epoxy exhibits a degree of tunability since a user can change the way either the resin or the hardener is used or synthesized in order to achieve the kinds of properties he/she wishes the epoxy to display. For example, its viscosity and final strength can be adjusted by changing the monomer density, chain length, curing agent and catalyst if used [105]. These properties are ideal for engineering as not only is epoxy a flexible material with a variety of possible properties, it also produces little to no harmful byproducts when undergoing the curing procedure [105]. Many of these wonderful properties are heavily attributed to a quantifiable means of determining how well epoxy is cured: the crosslinking density [108].

With this knowledge in mind, it is clear that the mechanical and physical properties of ECAs are heavily dependent on the type of polymer matrix chosen, influencing the ECA's rheology, adhesion strength and durability as will be seen in the coming sections.

2.4.4 The Rheological Properties of a Composite: Flow and Workability

As mentioned in the previous section, understanding the rheological and viscoelastic behavior of a composite system is important in the perspective of engineers. Studies give insight to the flow mechanics of the most common type of polymer liquid systems, and non-Newtonian fluids are useful for a variety of applications such as paint systems, ink printing processes or generally any system that handles dispersions [111,112]. Figure 2-12 shows viscosity as a function of shear rate as well as different colored lines to denote different flow curves for different rheological behaviors [113,114].

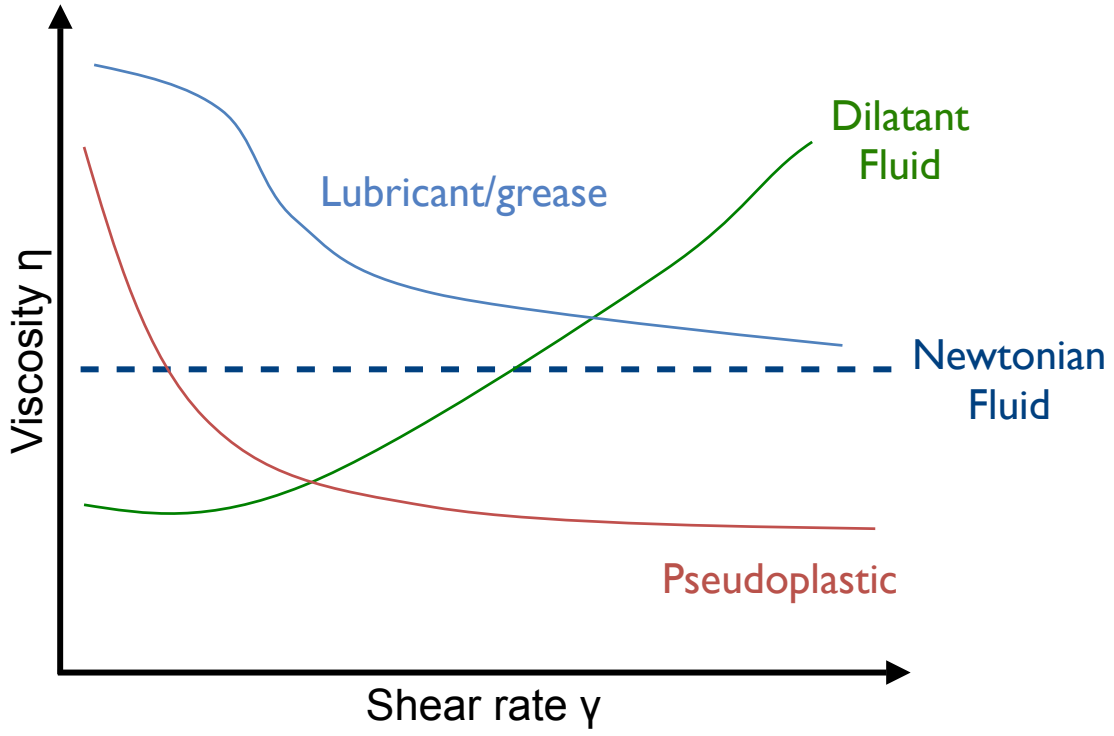

Figure 2-12: Viscosity as a function of shear rate to show the different rheological behaviors of fluids using flow curves

An example of why rheology is important can be seen in the behavior of polymer liquids under confinement (i.e. is very close to 2 Dimensions in that the paste is very thin).

Systems exhibiting this confined nature tend to behave very differently when compared to bulk behavior because the thickness of the polymer is approaching the magnitude of the polymer coils, giving rise to interactions that do not exist in the bulk scale: a behavior elucidated through only through rheology. The dynamics and statistics of these confined polymers have great value for industrial fields concerned with tribology, adhesion, lubrication and catalysis [115], while on a laboratory level they can help estimate important properties that we are concerned with composites such as dispersion quality of carbon fillers and the mechanical strength of composites [116]. Furthermore, viscosity has been used as a practical tool for determining the percolation threshold and saturation point of composites, which allow researchers spend less time on optimizing formulations despite the many compounding conditions that are associated with mixing filler materials in polymer matrices [117].

The understanding of rheological and viscoelastic behaviors is useful for different applications in industry as it gives engineers a better idea of the conditions required for easier processing control [118]. Moreover, this understanding can lead to the possibility of researchers shedding light on properties that a filler material expresses only within the polymer matrix. White et al reported that while graphene offers a variety of marvelous properties that are required to produce excellent properties as a composite, more often than not the resulting composite falls short. This problem could be caused by surface defects, lack of exfoliation, aggregation, wrinkles, poor dispersion, unexpected interfacial interactions and so fourth [118]. With rheological knowledge, it is possible to characterize particle structure and interactions for specific applications such as ECAs that require specific viscosity parameters for proper paste spreading as specified by A. Ryan et al [4]. Finally, it is important to realize that rheology is not a mature field as it still has not reached the point where researchers can develop high-level computational simulations and models that can simulate how the flow mechanics affect the composite performance without being limited to the existing continuum-level models [118]. As such, it is good to continue researching and expanding our knowledge regarding the rheological behavior of composites so that one day, researchers can have enough data to be able to create models and simulations that help draw out the full potential that

composites can offer. This thesis presents rheological work on Gr- and Gr(s)-loaded epoxy using a cone and plate viscometer at room temperature to help understand the impact of carbon fillers on the composite.

2.4.5 Mechanical Properties of a Composite: Lap Shear Strength

ECAs are first and foremost adhesives with the task of adhering electrical components down onto a substrate (PCB). As such, ECAs are required to exhibit good adhesion strength to be able to fulfill its purpose. Many works have focused on improving the electrical conductivity of ECAs as outlined in previous sections of this thesis. However, there is a significantly smaller number of works that focus on the characterization and improvement of ECA's mechanical properties such as adhesion strength [36]. It is mentioned in one of the upcoming chapters that quantifiably predicting both the performance and strength of an adhesive is difficult and complex, owing to the many factors that must be accounted for between the adhesive and the surface where it is bonded to [119,120]. Moreover, predicting the failure mechanisms occurring at the microscopic level is not a simple task without using complicated models and software. Figure 2-13 shows an example of a MATLAB software used by researchers that compares between analytical and experimental data for adhesive lap-shear joint failures.

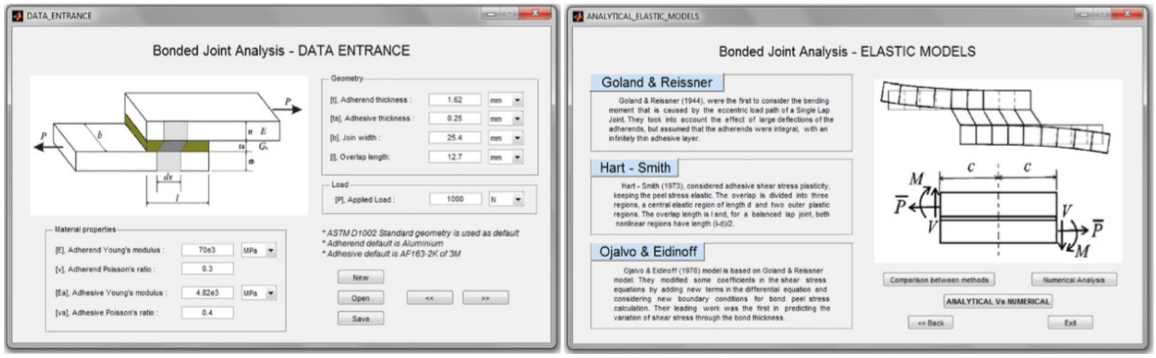

Figure 2-13: MATLAB program designed to do an analytical VS experimental comparison for bonded joints (Reproduced with permission Copyright 2012, Elsevier) [121].

In order to work around this problem, efforts were made to simplify the mechanical testing of adhesives by focusing on identifying stress distribution for the lap-joint of interest [122]. It is in the interest of both researchers and industry to adapt similar test

procedures so that both parties can accept a universal practice of determining the adhesive's mechanical strength. The way both researchers and industry achieved this is through the formation of test such as American Society for Testing and Materials (ASTM), which is a test standard association responsible for developing strict black-box protocols that heavily simplify the test procedure, preparation and calculations involved with finding a property of interest. In other words, as long as the tester follows the standard, they can then not only avoid experiencing issues with calculations and invalidating any approximations or assumptions made by the test standard, but also, the tester will have full confidence that their results are relevant and universally acceptable. In the case of adhesion strength, ASTM uses the lap-shear strength (ASTM D1002) [123] to quantify the adhesion strength of metal-to-metal joints, and is a commonly recurring mechanical property found in technical datasheets. Further examples of this test can be seen in subsequent chapters that utilize this test standard in hopes of determining the mechanical performance of ECAs.

2.4.6 Mechanical Properties of a Composite: Elastic Modulus

The concept of understanding the macro-scale mechanical properties of a given material using information gained from the micro-scale structure has been a recurring objective of material science and researchers [124]. As was discussed in the previous section, the adhesion strength is a mechanical property of great importance to ECAs. It is known that there are two ways to improve this property: a) using surface functionalization by adding a chemical that contains both an organic component and metallic component thereby assisting in the "coupling" of the two different solid surfaces; b) decreasing the elastic modulus of the resin to acceptable levels that do not encourage the adhesive from experiencing cohesive failure [41]. Although the method of using coupling agents has been well explored by other researchers [38], the studies outlined in this thesis concentrate on the latter, using micro-indentation in order to characterize the elastic modulus of ECAs. Figure 2-14 shows adhesion strength as a function of elastic modulus to illustrate how there is an optimal point at which the material enjoys high adhesion strength without decreasing the elastic modulus too far to the point of provoking cohesion failure.

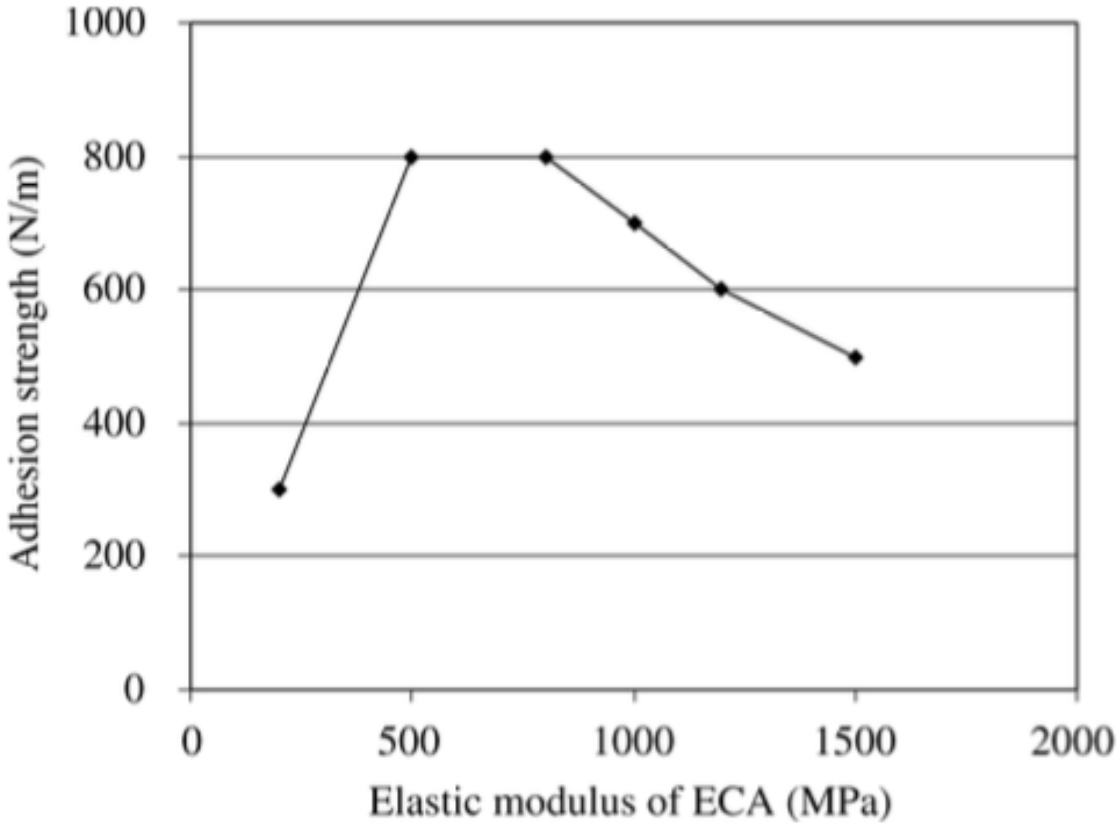

Figure 2-14: Adhesion as a function of elastic modulus for ECA composites (Reproduced with permission Copyright 2008, Taylor & Francis) [41]

By definition, the elastic modulus of a material is a measure of a material's ability to resist deformation within the elastic region (the area that permits deformation before irreversible deformation occurs) as an external force is applied [125]. Although it is simple to just characterize elastic modulus of ECA composites to see if it is possible to obtain a map to determine at which point we are able to have high adhesion strength yet high elastic modulus to prevent cohesive failure, predicting the elastic moduli of systems that are comprised of more than one component is not simple because many factors affect the readings, for example, system morphology, shape of the components as well as any interaction effects (i.e. if the components bond to themselves) [126]. Therefore, results from our studies will be focused on observable trends rather than focus on single values that fully define our composite system.

This study uses indentation as the primary method to determine elastic modulus (dubbed as Hertzian indentation in this thesis). According to Oliver and Pharr, elastic modulus *E* and hardness *H* are the two most common mechanical properties that are characterized using indentation [127]. The elastic modulus is connected to the force VS displacement curve generated from the indentation test using an equation solved by Hertz [128,129] and Reine [128] (dubbed Hertzian equation in this thesis) and can be seen below as equation 5:

$$a^3 = \frac{3PR}{4E^*} \qquad \textbf{Eq. 5}$$

where a^3 is the radius of the contact area, *P* is the indentation load (in force), *R* is the radius of the indenting tip, and E^* is the elastic modulus [128,129]. This equation acts as the basis upon which our elastic modulus information was calculated and will be explained further in a future chapter.

Chapter 3 SDS Decoration of Graphene and its Effect on the Rheological and Electrical Properties of Epoxy/Silver Composites

3.1 Introduction

As was discussed in the previous chapter, engineers consider the rheological and viscoelastic behaviors of a composite system as important physical properties to understand. The rheological and viscoelastic behavior can be used to give a better idea of the conditions required for easier processing control and in the end, workability that is essential to making ECAs become commercially friendly and practical to manufacture. This study uses SDS decorated graphene (Gr(s)) because previous works by T. Filleter et al and J. Lin et al suggest that single layer graphene possesses properties that allow it to behave as a solid lubricant [130,131]. This concept is useful as J. Coo et al and R. Bowman et al explained that frictional force (that lubricants decrease) is proportional to viscosity [132,133]. These rheological studies for graphene and epoxy composites are in specific useful for electrically conductive adhesives (ECAs); a material intended for replacing traditional alloy-based solders [134]. The viscosity and rheological properties of an ECA is key to determining its performance and feasibility as it is applied to stencil and screen-printing techniques [134].

It is important to note that this study cannot use a solvent-assisted approach, because both trace amounts of solvent and bubbles formed during the curing are unavoidable even with long desiccation time [76,135]. Furthermore, the yield from such a process is expected to be very low because of a small amount of material, as a large amount of solvent is needed [18]. M. L. Gupta et al addressed a similar problem when it came to making composites, however, instead of using graphene, they used carbon nanotubes (CNTs) as the nanofiller. They successfully determined how to disperse and mix the nanofiller without solvent when it came to forming composites through the use of a planetary shear mixer (PSM), as well as other high shear mixing machines [76]. Our method also used a PSM to carry out a solvent-free method to disperse nanofillers, synthesize hybrid ECAs, as well as investigate nanocomposites that were not loaded with silver flakes. This work

systematically investigated how adding graphene and SDS decorated graphene will affect the viscosity and the electrical performance of the composite. The way this mixing method affects the ECA properties will be briefly discussed by examining the morphology of the ECA using SEM. We will also determine the electrical conductivity of the material as it is suspected that the absence of the solvent will directly affect the dispersion of graphene and thus affect its ability to decrease bulk resistivity.

3.2 Experimental

3.2.1 Stabilizing/Decorating graphene nanosheets with SDS

Graphene nanosheets (Gr) were purchased from ACS Materials (USA) and used as received. The size of the graphene nanosheets according to the supplier is 0.5 to 5 μm and is confirmed using TEM by Amoli et al to be around 1 μm [18]. SDS was purchased and used as received from Sigma Aldrich. Although the procedure before the nanocomposites preparation requires the use of solvents (ultra-pure water and HPLC Ethanol) in order to properly functionalize and stabilize the Gr with surfactant, the mixing procedure for preparing the nanocomposites is solvent-free.

Our previous work provided us with the inspiration to decorate graphene with the non-covalent surfactant method, which is illustrated below as a schematic in Figure 3-1:

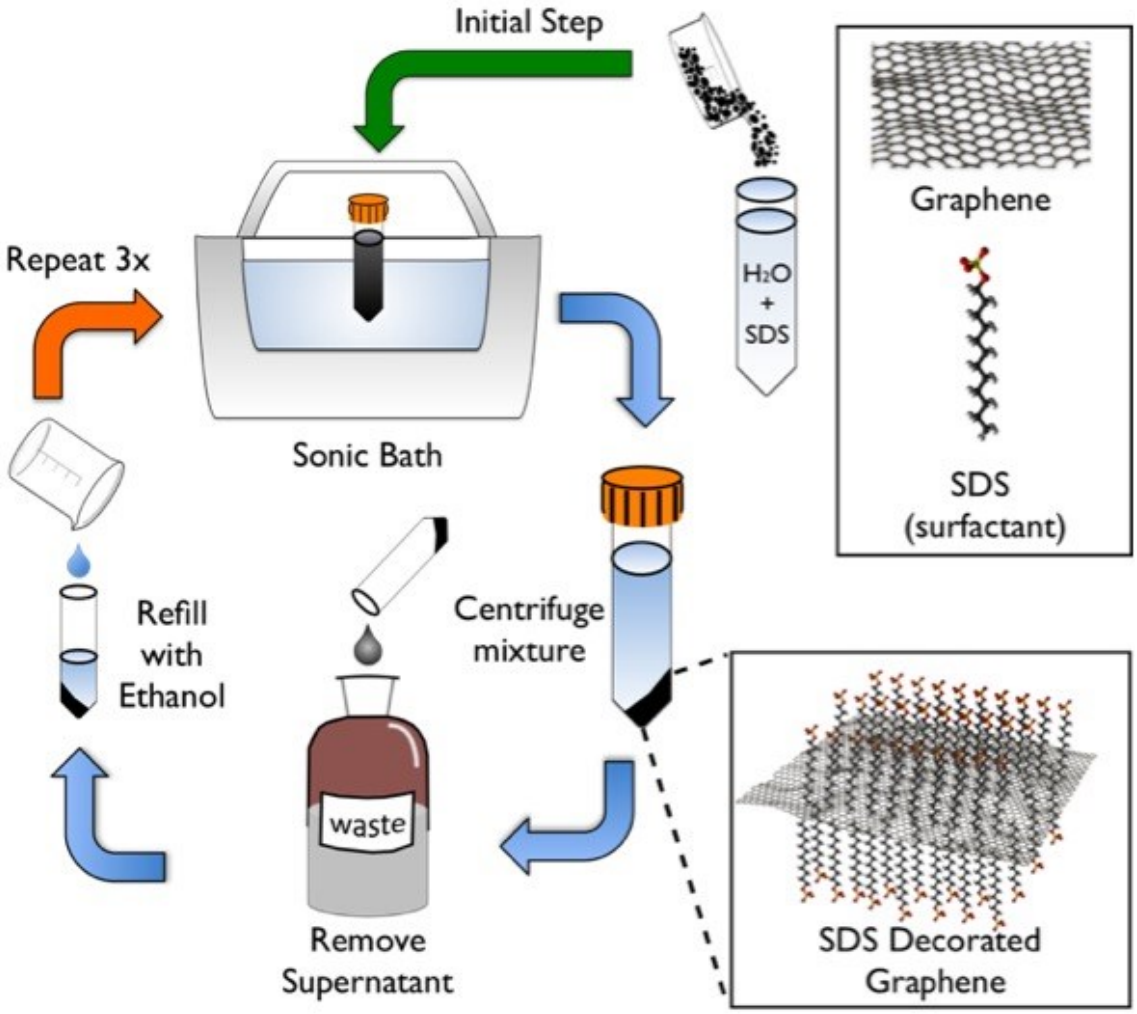

Figure 3-1: Schematic illustration showing the decoration of the graphene nanosheets with surfactant SDS

This process uses a liquid solution that is prepared by mixing SDS powder with ultra-pure water at a concentration of 60 mmol L^{-1}, which is 20 mmol L^{-1} lower than the critical micelle concentration (CMC) of SDS in water [136,137]: the point where the excess surfactant forms micelles. The aim of the SDS decoration is not to make micelles, but rather, to decorate and self-assemble onto the graphene and non-covalently exfoliate the graphene sheets. This solution was then placed in low power sonic bath (Branson 2510R-MT) to undergo ultrasonication for 30 minutes, and allows for the hydrophobic backbone of the SDS to adsorb onto graphene's surface. The solution is centrifuged at 8500 RPM for 10 minutes and the supernatant is removed. The remaining precipitate is washed four

times using HPLC ethanol as its dispersant which is then sonicated for 5 minutes. This process is repeated three times in order to remove remaining un-bonded SDS from the precipitate. Finally, after completing the repetitions, the precipitate is then placed in a vacuum oven at 75°C overnight to allow any remaining solvent to evaporate wherein the leftover precipitate of SDS stabilized graphene (Gr(s)) is harvested.

3.2.2 Preparing the nanocomposites

Liquid epoxy resin (D.E.R.™ 331) Diglycidyl Ether Bisphenol-A (DGEBA) and curing agent (D.E.H.™ 24) triethylenetetraamine (TETA) were purchased and used as received from DOW Chemical Company (USA). Silver flakes (~10 μm) were purchased from Sigma Aldrich and used as received. The following combinations denoted below in Table 3-1 were combined in one container where they were mixed at 2000 RPM for 4 minutes and de-foamed at a speed of 2200 RPM afterwards for 1 minute using a Thinky Mixer (ARE-310).

Table 3-1: List of the combinations of compositions used for nanocomposites

Sample	Composition	Ag flakes [wt %]	Gr/Gr-s [wt %]
1	Epoxy	0	0
2	Epoxy + Silver flakes	60	0
3	Epoxy + Graphene	0	0.25, 0.5, 1, 1.5 and 2
4	Epoxy + Graphene-SDS	0	0.25, 0.5, 1, 1.5 and 2
5	Epoxy + Silver flakes + Graphene	60	1
6	Epoxy + Silver flakes + Graphene-SDS	60	1

3.2.3 Measuring Viscosity

A cone & plate viscometer (Brookfield CAP2000H+, USA) was used to determine the effects of filler concentration on the viscosity of the system at room temperature. Cone & plate viscometers operate under the principle of measuring a torque felt by a cone shaft undergoing a constant shear rate and known spindle dimensions. As seen in Figure 3-2, this viscometer is comprised of a flat plane where the sample is located and a rotating shaft (housing a cone shaped spindle at the end).

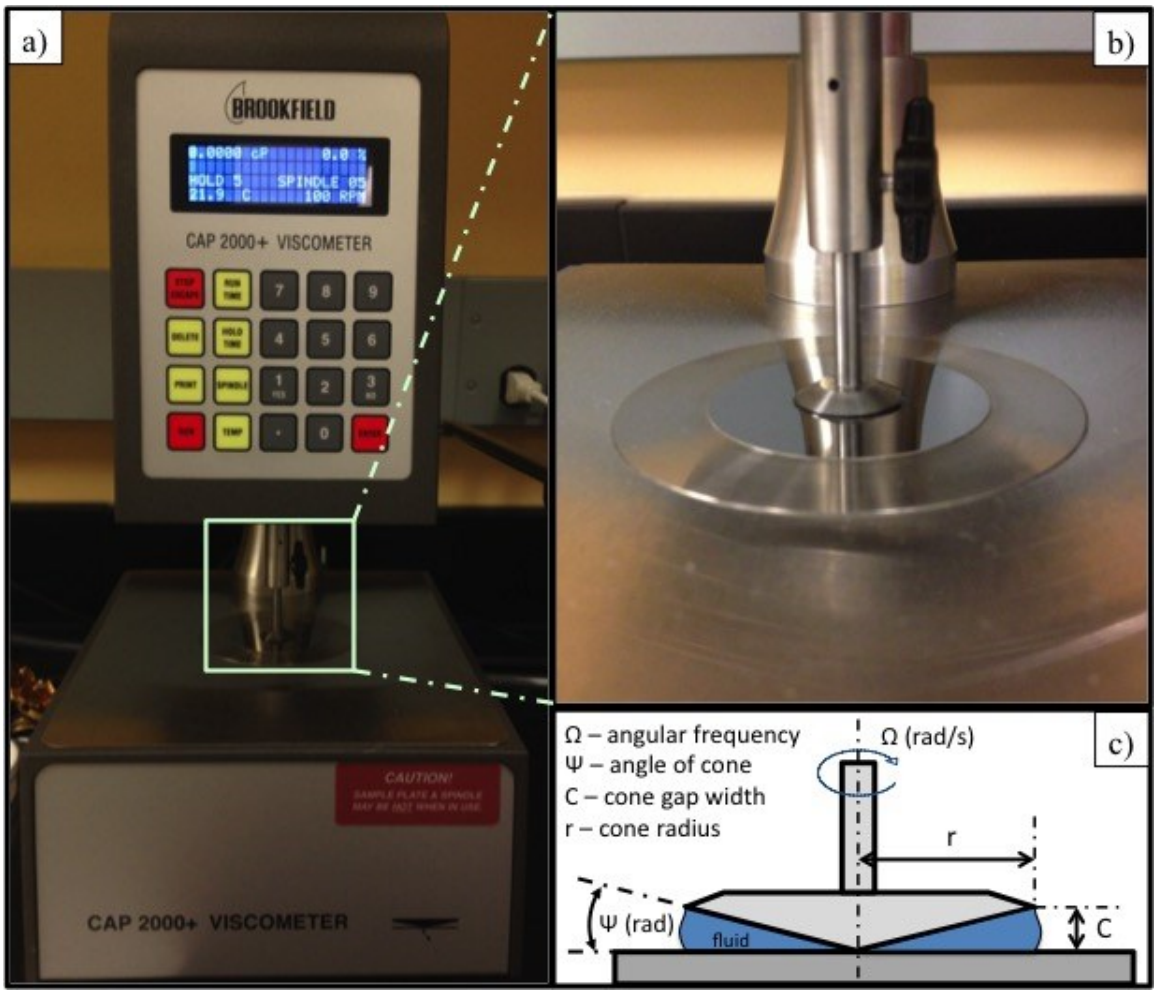

Figure 3-2: a) Optical image of the cone & plate viscometer; b) zoom-in of cone & plate loaded with epoxy resin; c) cross-sectional diagram of the cone & plate with the terms used in the viscosity equation

The cone itself has an obtuse angle propagating away from the apex of the shaft; the gap between the cone and plate once the apex touches the plane is filled with the sample where the linear velocity is proportionate to the radial distance resulting in a constant shear rate as the spindle rotates [138]. Shear stress τ is denoted below as a ratio between torque G felt by the spring and radius r of the cone [138]:

$$\tau = \frac{3G}{2\pi R} \qquad \textbf{Eq. 6}$$

Moreover, the shear rate γ is determined through the ratio between the velocity of the cone Ωr and cone gap C:

$$\gamma = \frac{\Omega r}{C} = \frac{\Omega}{\psi} \qquad \textbf{Eq. 7}$$

The viscosity η obtained using a cone & plate viscometer is defined as the ratio between shear stress and shear rate:

$$\eta = \frac{\tau}{\gamma} = \frac{\frac{3G}{2\pi R}}{\frac{\Omega}{\psi}} \qquad \textbf{Eq. 8}$$

The above equation for determining the viscosity of a material under a cone & plate viscometer is heavily dependent on the both the torque felt by the spring as well as the rotation speed of the cone. In this viscometer, a cone CAP-05 ™ was used, having a radius $r = 0.953\ cm$, a cone angle $\psi = 0.0314$, and finally, a cone gap of $C = 0.0299\ cm$.

3.2.4 SEM of Nanocomposites

A Field Emission Scanning Electron Microscope (FE-SEM, LEO-Ultra, Gemini, Germany) was used in order to carry out a qualitative study on the morphology and degree of dispersion of graphene nanosheets within the nanocomposites produced. The samples were placed on a 90-degree stub to view the cross-section of the ECA.

3.2.5 Electrical Conductivity Measurement

The resulting composites that contained silver flakes were casted into a glass slide that had a square mold (7mm x 7mm x 0.5 mm) made of adhesive tape. A clean, flat copper sheet was placed on top of the paste in the mold to ensure a flat surface and consistent thickness. The sample was then inserted into the oven and pre-cured at 60°C for 30 minutes, and then cured at 150°C for two hours. Once the curing was complete, the copper sheet and adhesive tape were removed in order to determine the bulk resistivity of

the sample using a sheet-resistance four-point probe measurement setup. The configuration consists of the probe unit (Cascade Microtech Inc.) and the digital multimeter & function generator unit (Keithley 2440 5A SourceMeter®, Keithley Instruments Inc.). The sheet resistance readings acquired from this configuration can then be converted into bulk resistance readings using the following equation [17,52,92]:

$$\rho = Ft\frac{\pi}{\ln 2}\left(\frac{V}{I}\right) \qquad \textbf{Eq. 9}$$

The t in the above equation is the thickness of the sample, I is the applied current, and V is the voltage drop measured by the SourceMeter®. The F in equation 9 is a correction factor for samples that have a finite thickness that is defined by the ratio between the sample thickness t and probe spacing s (1 mm). The correction factor F can be approximated to 1 if $0.4 < \frac{t}{s} < 1$. The mold is 0.5 mm while the probe spacing is 1 mm, which leads to a ratio of 0.5: a value that allows F to be approximated to 1.

3.3 Results and Discussion

3.3.1 Viscosity behavior of composites

Six samples of varying compositions were measured for viscosity (summarized in Table 3-2) at room temperature and a shear rate of $33.3s^{-1}$ (or 10 RPM). We quantified the behavior and characteristics of the uncured composites in order to obtain a preliminary dataset that will assist us in figuring out where our composite stands.

Table 3-2: Viscosities for the different compositions at 10 RPM

Sample	Composition	Viscosity [cP]
1	Epoxy	11400
2	Epoxy + Silver flakes (60 wt%)	30660
3	Epoxy + Graphene (1 wt%)	49470
4	Epoxy + Graphene-SDS (1 wt%)	18263
5	Epoxy + Silver flakes + Graphene	Above 1000000
6	Epoxy + Silver flakes (60 wt%)+ Graphene-SDS (1 wt%)	160500

The addition of any form of fillers resulted in an increase in viscosity. If we compare the 60 wt% silver to the added 1% graphene, a very pronounced effect on the viscosity of the composite is observed, reflecting the fluffy nature of graphene nanosheets. Moreover, the fourth sample containing Gr(s) exhibits lower viscosities as opposed to the third containing Gr, indicating that SDS plays an important role in the viscosity behavior of the composite. The main function of SDS decoration is to improve the dispersion of graphene nanosheets with in the epoxy resin [18]. However, some studies have shown that the presence of an anionic surfactant molecule such as SDS can disrupt the inter-chain contact or entanglement of the hydrophobic polymer chains (in our case, Bisphenol A diglycidyl ether) causing a decrease in viscosity [139]. This decrease in viscosity can also be explained by considering that the surfactant (that self-assembles on the polymer and graphene) participates in an untying process that severs the connections between different polymer chains [140]. This means that the presence of SDS in our system may have not only prevented the aggregation of the graphene but also the entanglement of the epoxy polymer, thus leading to lower viscosities.

The effect of Gr/Gr(s) on the viscosities of the composites were systematically investigated by varying the amount of added Gr/Gr(s) and the shear rate, with a particular goal of observing the role of SDS decoration. Figure. 3-3 uses bar graphs to show the viscosities of epoxy with Gr (Figure 3-3a) and epoxy with Gr(s) (Figure 3-3b) nanocomposites as a function of increasing weight concentration at a constant 20 RPM (or a shear rate of 66.7 s^{-1}).

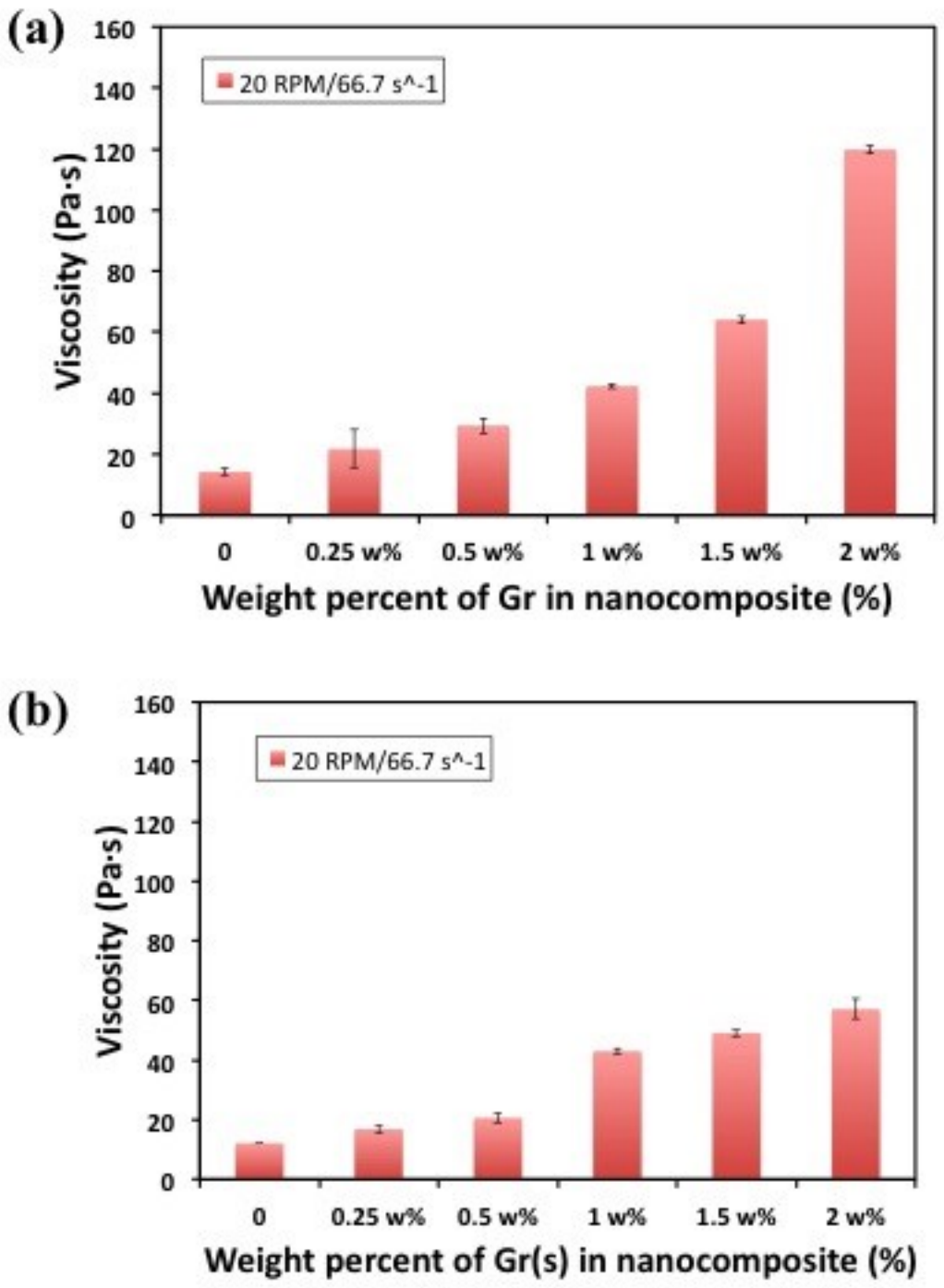

Figure 3-3: a) Viscosity as a function of weight loading of the pristine graphene (Gr) in epoxy resin at 20 RPM; b) viscosity as a function of weight loading of SDS-decorated graphene Gr(s) in epoxy resin at 20 RPM.

It is seen that the Gr(s) graphs show much lower values when compared to the Gr graphs. The maximum value in Gr(s) graphs is close to 60,000 cP whereas the maximum value of the Gr graphs is doubled, almost exceeding 120,000 cP. The dependence of viscosity on the weight concentration of pristine Gr is an exponential increase; this same trend was not seen for Gr(s).

Figure 3-4 and Figure 3-5 show plots of viscosity as a function of shear rate in log base 2, providing a different perspective on what happens to the viscosity of the system as the rotational speed of the cone & plate is increased, where Figure 3-4 is Gr and Fig 3-5 is Gr(s). It can be observed that the way shear rate affects the viscosity depends on the amount graphene added to epoxy.

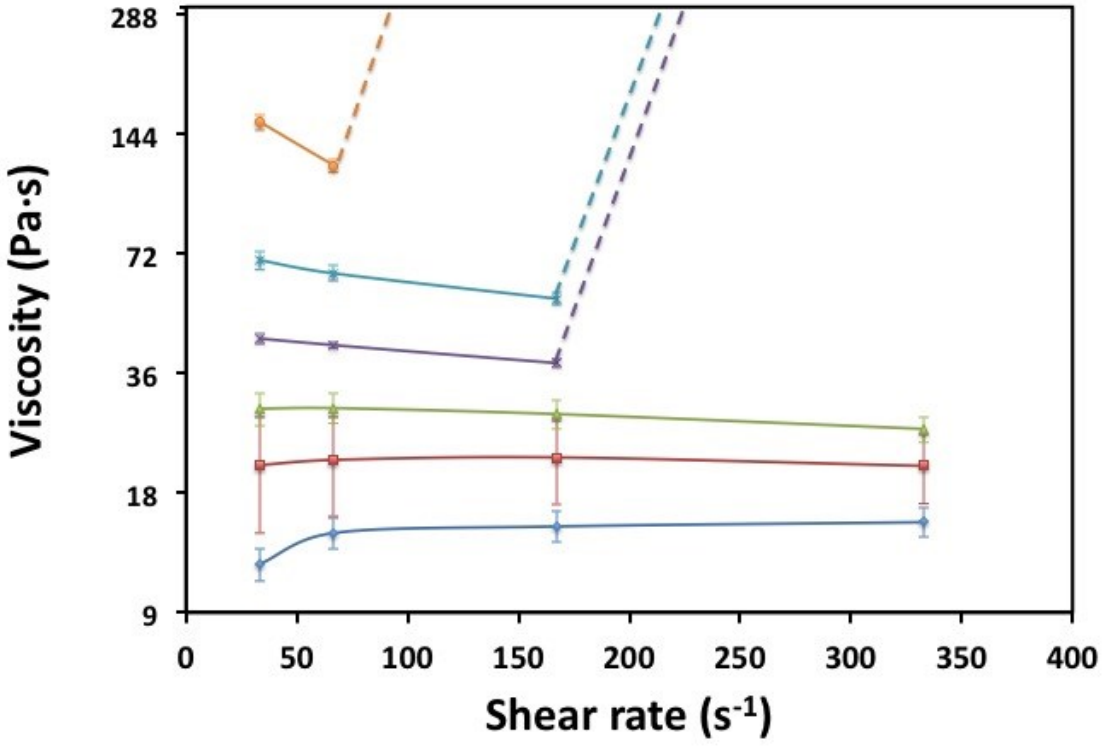

Figure 3-4: Viscosity in log scale as a function of Shear Rate of Gr and Epoxy where dotted lines indicate viscosity readings too high for the viscometer to display; Note: All values in graphs that contain error bars represent standard error.

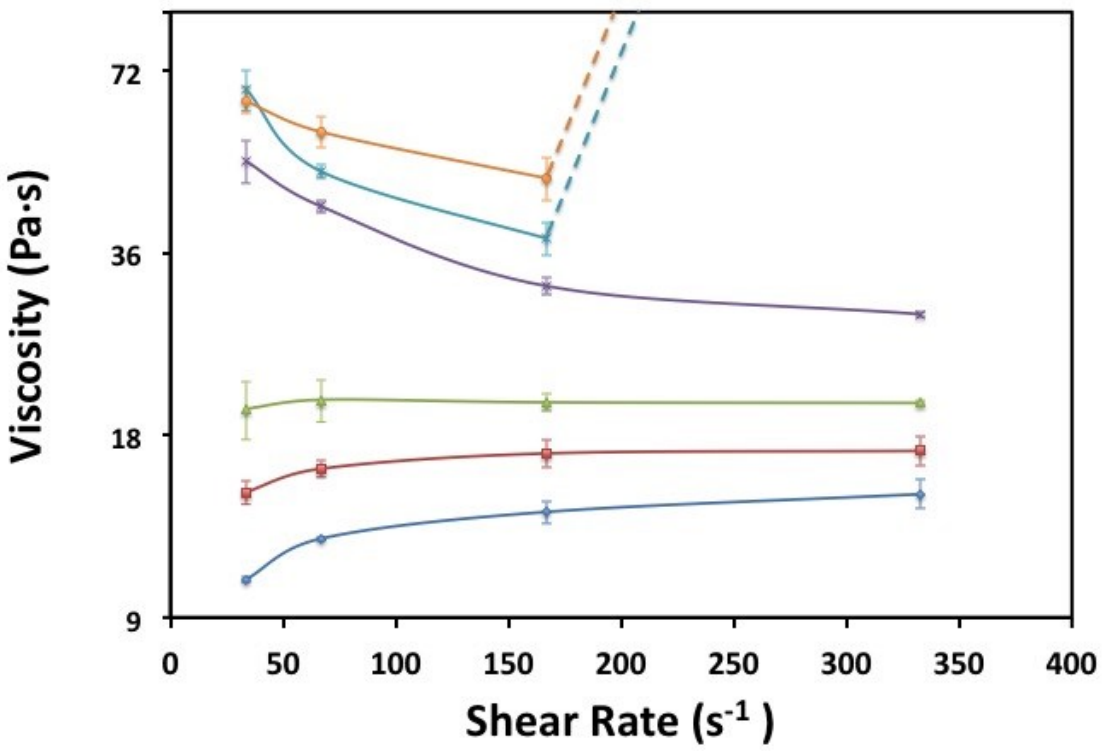

Figure 3-5: Viscosity in log scale as a function of Shear Rate of Gr(s) and Epoxy where dotted lines indicate viscosity readings too high for the viscometer to display; Note: All values in graphs that contain error bars represent standard error.

For the samples of lower wt% (0-0.5 wt%), the viscosity increased with the shear rate, following a known behavior where the non-aggregated solid particles show high viscosities at low shear rates, but then begin showing lower viscosities upon higher shear rates [141]. On the other hand, for the samples of higher wt% (1-2 wt%), the viscosity first decreased with the shear rate but exhibited spikes (i.e. sharp increase) that thus far appears after going past what appears to be a critical shear rate of 167 s^{-1}. The dotted lines indicate spikes in the viscosity that can no longer be measured by the cone and plate viscometer as the viscosity rapidly increased at those high shear rates. This type of spike was observed both in Figure 3-4 and Figure 3-5, occurring at higher shear rates for sample loadings of 1-2 wt%.

The effects of increasing shear rate on the viscosity of the nanocomposites system are further interpreted in terms of the concepts of shear thickening and shear-thinning. Shear

thickening is a behavior seen in fluids that experience a sharp increase in viscosity above a critical shear rate, where the fluid often transitions from a liquid-like dispersion into a solid-like material as a result of the particles forming clusters [142]. Conversely, fluids that behave in the opposite manner are known as shear-thinning fluids; for example, colloidal dispersions are typically shear-thinning fluids [143]. When this type of fluid is subjected to flow, the colloidal particles begin to form layers resulting in lower flow resistance as well as lower viscosity [142]. As shown in Fig. 4 and Fig. 5, the viscosity of the pure epoxy (D.E.R. 331 DGEBA) increases with the shear rate, behaving as a shear thickening liquid. Note that DGEBA can render either shear thickening or shear-thinning behavior depending on the supplier [144]. The viscosity of the epoxy nanocomposites with 0.25 and 0.5 wt % Gr and Gr(s) are almost constant with higher shear rate. An explanation for this shear-thickening behavior of the nanocomposites containing low loading of graphene (0 to 0.5 wt%) is that the composite is in a regime where the system is dominated by the molecular strands of the epoxy resin, which is similar to the one-dimensional particle arrangement discussed by D. Smith et al [145]. As a result of the viscometer applying force, the polymer strands become entangled and take a three-dimensional arrangement, resulting in higher viscosities [141] within the higher shear rate region. On the other hand, the behavior of the epoxy composite with higher loadings (1-2 wt%) of Gr and Gr(s) starts to show signs of shear-thinning, hinting the possibility that the addition of graphene nanosheets suppressed the shear thickening properties of the epoxy. It is well known that the presence of a layered structure (in our case, graphene) can suppress the onset of shear thickening, as it reduces the efficacy of the shear flow to create the hydrodynamic clusters [143]. Similar results indicating that shear-thinning of polymer-filled graphene at higher weight concentrations are found in D. Wu et al's work, where they reported that graphene at 1 wt% showed stronger shear-thinning behavior, and further reported that graphene nanosheets were responsible for the suppression of the shear flow of their polylactide polymer chains [146].

Figure 3-5 revealed a stronger shear-thinning behavior in Gr(s) when compared to Figure 3-4, which happens at higher loadings of the Gr: in particular, at the 1 wt %, suggesting the some influence resulting from the SDS molecules decorated on the graphene surface.

It was suspected that the SDS molecules formed additional intermolecular bonds between the graphene and epoxy [147], which resulted in the increase of viscosity at low shear rates. However, applied force at high shear rates break the bonds thus resulting in the shear-thinning behavior. Other than the 1 wt% Gr(s) curve, all other curves at higher loadings above 0.5 wt % in Figure 3-4 and 3-5 show an initial shear-thinning behavior, followed by a sharp increase in viscosity at higher shear rates. This phenomenon is similar to the typical Order-Disorder flow curve of stable suspensions of Brownian hard particles [142,148]. The Order-Disorder theory describes the sliding of particles over one another, forming layers during shearing; after exceeding a critical shear rate, the hydrodynamic forces would pull out the particles from their ordered layers to enter a different regime where the particles agglomerate with one another to form a disordered state resulting in a sharp increase in viscosity [142].

Overall, Figure 3-4 and 3-5 reveal that the addition of Gr(s) led to lower viscosities for the epoxy nanocomposites than the pristine graphene Gr. This finding has profound implications for the future applicability on these conductive composites as some printing techniques that already focus on dispensing conductive ink are concentrating on ways to improve their printing process (which involves the use of shear-thinning conductive inks) [149]. Furthermore, conductive adhesives used for surface mount assemblies are recommended to exhibit strong shear-thinning, highly stable yet low viscosities at high shear rates, and good recovery of the pastes after the process is complete [150]. This suggests that Gr(s) may be useful as a dilatant-suppressor when formulating ECAs that are dispensed through printing techniques.

On another note, it has been reported that negative effects (such as excess deposition or non-smooth flow across the stencil) are associated with conductive adhesives that do not fall within the desired viscosity ranges (recommending a range of 100,000 cP, although the conductive adhesive used in that work was 70,000 cP) [4]. It can be seen that sample 6 is reaching the range of the recommended viscosity and that the use of exfoliated graphene as a lubricant is indeed successful. Further work for optimization can give us the opportunity to reduce the viscosity to even lower, more acceptable levels, which is

especially relevant for other applications such as dispensing through printing technology [134].

3.3.2 Morphology and electrical conductivity of composites

The morphology and conductivity of the cured nanocomposites were characterized. The SEM images in Figure 3-6 show the morphologies of the epoxy and Gr/Gr(s) nanocomposites at different magnifications. Figure 3-6a and 3-6b compare the difference between low weight percent and high weight percent of Gr as seen in Figure 3-6c and 3-6d. It is seen that the increase of filler content changes the morphology from a smooth, flat surface to a flakier and mountainous appearance. As such, the higher weight percent Gr contains a morphology that is overall sharper and higher in surface area even when compared to Gr(s) at the same weight percent. Figure 3-6e is the SEM image of the nanocomposite with 2 wt% Gr(s), showing a similar morphologies to that of 2 wt % Gr, containing moderately hilly or mountainous terrain. The transparent-looking sheets at the edge of the flakes found in the high magnification zoom in Figure 3-6f indicate that the Gr(s) are better exfoliated.

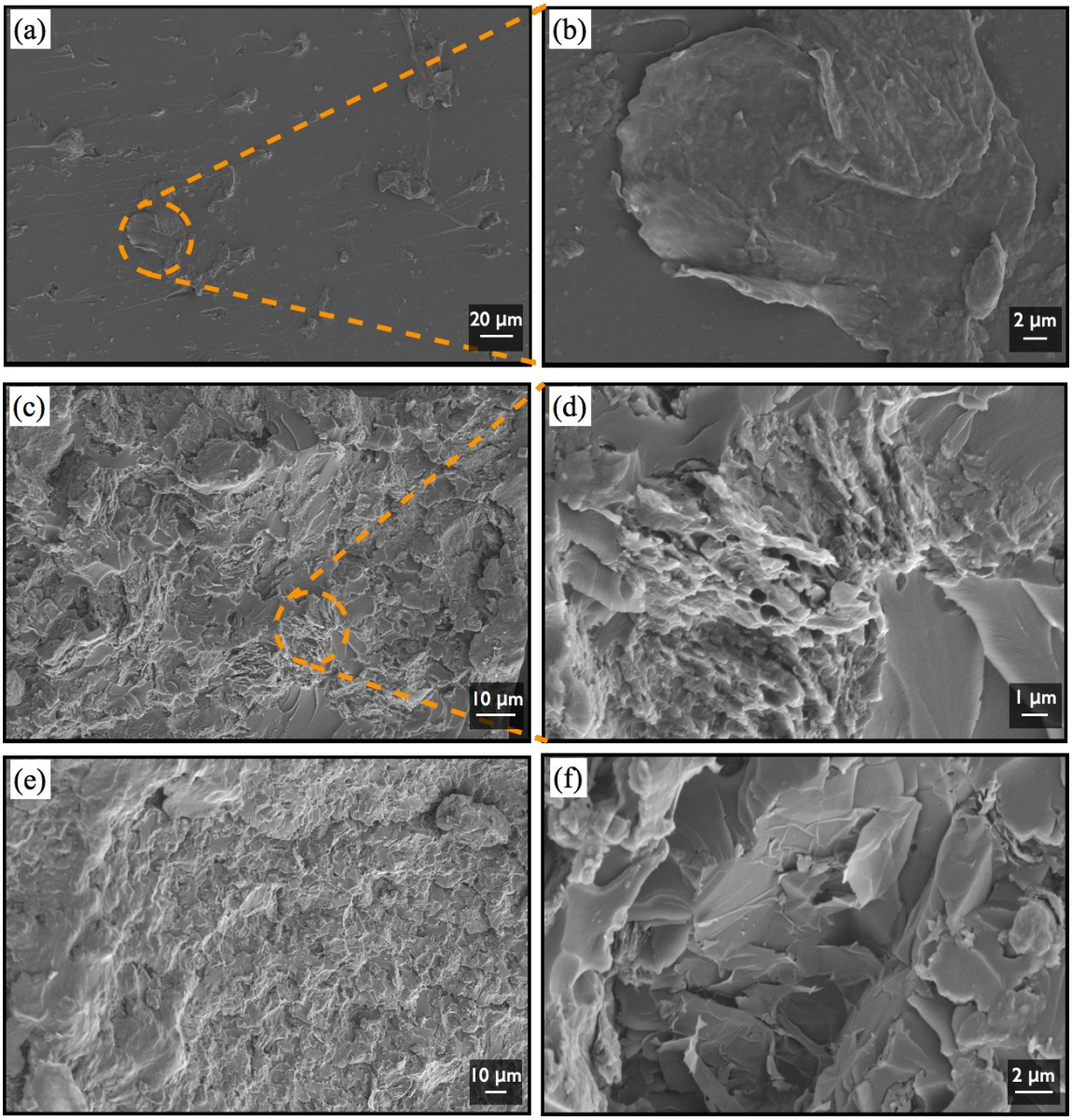

Figure 3-6: SEM images of the epoxy composites with 60% silver and Gr or Gr(s); a) Low zoom view of Graphene and epoxy [Gr] at 0.25 wt%; b) Highest zoom view of Gr 0.25 wt% on a large flake; c) Low zoom view of Gr 2 wt% showing a mountainous morphology; d) Highest zoom view of Gr 2 wt% taken of an area from 6c; e) Low zoom view of Gr(s) 2 wt% showing a similar morphology to 6c; f) Highest zoom view of Gr(s) 2 wt% showing smoother morphology likely as a result of the SDS decoration

The electrical conductivities for the synthesized hybrid ECAs were investigated using a four-point probe method. Figure 3-7 plots the electrical bulk resistivity of the ECAs as a function of the weight loading of two nanofillers Gr and Gr(s) added into the composites without the use of solvent (identified as solvent-free method and denoted by solid lines) in this work and with the assistance of ethanol solvent used in our previous work (identified as solvent-assisted and denoted by dashed lines) [18].

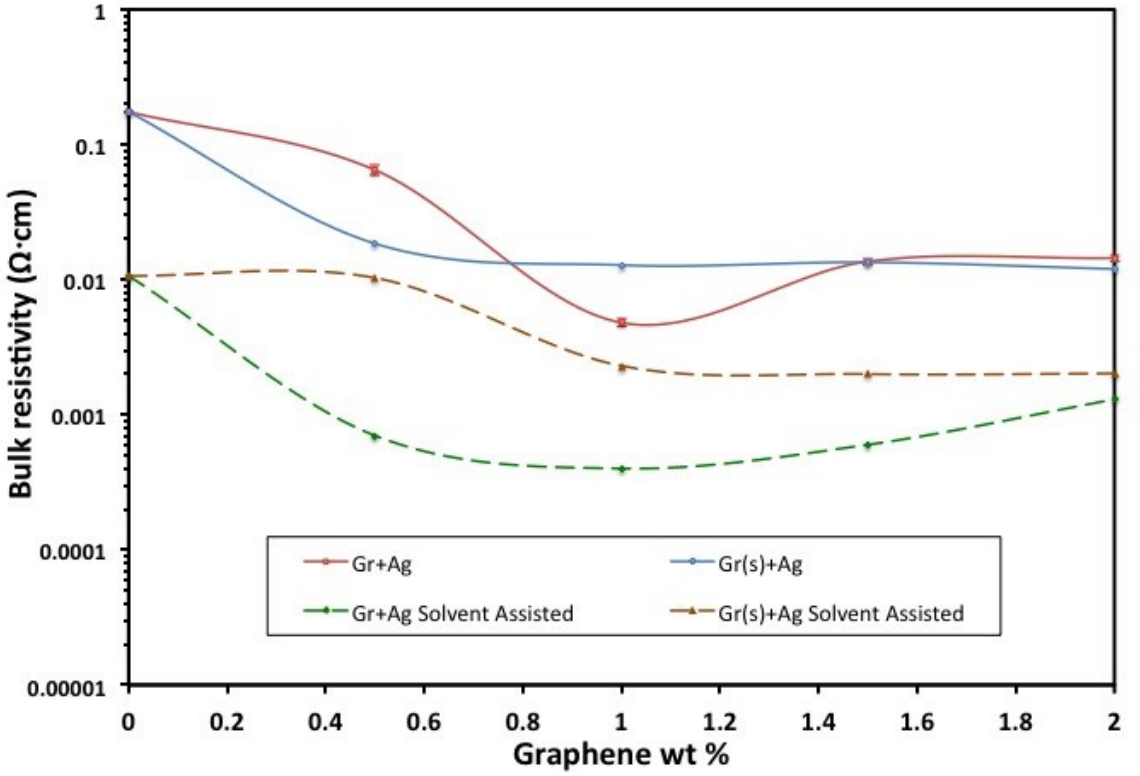

Figure 3-7: Bulk resistivity as a function of weight percent comparison graph between Gr and Gr(s). The solid lines denote (solvent-free) results from our work. The dotted lines show results from previous work that used ethanol to assist in the dispersion of filler content.

The electrical resistivity values of the ECAs filled with Gr(s) are in the same order of magnitude as those of the ECAs filled with Gr; in general, the resistivity decreased with the addition of graphene. This observation confirms the positive effect of adding graphene on improving the electrical conductivity when compared to conventional ECAs

and suggests that the SDS decoration of graphene has a negligible effect on the conductivity improvement. However, a slight increase in the resistivity between 1-1.5% wt Gr was noticed, perhaps because of the uneven dispersion of the Gr at higher concentrations. The bulk resistivity values for the solvent-free method are in the range of $1 \times 10^{-2}\ \Omega \cdot cm$, which is one magnitude higher compared to the solvent assisted method. This is reasonable considering the role of solvent was to improve the filler dispersion and deliver better conductivity. It is important to note that we see this solvent effect even for conventional ECAs that do not contain graphene nanofillers. Even though the solvent-free method may hold the advantage in the simplicity of the manufacturing process and the workability of the paste itself, the graphene-filled ECAs prepared in this work may be suitable for the applications where only moderate conductivity is needed. Further work is necessary to improve the electrical conductivity and as a result, broaden its potential applications.

3.4 Conclusions

We systematically investigated the rheological and electrical properties of graphene/silver-filled composites, and particularly focused on elucidating the effect of SDS decoration of graphene. Gr(s) exhibited lower viscosities when compared to Gr (with or without the presence of silver), revealing a positive effect of SDS on reducing the viscosity. Our findings also show that weight concentrations from both Gr and Gr(s) appeared to exhibit shear thickening from 0 to 0.5 wt% owing to the potential transition of the resin going from 2 dimensional to 3 dimensional conformation as well as the intrinsic properties of the epoxy chosen. However, above 0.5 wt%, it is suggested that due to the presence of a layered structure suppressing the shear thickening behavior of the system, the Gr and Gr(s) viscosities began exhibiting shear-thinning behavior. Both systems follow the order-to-disorder theory and curve at higher weight concentrations. Gr(s) has been shown to follow the typical curve for stable suspension of Brownian hard particles after a high enough concentration is present within the epoxy matrix. As a result, the presence of graphene in general has been shown to play a key role in the shear-thinning behavior of these composites. The compositions that use Gr(s) were shown to exhibit better workability, while also falling within the higher section of the

recommended viscosity range. Furthermore, this work revealed new rheological behavior upon the addition of surfactant SDS on graphene as the decoration of graphene is usually exploited to improve dispersion; however, in our case it has an added unique effect. It is clear that the multiple effects of surfactant should be considered in the development of ECAs: not simply for the improvement of filler dispersion, but also the suppression of dilatant behavior. Future work can incorporate this finding into the optimization of ECA fabrication processes, as well as any other endeavors that require a shift in rheological behavior.

Chapter 4 Residual Solvent and its Negative Effect on the Lap-Shear Strength of SDS-Decorated Graphene Hybrid ECAs

4.1 Introduction

Most ECA research today focuses on improving its electrical conductivity [6,17,18,47,151] instead of on its mechanical properties [36] because quantifiably predicting the performance and the strength of the bond is difficult and complex without using simulations and modelling software, since it must account for factors such as geometric complexity, inherent discontinuity signature between the adhesive and the surface it is being bonded to, or even the failure mechanisms happening in the microscopic level [119,120]. As a result, there are limited studies that evaluate the mechanical properties of ECAs [36]. This work is focused on using lap shear testing as a way to determine how well nine different formulations of conductive adhesives bond onto the FR-4 surface using the most common test standard: ASTM D1002 [121,122].

This work investigates the influence of residual solvent presence (within the composite) on the mechanical properties (and to a smaller degree, the electrical properties) of both hybrid and conventional ECAs compared to solvent-free formulations. Although the utilization of solvent is integral for properly dispersing the SDS modified graphene nanofiller [18,27] within the composite, the presence of solvent within the system was suspected to have a negative impact on the mechanical properties of the cured adhesive. This is especially true if the functional groups of the solvent unfavorably interact with either the polymer matrix or the surfactant in our case based on previous works that also attempted to disperse carbon-based nanofillers within a polymer matrix [76,135,152,153]. Our suspicion was further outlined in a previous work according to the TGA and DSC, which will be explained in a later section [18]. To follow up on these results, we will compare the solvent-assisted formulation results to the solvent-free formulation and in the end, shed light on whether or not residual solvent indeed has a negative impact on the curing mechanics as it will become evident in the mechanical properties of the ECA. Moreover, we will confirm that solvent presence has negative effects on the mechanical

properties of the system; we will then take a closer look to identify any potential factors that could directly impact the mechanical strength so as to gain a better understanding on what is happening to the post-cured material. This work also plans to identify an optimal composition that possesses both high shear strength and electrical conductivity for further investigation and future work that can be further tested in practical settings.

4.2 Experimental

4.2.1 Materials

The polymer matrix used in this study was the liquid epoxy resin (D.E.R 331™) Diglycidyl Ether Bisphenol-A (DGEBA) and amine-based curing agent triethylenetetraamine (TETA). Both were purchased and used as received from DOW Chemical Company (USA). Silver flakes (~10 μm) purchased from Sigma Aldrich were used as received, and acted as the conductive filler for the composite. Graphene nanosheets with a size range of 0.5 to 5 μm were purchased from ACS Materials (USA) and were used as received [18,27]. The surfactant Sodium dodecyl Sulfate (SDS) was purchased and used as received from Sigma Aldrich and was responsible for exfoliating the graphene nanosheets. HPLC ethanol solvent at 99.8% purity was purchased and used as received from Fisher Scientific (USA).

4.2.2 ECA Preparation

The process for preparing the composites required the following steps: (a) adding the appropriate amounts of epoxy resin and silver flakes according to the desired composition as denoted in Table 4-1; (b) adding SDS modified graphene that was prepared by suspending SDS and graphene in ultra pure water, using an ultra sonic bath to allow the surfactant so self-assemble onto the graphene sheets, and finally extraction by centrifugation and evaporation of any remaining supernatant [27]; (c) steps exclusively for solvent-assisted formulations include taking the mixture and adding 250 mL HPLC ethanol, running the mixture through a planetary shear mixer (PSM), and then doing a combination of vortex mixing and desiccation [18,27]; (d) adding curing agent, mixing the composite via PSM to form the ECA paste [18,27] and then applying the paste onto

the appropriate test coupons (i.e. FR-4/electrical/microscopy). A schematic in Figure 4-1 illustrates the above method.

Table 4-1: List of the combinations of compositions used for nanocomposites

Composition	Ag flakes [wt %]	Gr(s) [wt %]
Epoxy + Silver	20, 40, 60	0
Epoxy + Silver + solvent	20, 40, 60	0
Epoxy + Silver + Graphene-SDS	20, 40, 60	0.75, 1.5
Epoxy + Silver + Graphene-SDS + solvent	20, 40, 60	0.75, 1.5

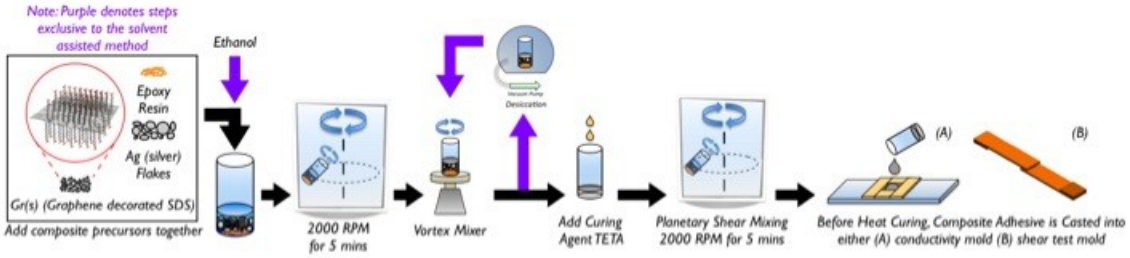

Figure 4-1: Schematic illustration of how the ECAs were mixed and prepared for testing

4.2.3 Lap Shear Test

The Universal Material Tester (UMT) Tribological Test Equipment (CETR Campbell), equipped with a pair of tensile wedge grips (G1061-2, Mark-10 Corp) was used to evaluate the lap shear strength (LSS) of varying ECA compositions. Test coupons (1/16" double-sided FR-4 boards, 590-540) were purchased and used as received from MG Chemicals. The specifications of the FR-4 boards were machined to follow the dimensions presented in Figure 4-2. The test procedure and calculations followed ASTM D1002 [123] with the exception of reducing the contact area of the joint to 12.7 mm x 12.7 mm in order to accommodate the limitations of the load cell used in the experiment.

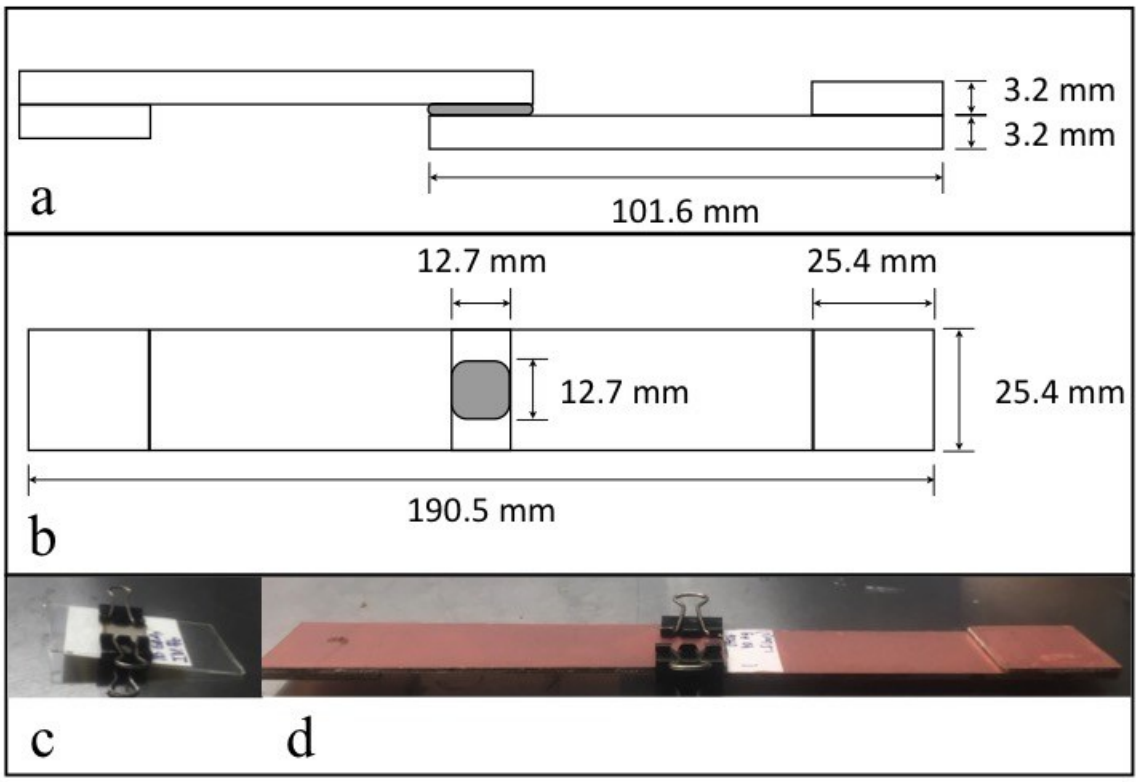

Figure 4-2: a) Schematic cross-section illustration of ASTM D1002 test coupon and its modified paste measurements; b) schematic top view illustration of ASTM D1002 test coupon and its modified paste measurements; c) example of test sample used for optical microscopy and optical profiling; d) example of test sample used for ASTM D1002 lap shear testing

4.2.4 Electrical Conductivity Test

A four-point probe fixture (Cascade Microtech Inc.) that is connected to a micro-ohm meter (Keithley 2440 5A Source Meter, Keithley Instruments Inc.) was used to measure the electrical sheet-resistance values of varying ECA compositions. These values were then converted to bulk resistance using the following equations [18,52]:

$$\rho = R_s \cdot t = Ft \frac{\pi}{\ln 2} \left(\frac{V}{I}\right) \qquad \textbf{Eq. 10}$$

The sheet resistance (R_s) obtained from the reading was used together with the caliper-measured ECA thickness (t). The (V) and (I) represent the applied current and measured voltage drop across the probe pins, from which the sheet-resistance is based upon. The correction factor (F) is ratio between the thickness of the ECA sample (t) and the probe gap (s) [18,52]. Under the condition where $0.4 < \frac{t}{s} < 1$, it is safe to approximate the correction factor (F) to equal 1 [18,52]. As the probe gap is 1 mm wide, the ECAs prepared were designed to have an average thickness of 0.5 to 0.7 mm, resulting in the fulfillment of the above stated condition.

4.2.5 Optical Microscopy and Optical Profiler

The cross sections of two ECA formulations were observed under manual operation using an inverted optical microscope (Carl Zeiss Axio Observer Z1m; Magnification 5x and 50x) equipped with a CCD camera (Axio Cam).

An optical profiler (MFP-D WLI 3D Surface Profilometer, RTEC Instruments USA) was used to observe the degree of flatness exhibited by the solvent-assisted and solvent-free ECAs as well as to generate a 3D plot to further illustrate the presence of bubbles as well as any other defects that are not easily detectable by optical imaging.

4.2.6 Scanning Electron Microscopy

A Field Emission Scanning Electron Microscope (FE-SEM, LEO-Ultra, Gemini, Germany) was used in order to investigate the morphology and find potential defects or bubbles associated with the solvent-assisted method compared to the solvent-free method of preparing the ECAs. ECA pastes were prepared and casted into a glass mold and thermally resistant tape onto a ½" x ½" area with a thin sheet of copper as a cover. The glass slide was then sliced and bent (at the middle of the copper sheet) in order to obtain a flattened cross-sectional sample of the ECA. The samples were placed on a 90-degree stub to view the cross-section of the ECA.

4.3 Results and Discussion

In order to conduct an investigation of how hybrid ECAs would behave as we change two different filler concentrations (in this case, silver flakes and SDS-modified graphene flakes), we created a two-variable system with our response curve being LSS (in MPa). Moreover, this two-variable system was completed for two processes for a comparison study: the solvent-free method as seen in Figure 4-3 and the solvent-assisted method as seen in Figure 4-4. A general comparison of the entire system in a 3D bar graph format can be seen in Figure 4-5a and 4-5b to give the reader an easy way to follow comparison between the solvent-free and solvent-assisted values.

4.3.1 Solvent-free method

The LSS values investigated for the solvent-free method are intended to be both the reference and primary baseline map as to which formulations benefit or suffer as the weight concentrations of two fillers Ag and Gr(s) are increased. Figure 4-3a illustrates the evolution of LSS as we increase the Gr(s) concentration whereas Figure 4-3b illustrates the evolution of LSS as we increase the Ag concentration. The influence that each filler exhibits on the composite as the weight concentrations will be explained in further detail below.

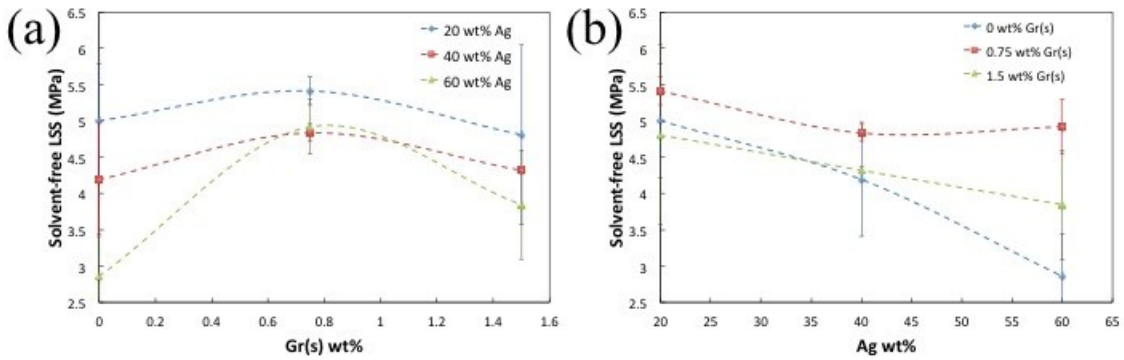

Figure 4-3: a) Solvent-free LSS as Gr(s) is increased; b) Solvent-free LSS as Ag is increased

4.3.2 The effect of Gr(s) on LSS of ECA without Solvent

In order to understand how increasing the Gr(s) content affects the LSS of the composite, Figure 4-3a was examined. For a constant Ag wt%, a parabolic trend can be seen where the LSS of the material is at its highest for a weight loading of 0.75 wt% Gr(s), and lower for both 0 wt% and 1.5 wt% Gr(s) (which applies for all three weight concentrations of Ag) in similar fashion to CNTs as demonstrated by H.P. Wu et al's work for aluminum substrate [20]. Furthermore, it is observed that 0.75 wt% Gr(s) has the smallest deviation among all of the formulations, hinting that Gr(s) has excellent potential to ensure that ECA is reliable on top of being mechanically robust. We suspect that the following reasons for the parabolic trend:

- Gr(s) is successfully increasing the strength of the composite, however, after a critical concentration, it begins to aggregate and act as a detriment to the system (possibly promotes bubble formation or something equivalent, creating defect sites, which will be examined further in this work)
- Gr(s) is unfavorably interacting with the epoxy curing process at higher weight concentrations (in particular the increase of SDS in the system) [18], and as a result is overtaking its potential to reinforce the composite
- A Combination of both

More experimentation where the Gr(s) is varied in smaller step sizes is recommended so as to generate a more comprehensive surface response plot and further verify this trend, giving better justification to the provided explanations above. Overall, by looking at Figure 4-3a and 4-3b, it is evident that the strongest formulations are those that contain 0.75 wt% Gr(s); among these, 0.75 wt% Gr(s) with 60 wt% Ag will be further tested for electrical conductivity and by microscopy techniques for a view of its morphology. The reason why the highest LSS value in the solvent-free process (20 wt% Ag and 0.75 wt% Gr(s)) was not chosen for further testing is because formulations with low silver content (20 wt%) express little to no electrical conductivity, thereby eliminating its potential to be used as a functioning ECA.

4.3.3 The effect of Ag on LSS of ECA with solvent

In order to understand how increasing the Ag content affects the LSS of the composite, Figure 4-3b was examined. It is evident that as the Ag wt% is increased for a constant

Gr(s) wt%, the LSS of the composite decreases. Formulations that contain 0.75 wt% Gr(s) display smallest decline while the sharpest decline is observed for formulations that do not contain Gr(s). It is also interesting to note that the LSS deviation from our results are consistently large for the formulations that only contain Ag, hinting that on its own, Ag is more of a detriment to the composite's LSS either through increasing unreliability (large error bars) or through the fact that higher weight concentration in hopes of attaining better electrical performance of the composite results in the compromising of its mechanical strength, similar to work reported by Wu et al [20]. The author suspects that the reason for this behavior is because the Ag flakes have an effect where the increase of the silver filler content in epoxy means the decrease of epoxy's shear strength since more of the composite is comprised of the filler rather than the actual binding component [20]. Furthermore, unlike Gr(s), Ag does not show any signs of composite reinforcement. It has been known that excess Ag content in conventional ECAs leads to issues such as higher material costs, little to no electrical conductivity improvement past the percolation threshold, and issues with environmental reliability [7,8,19,20,154]. However, this work also shows there is a detrimental effect to the LSS of the composite when using an excess amount of Ag filler content, which supports the need to reduce the amount of Ag in conventional ECAs.

When comparing the two filler materials, it has been shown that Gr(s) has the potential to act as a reinforcing agent upon a critical concentration. Moreover, there is little variance between samples resulting in a mechanically reliable and robust ECA. On the other hand, it has been shown that excess addition of Ag into the composite is detrimental to its mechanical strength and should be avoided to prevent introducing weakness into the composite, and also to reduce cost and to avoid issues with environmental reliability at the same time.

4.3.4 The effect of Ag on LSS of ECA with solvent

The LSS values investigated for the solvent-assisted method are intended to follow up initial suspicions from other references that hinted potential repercussions involved with the presence of residual solvent in the ECA composite, in particular, on its mechanical

properties [18,76]. Experimental results in Figure 4-4a when compared to Figure 4-3a illustrate a significant drop in LSS: in particular for the formulations containing Gr(s).

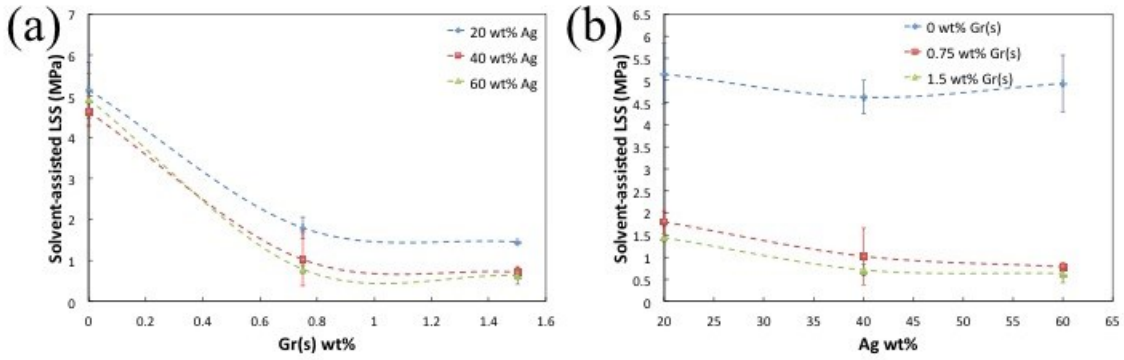

Figure 4-4: a) Solvent-assisted LSS as Gr(s) is increased; b) Solvent-assisted LSS as Ag is increased

According to our previous work, three findings were stated that would help elucidate the results seen in Figure 4-4: (a) it is known and accepted that silver flakes have no significant effect on the curing of epoxy [155]; (b) the presence of trace ethanol in the composite reduced both the ΔH_{Tot} and $T_{g\infty}$ indicating a drop in epoxy's crosslinking density [18]; (c) the DSC data experienced a sudden increase to ΔH_{norm} for ethanol-diluted epoxy VS neat epoxy, and again for the hybrid ECA containing graphene VS the hybrid ECA containing SDS decorated graphene [18].

The results from Amoli et al's thermal test indicate that despite the lack of change in $T_{g\infty}$, the change in ΔH_{norm} and ΔH_{Tot} point to an unknown mechanism that is caused by the presence of SDS [18]. Moreover, it has been suspected that SDS and ethanol are interacting with each other resulting in the changes in thermal data and inevitably, the crosslinking density of the final product.

From the above statements, we can firstly rule out any effect that Ag flakes have on the solvent-assisted system [155], which explains why the samples that had 0 wt% Gr(s) exhibited very similar LSS results to the solvent-free system. Note that the outlier for 60 wt% Ag in Figure 4-3b was noticed but not further investigated because: a) the standard deviation is large enough that if more tests were done, the option that it is in the lower

bounds exists; b) further investigation of this incident will go beyond the scope of what this work is investigating. Secondly, we can confirm that the presence of residual ethanol alone in the system is in fact not enough to disrupt the curing mechanism of the ECA. According to the data, it appears that both SDS and residual ethanol are required to generate the competing mechanism that is responsible for the drop in crosslinking density, as residual ethanol was not enough to cause a significant drop in LSS for the formulations that did not contain Gr(s). Thirdly, the formulations that did contain Gr(s) were shown to experience a drop in LSS, and as such, at the very least, these results support the initial suspicion of a drop in crosslinking density (a factor that is heavily related to the mechanical strength of the bulk material) for the solvent-assisted Gr(s) containing formulations. Although the mechanism itself was not discovered, findings in this work prove that the initial suspicions outlined in previous work coincides with what is happening in the composite system, as the presence of solvent and surfactant negatively impacts one of the mechanical properties of the cured adhesive. Further work using thermal characterization techniques is recommended to verify that the interaction of solvent with surfactant negatively affects the crosslinking density. Figure 4-5 is shown below to illustrate a summary of what was found in this study.

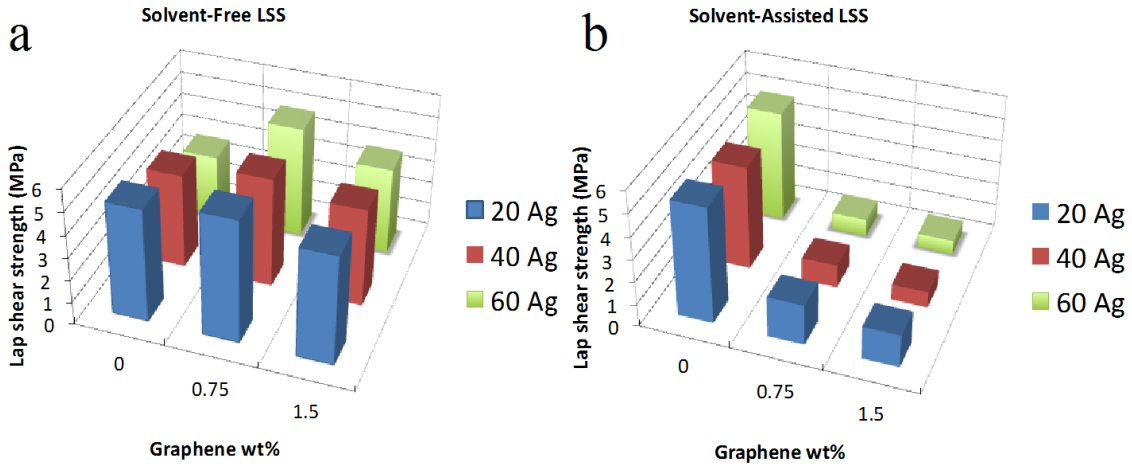

Figure 4-5: a) Solvent-free LSS in 3D format; b) Solvent-assisted LSS in 3D format

4.3.5 Electrical conductivity

Although the intention of this work is not to optimize or improve the electrical conductivity of the conductive adhesive, it is still important to choose an adhesive that not only exhibits excellent LSS, but also possesses sufficient electrical conductivity to ensure that the composite continues to perform as a conductive adhesive. As such, the formulations that exhibit the strongest LSS: 20 wt% Ag/0.75 wt% Gr(s), 20 wt% Ag/0 wt% Gr(s), 40 wt% Ag/0.75 wt% Gr(s) and 60 wt% Ag/0.75 wt% Gr(s) were measured for bulk resistivity. The first two samples exhibited no electrical conductivity despite the highest LSS values and as a result, will not be further tested or looked into within this work. However, the next two formulations exhibited bulk resistivity values ranging from $2.5 \times 10^{-1}\ \Omega \cdot cm\ to\ 1 \times 10^{-2}\ \Omega \cdot cm$ and is presented below in Figure 4-6 (where a current of 1 mA was used for all of the values measured).

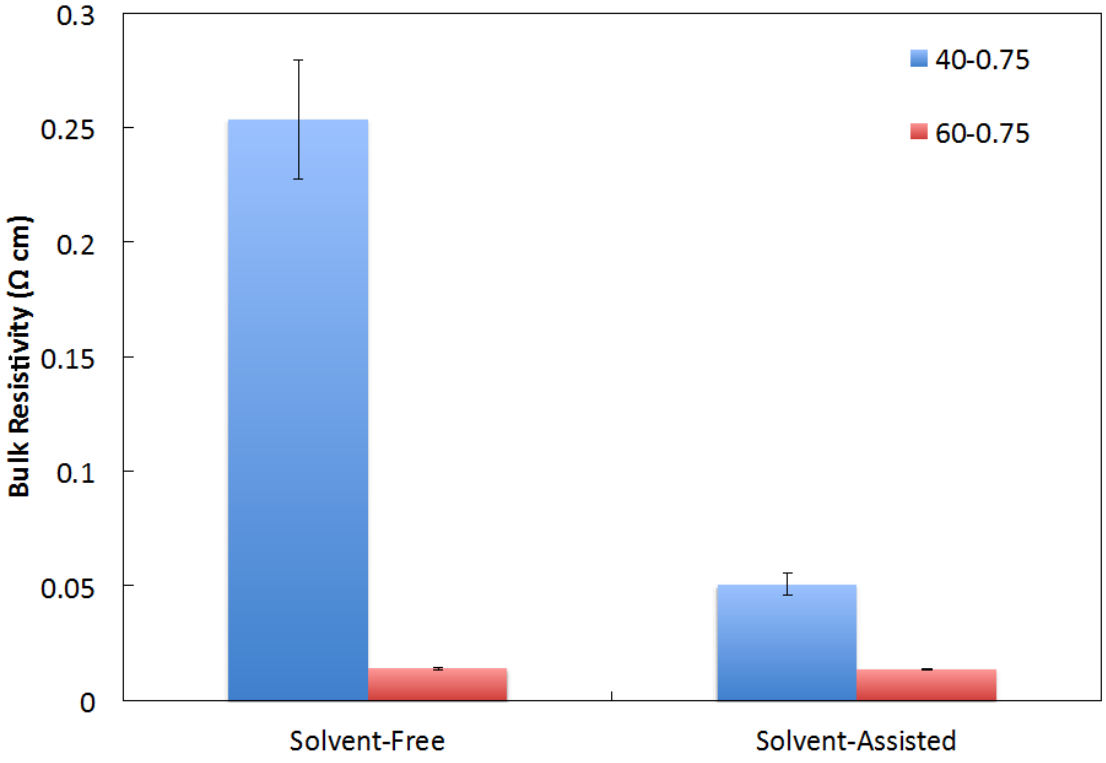

Figure 4-6: Bulk resistivity comparison of solvent-assisted and solvent-free 40 wt% Ag/0.75 wt% Gr(s) and 60 wt% Ag/0.75 wt% Gr(s) formulations

It can be seen that the presence of solvent matters for the 40 wt% Ag/0.75 wt% Gr(s) formulation as the solvent-assisted method is observed to have bulk resistivity that is 18x smaller than the solvent-free method. However, similar results were not observed for the

60 wt% Ag/0.75 wt% formulation as the two samples regardless of solvent presence exhibit roughly the same bulk resistivity values of $1 \times 10^{-2}\ \Omega \cdot cm$. As such, a difference exists, further values are required to gain a thorough understanding of the solvent effect on conductivity. Instead, it is better allocated for future work, as it is not within the scope of this work to further elucidate the details of the differences between bulk resistivity values.

It should be noted that the electrical conductivity values are congruent with Trinidad et al's findings [27]. However, when it came to Amoli et al's findings using their own solvent-assisted method, the electrical conductivities found in this work were lower by a factor of 10 [18]. This was to be expected due to the different process that Trinidad et al's work utilized, where SDS decoration of graphene was conducted independently from the composite itself and the PSM was applied over regular vortex mixer (which is known for better dispersion efficiency) [27]. As such, it is expected that the pre-treated Gr(s) would benefit less from the presence of ethanol when compared to Amoli et al's process that fully utilized the solvent, achieving higher success with the mixing process at obtaining well dispersed and decorated graphene.

This study verified that the chosen solvent-free composites exhibited conductivity values acceptable for electrically conductive adhesives, while also showing high LSS values. These findings conclude that 60 wt% Ag/0.75 wt% formulation is the optimal formulation for high LSS and high conductivity while retaining a relatively simple preparation method when compared to the solvent-assisted approach.

4.3.6 Optical microscopy and profiler

Another factor that is suspected to contribute to the decrease of the mechanical strength of the solvent-assisted mechanism is the formation of bubbles during the curing process. The presence of bubbles will inevitably decrease the smoothness of the paste as well as the contact area between the adhesive and substrate. If the paste is not smooth on the microscopic level, the actual contact area of the adhesive is reduced, leading to the adhesive failing at lower applied forces.

In order to verify this, we assumed that bubbles would form in the paste regardless of the type of surface it is embedded to; as such, other factors besides substrate choice are kept constant (for example, applied pressure and curing time/temperature). We chose to use glass as the alternate substrate for its transparency so that optical microscopy and optical profilometry techniques could be used to inspect the surface of both the solvent-free and solvent-assisted method. The goal was to search for any evidence of bubbling at the interface or cross-section of the paste. Optical microscopy is used to qualitatively check for pits, dimples or other forms of discontinuity when adhering to the surface of the glass, while the optical profiler is used to generate a 3D plot to show any possible changes in flatness as well as obtain a quantitative measure of the sample's surface roughness.

4.3.7 Optical microscopy results

The first method used to characterize the surface between the substrate and paste is the optical microscope. Both solvent-free and solvent-assisted 40 wt% Ag/0.75 wt% Gr(s) and 60 wt% Ag/0.75 wt% Gr(s) formulations were observed at 5x and 50x magnifications. Figure 7-7 is for 40 wt% Ag/0.75 wt% Gr(s), where 7-7a and 7-7b is solvent-free and solvent-assisted at low magnification, and 7-7c and 7-7d is solvent-free and solvent-assisted at high magnification.

Figure 4-7: a) Optical microscopy image of 40 wt% Ag/0.75 wt% Gr(s) at low power for solvent-free formulation; b) low power for solvent-assisted formulation; c) high power for solvent-free formulation; d) high power for solvent-assisted formulation

A similar pattern is followed for the next formulation as Figure 4-8 is for 60 wt% Ag/0.75 wt% Gr(s), where 4-8a and 4-8b is solvent-free and solvent-assisted at low magnification, and 4-8c and 4-8d is solvent-free and solvent-assisted at high magnification.

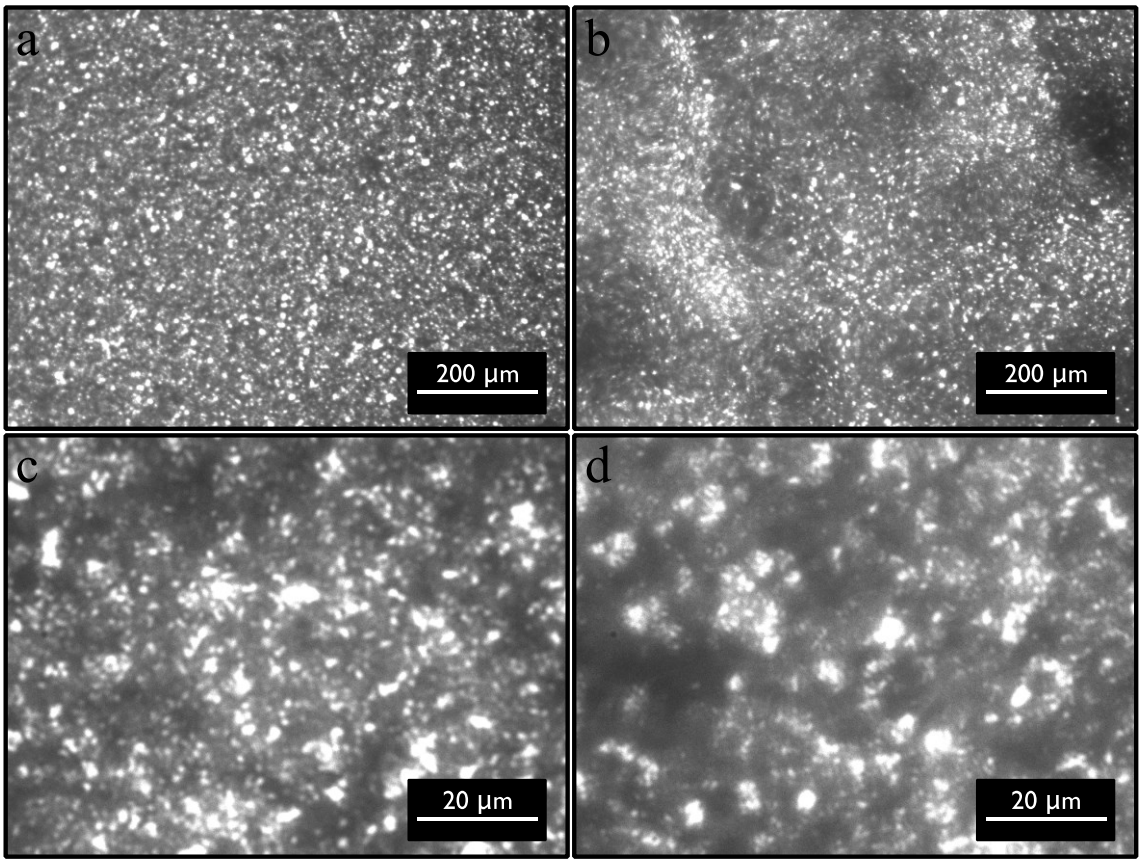

Figure 4-8: a) Optical microscopy image of 60 wt% Ag/0.75 wt% Gr(s) at low power for solvent-free formulation; b) low power for solvent-assisted formulation; c) high power for solvent-free formulation; d) high power for solvent-assisted formulation

Based on the optical microscope images at low magnification for 40 wt% Ag/0.75 wt% Gr(s), Figure 4-7a shows a smooth speckled pattern (indicating a smooth surface) as opposed to its solvent-assisted counterpart Figure 4-7b, which shows many light-colored lines and grooves, as well as what appears to be rough patches resulting in lower contact with the glass substrate. Under higher magnification, it is seen that the solvent-free formulation in Figure 4-7c contains less of the light-speckled patterns as opposed to Figure 4-7d, hinting that there are more pits and holes in the solvent-assisted formulation compared to the solvent-free formulation, which agrees with the findings from the lower magnification images that the solvent is causing pitting and contact area reduction between the substrate and the paste.

The next formulation observed with the optical microscope is 60 wt% Ag/0.75 wt% Gr(s) at low magnification. Figure 4-8a shows a speckled pattern that is similar to Figure 4-7a except that it is not as smooth, contains larger light speckles and overall higher particle density, likely due to the increase in Ag wt%. Figure 4-8b shows smaller light speckles but in more clumps, indicating that some form of aggregation may be occurring or that certain spots have more adhesion to the substrate than others. However, this still hints that the solvent-assisted formulations have smaller contact area to the substrate compared to the solvent-free formulations. This is again evident in the higher magnification in Figure 4-8c and 4-8d as there are more clumps visible for the solvent-assisted formulations.

These qualitative findings support the idea that the solvent-assisted formulations are indeed forming more bubbles post-cure as opposed to the solvent-free formulations, because the solvent-free formulations tend to exhibit better smoothness and uniformity, resulting in higher contact area between the paste and substrate and thus leading to higher LSS. However, a more quantitative approach will be presented below in order to verify and further support these observations.

4.3.8 Optical microscopy results

In order to quantitatively determine the roughness of the surface between the paste and substrate, an optical profiler was used to find any pits and dimples that were suspected to form bubbles during the curing procedure. Similar to the optical microscope, both solvent-free and solvent-assisted 40 wt% Ag/0.75 wt% Gr(s) and 60 wt% Ag/0.75 wt% Gr(s) formulations were observed at a magnification of 10x. Figure 4-9a and 4-9b show the optical profile of the solvent-free paste surface and the 3D render of the surface, respectively. Figure 4-9c and 4-9d show the optical profile of the solvent-assisted paste surface and the 3D render of the surface, respectively.

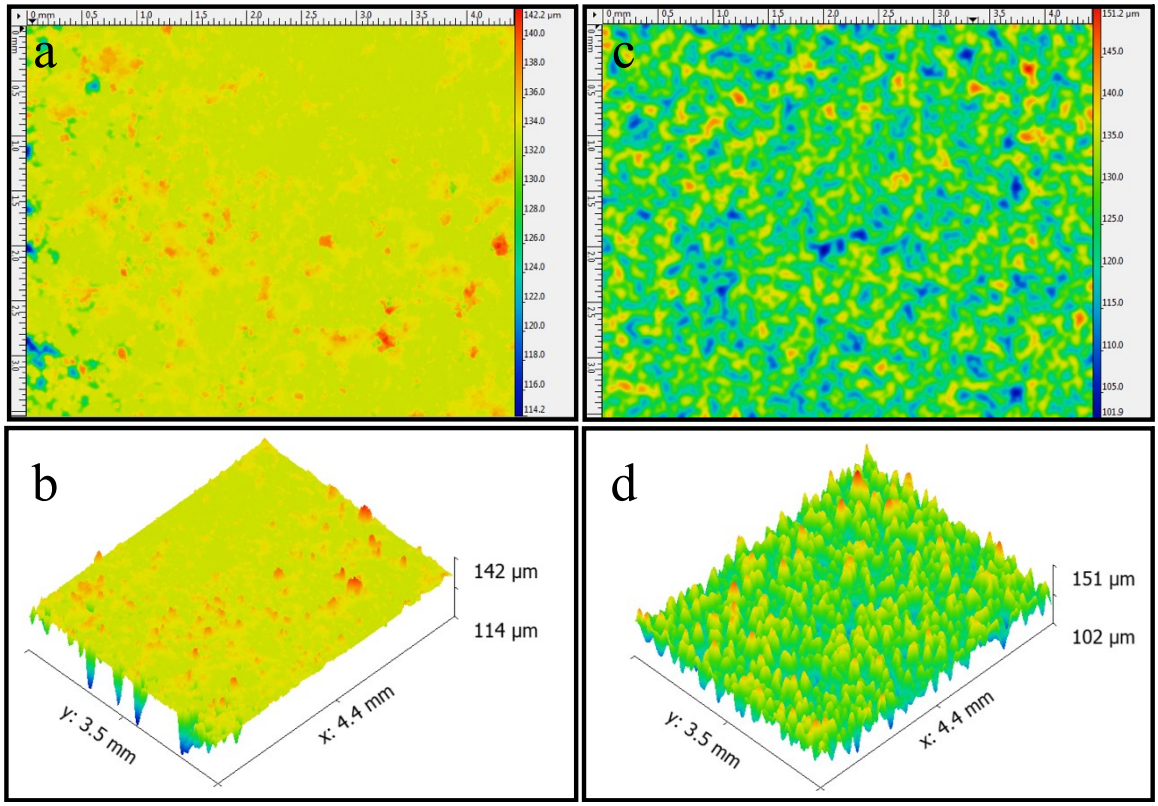

Figure 4-9: a) 40 wt% Ag/0.75 wt% Gr(s) 2D surface profile of solvent-free formulation; b) 3D surface profile of solvent-free formulation; c) 2D surface profile of solvent-assisted formulation; d) 3D surface profile of solvent-assisted formulation

The surface roughness values are presented below in Table 2. After comparing the solvent-free and solvent-assisted surfaces for the 40 Ag – 0.75 Gr(s) composites, it was found that the solvent-assisted formulations exhibited both lower average roughness (Ra) as well as root-mean square roughness (Rms) when compared to the solvent-assisted formulations for each corresponding formulation counterparts. It is important to note that larger dimples and pits are observed for the solvent-assisted 40 Ag – 0.75 Gr(s) when compared to the solvent-assisted 60 Ag – 0.75 Gr(s) which skews the surface roughness to a higher Ra value. One explanation for this occurrence is that the lower Ag content prevents resistance to larger bubble formation; however, more investigation is needed to verify this phenomenon.

Table 4-2: Summary of surface roughness values from optical profiler

Formulation	Ra (µm)	Rms (µm)
40 Ag – 0.75 Gr(s) solvent-free	0.59	1.27
40 Ag – 0.75 Gr(s) solvent-assisted	5.27	6.48
60 Ag – 0.75 Gr(s) solvent-free	3.68	4.52
60 Ag – 0.75 Gr(s) solvent-assisted	3.77	4.65

Moreover, the same can be observed with the 60 Ag – 0.75 Gr(s) composites as seen below in Figure 4-10a and 4-10b for the solvent-free optical surface profile and 3D render respectively, and correspondingly Figure 4-10c and 4-10d for the solvent-assisted formulation. This finding leads to the conclusion that overall, the solvent-free formulations have smoother surfaces that contain less pits and dimples when compared to the solvent-assisted formula. This conclusion can be seen visually through the surface diagrams of 40 Ag – 0.75 Gr(s) composites in Figure 4-9a and 4-9c where Fig 4-9a contains little to no blue areas – blue regions correspond to pits and dimples found on the surface of the paste that are not in contact with the glass substrate while Figure 4-9c in comparison contains many. The same can be said for 60 Ag – 0.75 Gr(s) composites in Figure 4-10a and 4-10c where Figure 4-10a contains fewer blue areas in comparison to Figure 4-10c further supporting the idea that bubble forming during curing is decreasing the contact area between the paste and substrate and as a result, exhibiting weaker LSS.

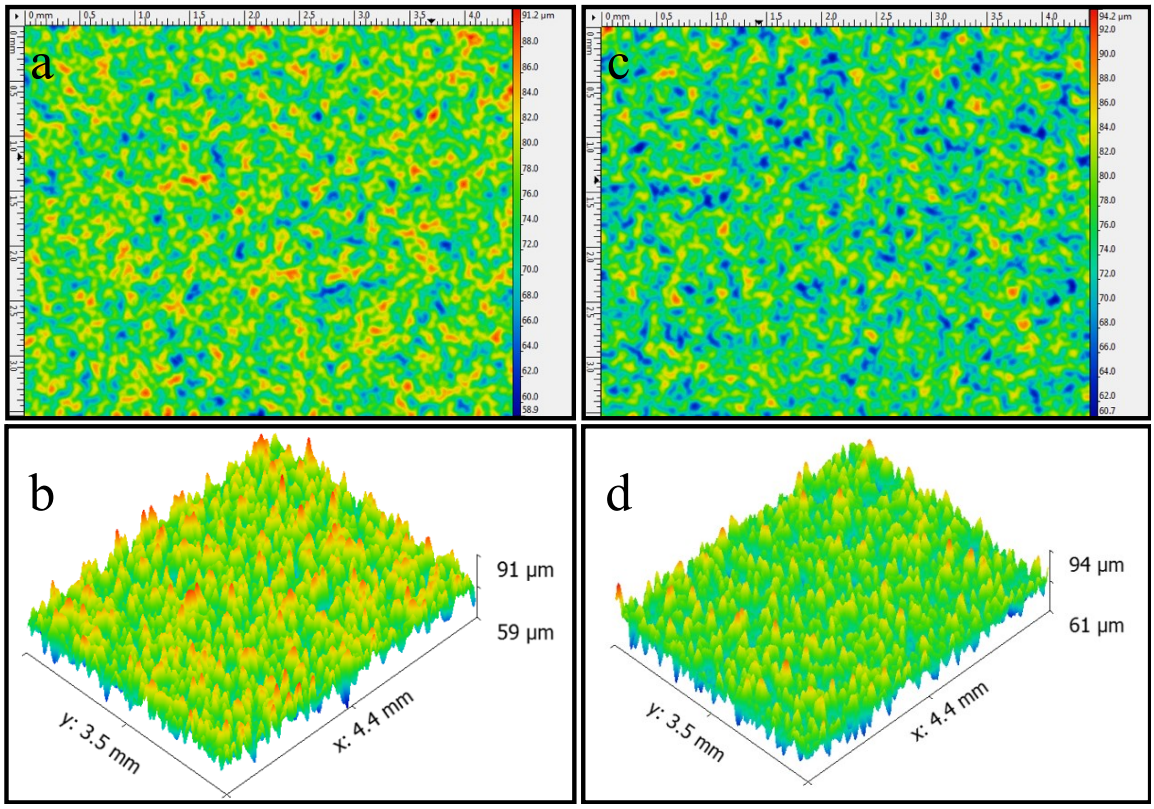

Figure 4-10: a) 60 wt% Ag/0.75 wt% Gr(s) 2D surface profile of solvent-free formulation; b) 3D surface profile of solvent-free formulation; c) 2D surface profile of solvent-assisted formulation; d) 3D surface profile of solvent-assisted formulation

4.3.9 Scanning electron microscopy results

We further verified the results by characterizing the morphology at the micron range by using a scanning electron microscope on the cross-section of the paste. Because the two strongest formulations 20 wt% Ag/0.75 wt% Gr(s) and 20 wt% Ag/0 wt% Gr(s) exhibited electrical resistivity values too high for ECAs, and were therefore deemed unsuitable for further investigation. The next two strongest formulations were chosen instead. Below shows the SEM images for 40 wt% Ag/0.75 wt% Gr(s) in Figure 4-11.

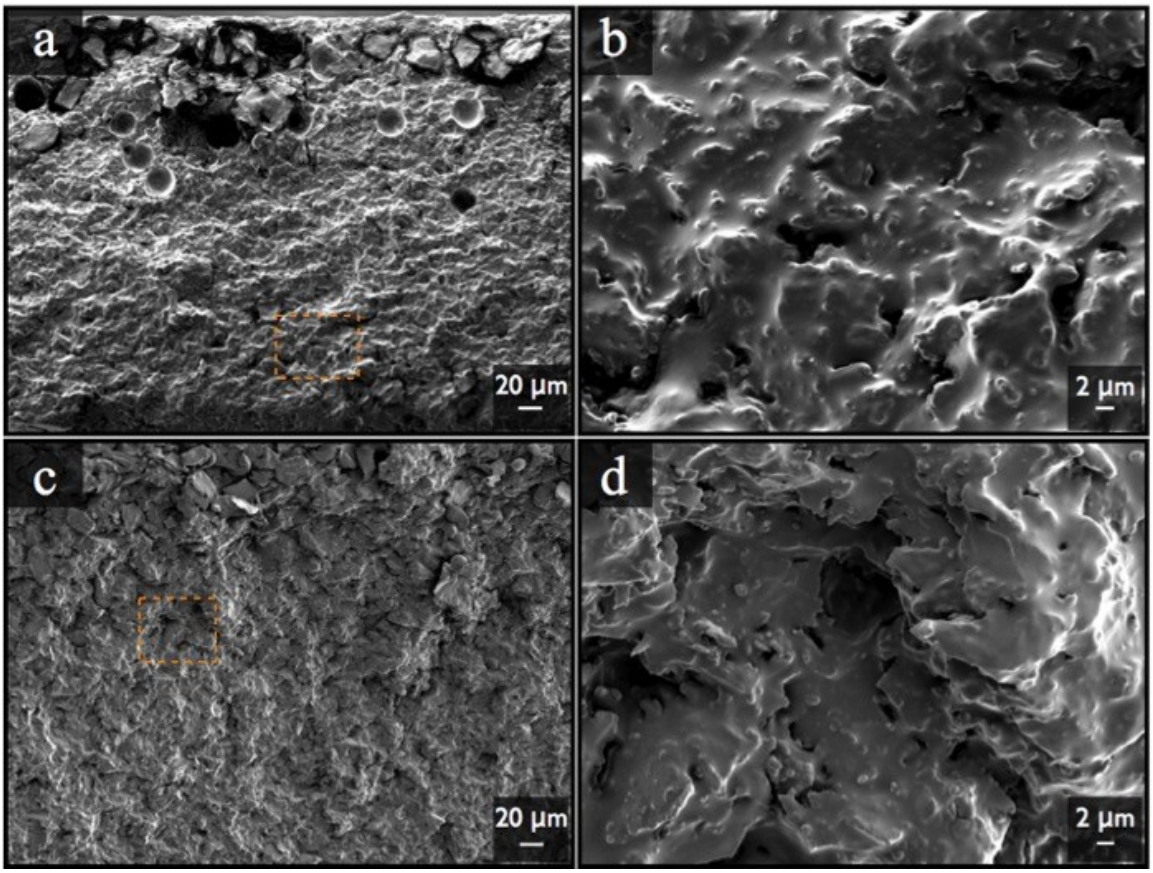

Figure 4-11: a) 40 wt% Ag/0.75 wt% Gr(s) SEM image of solvent-free formulation at low magnification; b) SEM image of solvent-free formulation at high magnification referenced from orange box; c) SEM image of solvent-assisted formulation at low magnification; d) SEM image of solvent-assisted formulation at high magnification referenced from orange box

The next formulation of 60 wt% Ag/0.75 wt% Gr(s) is shown below in Figure 4-12.

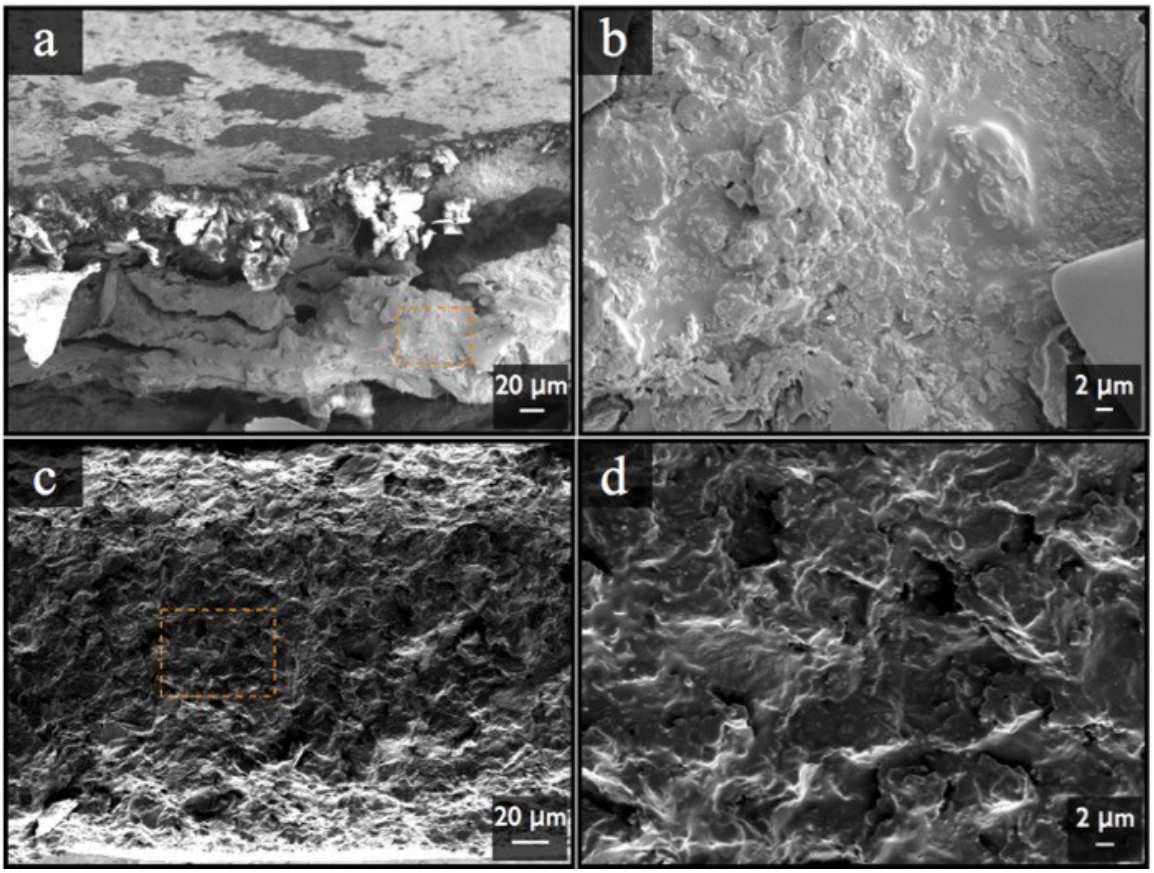

Figure 4-12: A) 60 wt% Ag/0.75 wt% Gr(s) SEM image of solvent-free formulation at low magnification; B) SEM image of solvent-free formulation at high magnification referenced from orange box; C) SEM image of solvent-assisted formulation at low magnification; D) SEM image of solvent-assisted formulation at high magnification referenced from orange box

In each of these figures, their respective a and c images denote a low power view of the cross-section of solvent-free and solvent-assisted formulations, respectively. Their b and d images show a high power view of the solvent-free and solvent-assisted formulations, respectively, with corresponding orange boxes in a and c that detail where these high power images are taken from. The compressed cross-sections of the solvent-assisted and non-solvent methods were compared. The images obtained from the SEM agree with the optical microscope and optical profiler, as the non-solvent methods for both formulations exhibit a smoother morphology and fewer pockets or dimples when compared to the solvent-assisted method. However, since the SEM images are able to capture the interior

structure of the composite (via cross-section), it is now clear that the phenomena observed on the surface extends all the way through the entire cross section, showing that bubbles are not limited to the surface alone, but are present throughout the entire paste. As such, it is confirmed that the detrimental effects of residual solvent within the composite can be attributed to the formation of dimples, bubbles and hollow structures both within the composite as well as on the surface, resulting in the weakening of its mechanical properties.

4.4 Conclusions

The LSS of both solvent-free and solvent-assisted formulations were systematically tested in this work. It has been determined that the combination of solvent presence and Gr(s) within the composite has a negative effect on the LSS of the material. We also determined that the two formulations exhibiting the highest LSS are 20 wt% Ag/0.75 wt% Gr(s) and 20 wt% Ag/0 wt% Gr(s). However, these formulations did not exhibit sufficient conductivity and therefore could not be considered for applications in ECAs. As such, the next two formulations that exhibited high LSS and electrical conductivity (60 wt% Ag/0.75 wt% Gr(s) and 40 wt% Ag/0.75 wt% Gr(s)) were further examined, primarily to determine why the LSS was lower for the solvent-assisted formulations and secondly, to verify that these formulations work as functional ECAs. The first property investigated was the electrical conductivity of these formulations to verify that these function as ECAs. It was found that the bulk resistivity (our measure of conductivity) of these two formulations ranged between $2.5 \times 10^{-1}\ \Omega \cdot cm\ to\ 1 \times 10^{-2}\ \Omega \cdot cm$. Furthermore, it was determined that 40 wt% Ag/0.75 wt% Gr(s) exhibited lower bulk resistivity when assisted with solvent, whereas solvent assistance for 60 wt% Ag/0.75 wt% Gr(s) showed little improvement of the electrical conductivity of the ECA.

The next investigation was made in order to follow up on two suspicions that could help explain the massive drop in LSS: the first is that a drop in crosslinking density has occurred either because of the presence of solvent, or due to the interaction between solvent and surfactant during the curing process. This factor was not further explored in this work, however, it is a recommended topic for future research. The second factor that

could affect the LSS was suspected to be bubble formation during the curing process. This factor was believed to cause a drop in contact area between the paste and the substrate, thus resulting in weaker mechanical properties because there is less contact with the substrate compared to the solvent-free formulations. This would be detectable through increased roughness and through microscopy visually as pits and dimples. To verify, the first method of characterization used was optical microscopy to check the presence of pits and dimples on the surface of the paste. It was found that the solvent-assisted formulations exhibit more pits and dimples when compared to the solvent-free formulations. To confirm, quantitative evidence was acquired using an optical profiler in order to determine if there is a difference in roughness between the solvent-assisted and solvent-free formulations. The findings from the optical microscope were successfully confirmed: the solvent-assisted formulations exhibit higher roughness when compared to solvent-free formulations, but also, the surface map generated from the optical profiler consistently showed more pits (denoted as blue) in the solvent-assisted samples confirming that those formulations offer smaller contact area between the paste and the substrate.

Further investigation of bubble formation during the curing process was undertaken by taking SEM images on the cross-section of the paste to determine whether these bubbles exist whith the material on a bulk level. The results showed that pits and dimples in the solvent-assisted forumlation, as well as higher surface roughness could be found in the cross section. This finding confirms that bubble formation does occur within the bulk of the material, not just on the interface between the paste and the substrate.

With clear evidence of bubble forming, leaving dimples and holes within the whole composite, it is safe to say that the large drop in LSS between the solvent-free and solvent-assisted formulations is caused by the formation of bubbles during the curing process at the micron range, leading to a decrease in contact area as well as holes within the bulk material. The findings of this work regarding LSS agree with and confirm the suspicions from previous works that a drop in mechanical strength will occur due to the presence of solvent in the composite. However, whether the drop is due to a decrease in cross-linking density should be studied and is best saved for another project.

Chapter 5 Elastic Modulus of Epoxy Composites Filled with Graphene

5.1 Introduction

Graphene holds great potential as a co-filler alongside silver in hybrid ECAs and has been shown by N.W. Pu et al to perform better in comparison to carbon black and CNTs [8]. Even so, graphene faces challenges toward its use in ECA fabrication such as the achievement of homogeneous dispersion and the preservation of its single-layer structure within the composite [18]. In our recent work [18], we employed sodium dodecyl sulfate (SDS) to decorate graphene in order to overcome these two concerns. In addition, it is known that increasing metal filler content in ECAs leads to a decrease in mechanical properties [20]. Therefore, SDS-decorated graphene is not only meant to help decrease the amount of silver necessary to retain acceptable conductivity values, but also meant to prevent the ECA from losing mechanical strength.

In this work, epoxy resin is loaded with two fillers: pristine commercial graphene nanosheets (Gr), and SDS-modified graphene nanosheets (Gr(s)). Different from our recent work [18], each nanocomposite is prepared using a solvent-free mixing procedure [27], giving rise to the ability to further scale up. The mechanical properties of cured epoxy with Gr(s) were evaluated and compared to those of epoxy with pristine graphene through Hertzian indentation studies. We observed that modifying graphene with SDS increased its maximum elastic bulk modulus at lower weight percentages compared to its unmodified counterpart.

5.2 Experimental

5.2.1 Preparation of hybrid composite ECA

The epoxy composites are primarily comprised of two components: the epoxy component that requires both the resin itself as well as the curing agent, and the filler material that usually comes in the form of a powder. Bisphenol-A liquid epoxy resin (D.E.R. 331) and epoxy curing agent (D.E.H. 24) triethylenetetraamine (TETA) were purchased from DOW Chemical Company and used as received. Graphene nanosheets with sizes ranging

from 0.5 to 5 μm were purchased from ACS Materials (USA) and were used as received [18,27]. The surfactant sodium dodecyl sulfate (SDS) responsible for exfoliating the graphene nanosheets was purchased and used as received from Sigma Aldrich. HPLC ethanol solvent at 99.8% purity was purchased and used as received from Fisher Scientific (USA). Gr(s) was prepared using the same procedure outlined in J. Trinidad et al's work [27] and was added into the vial together with all other materials before mixing. These materials (which include the graphene/modified graphene in the case of the hybrid ECAs) are combined within the same container where they are mixed at 2000 RPM for 4 minutes and de-foamed afterwards at 2200 RPM for 1 minute using a Thinky Mixer (ARE 310). After complete mixing of the materials, a paste-like substance is obtained and casted into a PDMS mold that holds the shape of a mechanical test coupon (following dimensions recommended by the ASTM D638 [156] standard for dogbone type IV). Afterwards, a copper sheet with dimensions 2 cm x 7.6 cm is placed on top. Finally, the sample is placed in the oven with a metallic block for compressing the mold. The material is heated at 60^{o}C for 30 minutes, and then ramped to 150^{o}C where it cures for 2 hours. Upon completion, the sample is removed from the mold and stored within a Ziploc bag.

5.2.2 Hertzian Indentation

In this study, we concentrate on determining the effects of Gr and Gr-s when mixed with epoxy. More specifically, our property of interest when investigating the mechanical strength for the nanocomposite is the elastic modulus. A Universal Material Tester (UMT) Tribological Test Equipment (CETR Campbell, CA USA) is equipped with an indenting tip used to record compression force and distance as the sample carries a maximum load of 750g at 1 mm/sec.

An estimation of its bulk modulus is determined by inputting the experimental data within the Hertzian indentation model that works under the principle of a hemispherical indenter indenting a flat surface [127]. The Hertzian equation is an indentation model for finding the elastic modulus [128,129]:

$$a^3 = \frac{3PR}{4E^*} \qquad \textbf{Eq. 11}$$

The above formula was rearranged in order to plot load *P* VS displacement *d*. But first, it is important to note that contact radius *a* found in the above equation is related to the displacement *d* as seen in the following equation:

$$d = \frac{a^2}{R} \; or \; a = \sqrt{Rd} \qquad \textbf{Eq. 12}$$

With the above equation being substituted into the contact radius equation, we can then rearrange it to take a form where load is a function of distance:

$$P = \frac{4E^* d^{1.5}}{3\sqrt{R}} \; or \; P = \frac{4}{3\sqrt{R}} \times E^* \times d^{1.5} \qquad \textbf{Eq. 13}$$

E^* is the modulus and R is the radius of the AISI Type 440-C stainless steel probe ($R=4.63 \times 10^{-4}$ m) used for indenting the sample.

With this equation, we apply a theoretical model to compare the data gained from the experimental results of the indentation. The way elastic modulus is estimated involves calculating the forward and backward force using the Hertzian equation and comparing those two forces to the actual forces reported by the UMT. We then take the square of the difference between the theoretical value and experimental value and add up all of those values: one for forward and one for backward force. Finally, we add those two values that were just obtained to be called the total sum of error and then use a solver function to estimate what the elastic modulus should be to best fit the model.

5.3 Results and Discussion

The elastic moduli of both Gr and Gr(s) were investigated using the UMT. Figure 5-1 illustrates the relationship between the elastic modulus of the nanocomposites and the weight percentage of the fillers within epoxy.

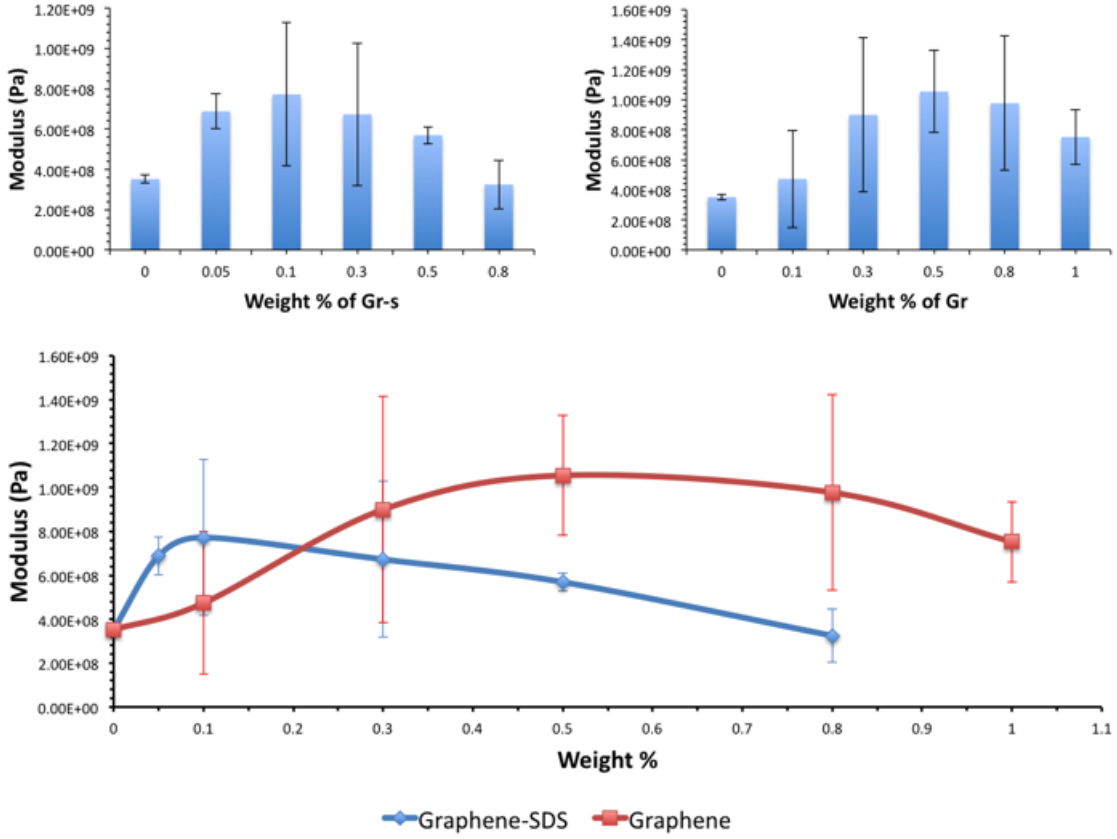

Figure 5-1: Plots of the elastic modulus as a function of filler fraction with Gr located at the top right and sample with Gr(s) is located at the top left. The bottom graph is a comparison chart illustrating the difference between the two co-fillers.

Both exhibit a parabolic-like trend indicating that too much or too little filler content can negatively impacts the performance of the material. Yan-Jun Wan et al reported a similar work regarding the positive effect of surfactants on graphene-filled epoxy on the modulus [25]. However, unlike our Gr(s), their work uses a different surfactant triton x-100 and also employs tensile, while this work uses indentation and SDS as the surfactant.

The first topic to discuss is the parabolic behavior of both Gr and Gr(s). This trend has been observed in other works that also utilize forms of graphene/epoxy composites

[25,82]. A hypothesized reason for this parabolic characteristic that Gr exhibits could be the following: the segment before the maximum modulus value is the region that follows an increasing trend, where the modulus increased as the amount of filler content increased; whereas a decrease of the modulus could also be due to excess graphene interfering with the crosslinking of epoxy. Further studies must be conducted to verify this.

The second topic to discuss looks into the differences between the elastic modulus of the composites as we add Gr and Gr(s). While Gr(s) also follows a parabolic characteristic similar to Gr, its optimal point arises at a lower weight percent and begins its fall at a lower weight percent. One explanation for this could be that the SDS aids in dispersing and exfoliating the graphene nanosheets more effectively. This modification could therefore play a key role in taking advantage single layer graphene's exceptional mechanical properties as a means to enhance epoxy's modulus. The decrease in mechanical properties on the other hand, could be caused by excess amounts of SDS interfering with the cross-linking procedure of epoxy as suggested in previous work by Amoli et al [18].

5.4 Conclusion

Hertzian indentation was used to determine how these epoxy nanocomposites behave mechanically by observing changes in elastic modulus. It was found that increasing graphene and SDS modified graphene as a function of weight percent yields an elastic modulus profile that roughly appears like a parabola. SDS modified graphene was determined to be inferior to the non-modified samples when it came to overall improving the mechanical properties of the nanocomposite. However, SDS modified graphene peaked at lower weight percentages compared to non-modified graphene indicating that less filler content is required to improve its elastic modulus. Overall, it was verified that the addition of either graphene or SDS modified graphene for a critical weight concentration generally yielded higher elastic modulus compared to that of pure epoxy.

Chapter 6 PEDOT:PSS as a co-filler for ECAs

6.1 Introduction

PEDOT is a conducting polymer classified as a polythiophene derivative [94,157–160]. PSS is another polymer with three functions: first, it acts as the medium at which PEDOT polymerizes and becomes stable in water [94,161]; second, it acts as a large dopant for PEDOT allowing for the introduction of charge carriers within the polymer backbone of PEDOT [158]; finally, PSS functions as a charge-balancing group (or counterions), providing a negative charge from the SO_3^- end-group for the positive charge on the thiophene group in PEDOT [94,161,162].

It has been a few decades since Shirakawa et al discovered the very first conductive polymers in 1977, but now, there are handfuls available in the market as outlined by R. Balint et al [158]. Conductive polymers are divided into three organic groups: sulfur-containing heteroatoms (thiophenes and sulfides), nitrogen-containing heteroatoms (polymerized pyrrole, aniline, etc), and non-heteroatom containing polymers with numerous alkenes. In specific, PEDOT:PSS was first produced by Bayer AG research laboratories in Germany [94,160] in the 1980s and has since been the topic of great research and industrial interest, being hailed as one of the most successful conductive polymers in commercial use today [159,160,163,164]. PEDOT:PSS has already been applied in many fields such as energy-based PV technologies [157,159–163,165], electronic semiconductor devices that require excellent electron/hole transport (e.g. field-effect transistors, LCDs, LED based technologies, and anti-static bags) [94,159,161–164,166], and bio-sensing/bioengineering applications [157,158].

PEDOT:PSS films contain work functions ranging from 5-5.2 eV and induces charge transfer at very high kinetic rates [160]. Its conductivity comes from a variety of factors, however, only two will be mentioned in this work. The first is its conjugated backbone that forms alternating double bonds. The weakly localized π-bonds overlap with each other, giving rise to the possibility for electrons to become delocalized and move or "jump" through the polymer backbone and as a result, move between groups of atoms

[158]. The second factor that makes conductivity possible is the presence of dopant(s) that act as counterions keeping the conducting polymer stable but at the same time is a charge carrier source that is responsible for adding/removing electrons from the polymer chains to become what are known as polarons or bipolarons [158]. These polarons/bipolarons move through the polymer chain as an electric potential is applied onto the system, which in turn allow for charges to pass through the backbone resulting in electrical conductivity. A more comprehensive explanation on what polarons/bipolarons are can be found from Bredas and Steer, who also explain the entire conducting mechanism of conductive polymers from a chemist's point of view, as well as explain the possible miscommunications that can arise as a consequence of using the term "dopants" to explain the conductivity mechanism in conductive polymers [167], whereas good diagrams and cartoons for the explanation of this mechanism in a simpler manner can be found in Balint et al's work [158]. In addition to this, Crispin et al presents a chart illustrating the conductive evolution of PEDOT:PSS as a function of weight percentage with the addition of diethylene glycol (DEG) [161]. Their chart shows a percolation curve between 0.1 and 1 weight percent showing synonymous trends to the percolation curves for conventional ECAs. As such, this work was inspired to explore the use of PEDOT:PSS as a co-filler within the conventional ECA in hopes of being able to either improve the conductivity limits of the conventional ECA, or at least reduce the silver content required to decrease material costs. In specific, this work will explore the electrical conductivity of a hybrid ECA that uses PEDOT:PSS as its co-filler, as well as investigate how adding increasing amounts of PEDOT:PSS will affect the mechanical properties (in this case, adhesion strength by means of evaluating shear strength). To the knowledge of the author, no work regarding the use of PEDOT:PSS in composite systems for the sake of improving electrical conductivity has been undertaken, as most current work utilizes PEDOT:PSS as a film for varying applications rather than a solution-based component. Therefore, this work will be primarily act as a preliminary study to determine its feasibility as a solution-based co-filler in hopes of opening a new avenue for modifying and improving the performance of conventional ECAS.

6.2 Experimental

6.2.1 Conductive composite preparation

Diglycidyl ether of Bisphenol-A liquid epoxy resin (D.E.R. 331) and Triethylenetetramine (TETA) epoxy hardener (D.E.H. 24) was supplied by DOW Chemical Company and were used as the resin base and the hardener respectively. A high conductive grade of Poly(3,4-ethylenedioxythiophene)-Poly(styrenesulfonate) (PEDOT:PSS 1.1% in water solution) was purchased from Sigma-Aldrich and used as the conductive filler material for the composite. Methanol in HPLC grade was purchased from Sigma-Aldrich and used as a common solvent between the water and the resin to assist with dispersion and mixing, as well as to wash out the PSS content in the solution. Silver micro-flakes (a density of 10.49 g/cm^3, a particle size of 10 μm) were purchased and received to act as the principle conductive material of the composite.

The procedure for making the conductive composites begins by adding the epoxy resin with both PEDOT:PSS solution and methanol solvent [162]. The resulting mixture is first mixed vigorously using a vortex mixer to ensure that the PEDOT:PSS solution is dispersed in the epoxy resin. Once completed, silver flakes are added into the mixture and then further mixed at 2000 RPM for 5 minutes using a Thinky Mixer (ARE 310). The mixture is then placed into the oven at 90 °C in order to allow both methanol and water to evaporate. Finally, epoxy hardener TETA is added into the system and again mixed at 2000 RPM for 5 minutes. The mixture is then placed into either a pre-cleaned 7 mm x 7 mm mold made of a glass slide, thermally resistant tape and a copper sheet (to ensure that the sample thickness remains constant) or a shear test coupon that is explained in an upcoming section. The samples are then placed into an oven to be baked at 150 °C for 2 hours. Below in Figure 6-1 is a schematic that illustrates and summarizes the entire procedure.

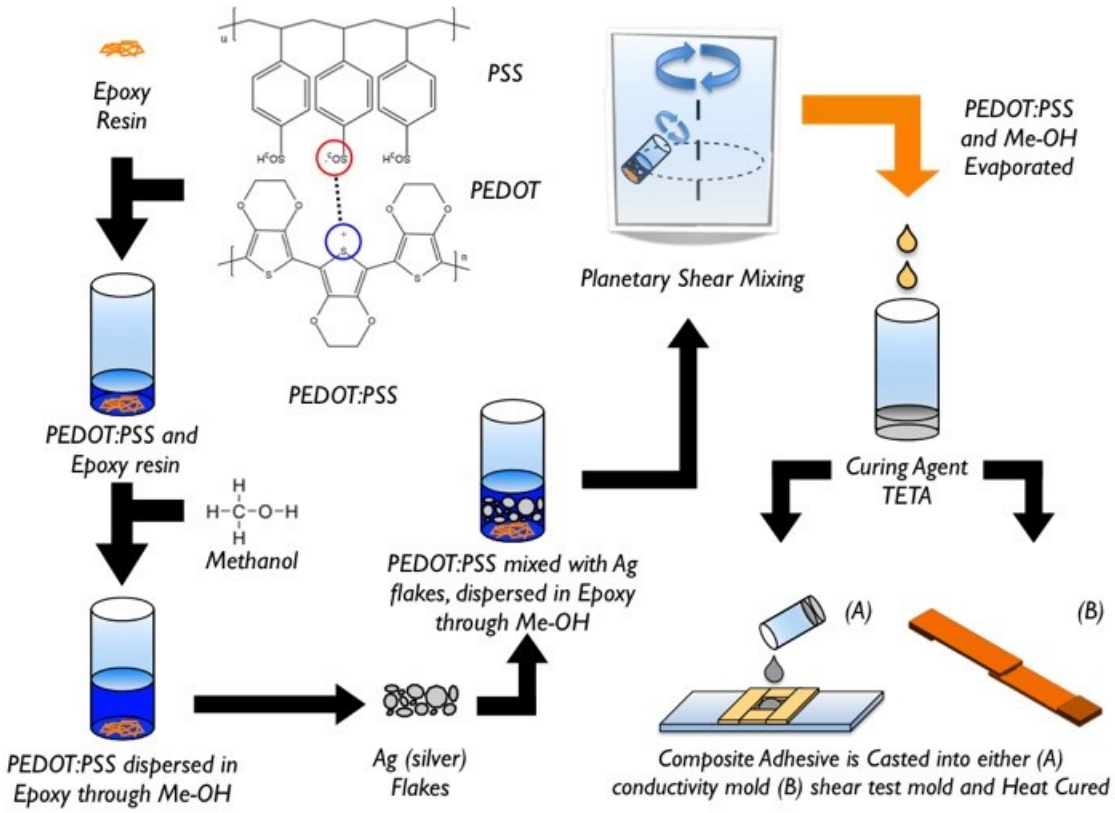

Figure 6-1: Schematic diagram of PEDOT:PSS as it is incorporated into conventional ECAs.

6.2.2 Characterization

The electrical sheet-resistance values of the cured composites were measured using a four-point probe setup that includes a probe fixture (Cascade Microtech Inc.) and a micro-ohm meter (Keithley 2440 5A Source Meter, Keithley Instruments Inc.). The sheet resistance R_s obtained can then be inserted into the bulk resistivity equation and then converted into conductivity with the following equations [17,27,52]:

$$\rho = R_s \cdot t = F \cdot t \ \left(\frac{\pi}{Ln\ 2}\right)\frac{V}{I} \qquad \textbf{Eq. 14}$$

as the bulk resistivity equation. However, bulk resistivity ρ can be converted to conductivity σ with the equation below:

$$\sigma = \frac{1}{\rho} \qquad \textbf{Eq. 15}$$

and if rearranged using equation 14, we can get the following equation:

$$\sigma = \frac{1}{F \cdot t}\left(\frac{Ln\ 2}{\pi}\right)\frac{I}{V} \qquad \textbf{Eq. 16}$$

where t represents the thickness of the sample, while I and V represent the applied current and measured voltage from which the sheet resistance value is based upon.

The lap-shear strength values of the cured composites were measured using a Universal Material Tester (UMT) Tribological Test Equipment (CETR Campbell) equipped with tensile wedge grips (G1061-2, Mark-10 Corp). The test procedure followed ASTM D1002 with the exception of reducing the contact area to 12.7 mm x 12.7 mm in order to accommodate the load cell used in the experiment [27,123]. 1/16 inch thick double sided FR-4 boards were used as lap shear coupons and were purchased from MG Chemicals. The boards were machined to meet the dimensions specified in Figure 6-2.

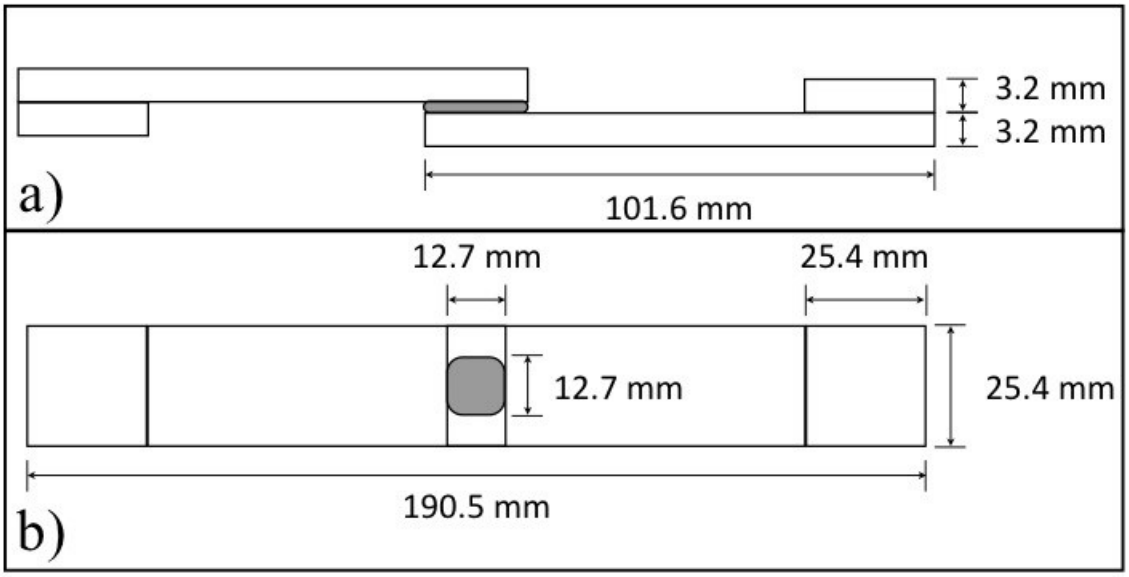

Figure 6-2: a) Top view of shear test coupon showing the modification of the paste area with measured values; b) Side view of shear test coupon with measured values.

6.3 Results and Discussion

6.3.1 Electrical Conductivity

The electrical conductivity of pristine PEDOT:PSS was characterized by a standard four-point probe setup in solution cast films. It was found that the electrical conductivity of pure PEDOT:PSS was about 15 S/cm. However, despite knowing how methanol treatment of PEDOT:PSS will improve electrical conductivity [162], we were unable to apply such a procedure to our samples as a perfect procedure that involved methanol treatment for the composite was not fully developed before the electrical conductivity testing commenced. This therefore meant that the samples were measured with the PSS still prevalent in the composite.

In order to investigate how PEDOT:PSS influences the overall electrical conductivity of their polymer composites, we used conventional ECAs containing only silver flakes at various weight fractions as a control. For all hybrid ECA samples with PEDOT:PSS co-fillers, the absolute amount of sliver flakes was kept constant, whereas the amount of PEDOT:PSS solution was increased. The formulations used for testing are summarized below in Table 6-1.

Table 6-1: Summary of different sample compositions and the masses of the conductive filler material

Sample	Composition	PEDOT:PSS+ H_2O mass (mg)	PEDOT:PSS mass (mg)
A	Epoxy + Ag 60 wt%	0	0
B	Epoxy + Ag 60 wt% + PEDOT:PSS 0.1 wt%	33.9	0.339
C	Epoxy + Ag 60 wt% + PEDOT:PSS 0.2 wt%	67.9	0.679
D	Epoxy + Ag 60 wt% + PEDOT:PSS 0.5 wt%	170.3	1.703
E	Epoxy + Ag 60 wt% + PEDOT:PSS 1 wt%	342.4	3.424

Figure 6-3a below illustrates the expected conductivity of conventional ECAs that typically contain only silver flakes as its main conductive filler as a function of weight percent loading. It is seen that past a certain point in the curve known as percolation threshold (within the range of 40 wt% loading), the composite transitioned from being an insulating material into a conductive material. Furthermore, by looking at the higher weight loadings, it is seen that adding more silver flakes into the epoxy matrix did not significantly improve electrical conductivity. In contrast, the electrical conductivities of the hybrid ECAs with a constant total amount of silver flakes at various PEDOT:PSS weight concentrations were plotted in Figure 6-3b below.

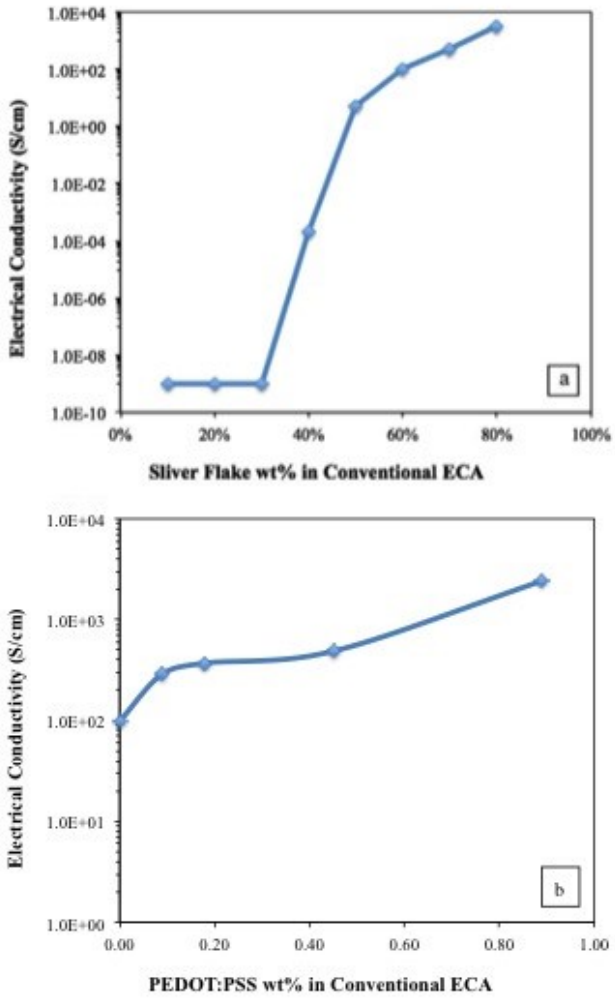

Figure 6-3: a) Electrical conductivity as a function of filler content silver flakes; b) electrical conductivity as a function of filler content PEDOT:PSS containing 60 wt% Ag

It was found that adding a small amount of PEDOT:PSS (0.1 wt%) remarkably improved the electrical conductivity to 289 S/cm, which is 3 times higher than that of the conventional ECA with 60 wt% sliver flakes. The maximum conductivity of 2422 S/cm was achieved at a weight loading of 0.89 wt% PEDOT:PSS showing that the combination of PEDOT:PSS and conventional ECAs produces highly conductive composites. Similar to conventional ECAs, excess PEDOT:PSS in the composite above a certain concentration yields appears to show diminishing improvement of electrical conductivity as seen in Figure 6-3b for higher weight loadings, however needs more experimental data to verify. This decrease in electrical conductivity may be attributed to the fact that increasing the amount of PEDOT:PSS into the system also increases the potential of residual water molecules from the PEDOT:PSS solution thereby decreasing the crosslinking density of the epoxy as it is being cured leading to fewer metallurgic interconnections between the silver flakes [7,11]. Thermal studies can be done to further investigate and verify this behavior.

6.3.2 Lap shear strength

The shear strength of the adhesive was measured in order to determine if the composite remains functional as a joining material after adding co-filler PEDOT:PSS into the system. The shear strength was investigated using (CETR UMT) universal mechanical tester with a load cell of 100 Kg and Mark-10 wedge grips G1061-2 with gripping force of 1-9 kN, while following ASTM D1002 with exceptions that were specified in a previous section. The shear strength as a function of PEDOT:PSS weight loading was investigated with the results summarized below in figure 6-4.

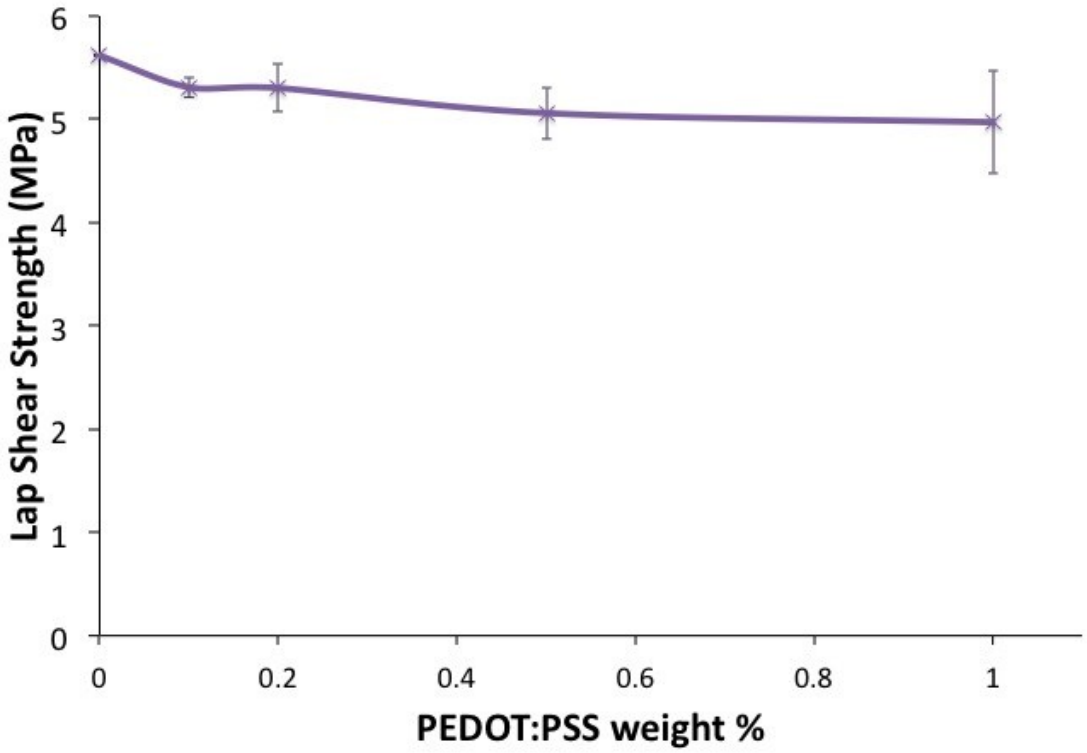

Figure 6-4: Lap Shear Strength as a function of PEDOT:PSS fraction for the hybrid ECAs.

Overall, it was observed that addition of PEDOT:PSS into the conventional ECA (where the weight loading of silver flakes was kept constant) shows an increase in variance with an increase in PEDOT:PSS. One possible explanation for this is that the addition of another component into the epoxy matrix resulted in more variability in the system (whether it comes from change in dispersion efficiency, addition of processing steps giving room for error, contamination issues or thermal instability), leading to weakened adhesion. However, it is important to note that the change in shear strength is insignificant when compared to the increase in electrical conductivity of the similar weight loading of PEDOT:PSS. Therefore, the addition of PEDOT:PSS as a co-filler towards conventional ECAs has not been found to negatively affect or compromise the shear strength of the bulk material in any statistically significant manner (only dropping around 1 MPa at worst case)

It is important however, to examine the reason for why the graph tends to decrease. One explanation must be taken into consideration is that the PEDOT:PSS comes as a polymer blend at a concentration of ~1%, whereas the rest of the solution is primarily water-based. As such, it is highly likely that the evaporation step intended to release all of the water introduced after adding PEDOT:PSS does not release all of the water in the system, leaving trapped water molecules within the resin.

It is well known that the presence of water in epoxy resin results in the compromising of its crosslinking density [168,169], thus leading to the degradation of both electrical conductivity and mechanical strength. With this in mind, it is very likely that the variability of how much water molecules are evaporated out of the system is directly related to both the bulk strength of the material, as well as its electrical conductivity. It is intuitive to know how increasing the crosslinking density results in better mechanical strength, however, the reason that crosslinking density is related to the bulk resistivity of the system needs to be explained through the concept of increasing shrinkage in epoxy. Increased shrinkage within the thermoset leads to better intimate contact between silver flakes, resulting in the formation of more conducting pathways [7,10,17,41,42,91]. Two avenues that were not explored in this study are the effects of methanol on the crosslinking density of the epoxy. Firstly, no explicit mention that methanol has a negative effect on crosslinking density of epoxy was found, however, it is suspected to be a potential contributing factor when it comes to the incomplete curing of the epoxy, or even the formation of air bubbles during evaporation. Secondly, dispersion issues could lead to problems in the utilization of PEDOT:PSS as it is not well known whether the actual active component is aggregated or isolated in small pockets within the composite system upon curing. Furthermore, poor dispersion is suspected to also act as potential weakness in the structure of the cured composite, leading to variance in its mechanical strength.

6.4 Conclusion

PEDOT:PSS was successfully introduced into a conventional ECA formulation; its electrical conductivity and shear strength were investigated. The electrical conductivity results have shown that the incorporation of PEDOT:PSS improves the conductivity of conventional ECAs to 289 S/cm, which is three times more conductive than without the co-filler. The maximum conductivity found in this investigation when incorporating 0.89 wt% PEDOT:PSS into the conventional formulation has a conductivity value of 2422 S/cm. The co-filler system is successful at reaching high conductivity values without introducing an extra 10-20 wt% of silver content within the ECA to achieve the same results.

The mechanical strength of the hybrid ECA was also investigated. By varying only the weight loading of PEDOT:PSS, it was found that the increase of the co-filler increased the variance of the shear strength of the system, as well as an insignificant decrease in shear strength of 1 MPa at worst case. It has been explained that the increase in variance could be from a variety of factors, however, it is suspected that the introduction of PEDOT:PSS at higher weight loadings resulted in excess water molecules that were trapped in the composite because of insufficient evaporation, leading to the varying shear values. Overall, it has been found that the incorporation of PEDOT:PSS on the point of view of both electrical conductivity and mechanical strength is positive. It increases the electrical conductivity of the conventional ECA while simultaneously reducing the required amount of silver to be functional, as well as exhibits negligible impact on its shear strength. This newfound use of PEDOT:PSS as a co-filler in conventional ECAs can lead to a variety of innovative applications in solder mount technologies, as well as flexible electronic joining materials.

Chapter 7 Concluding Remarks, Recommendations and Future Research

7.1 Concluding Remarks

We explored the use of Gr(s) as a co-filler for CCAs using a PSM as a modified method of composite preparation and high shear mixing. The rheological properties of epoxy-based composites that are loaded with Gr and Gr(s), as well as combinations with silver and Gr/Gr(s) were successfully investigated. Although the total viscosity of the system increases upon addition of any filler in epoxy, the addition of Gr or Gr(s) in specific produces a shear-thickening suppression effect that is clear and visible at weight concentrations above 0.5 wt%. This new phenomenon could prove useful to future applications that involve the need for shear-thinning liquids, especially those used for electronic printing techniques.

Furthermore, a comparative study between the LSS of Gr(s) and Ag (both independently and in combination of one another) using a solvent-free and solvent-assisted environment was undertaken. It was found that samples containing Gr(s) prepared by solvent-assisted method show significantly weaker LSS values when compared to those that do not use solvent. It was initially suspected that solvent and surfactant were the primary cause for the decrease in the cross-linking density of epoxy; however, this was not proven in our work. Instead, we noticed another factor that could cause the decrease in LSS: formation of bubbles during cure, resulting in dimples and pits post-cure. We used multiple forms of microscopy to qualitatively and quantitatively determine that there are more dimples and pits found in the entire bulk of the structures prepared by the solvent-assisted. This finding gave traction to our suspicion that the pits and dimples were in effect decreasing the contact area between the paste and the substrate, and as a result, decreasing the amount of force required to fail as well as decreasing the LSS of the system. Electrical conductivity was also examined using the same procedure for making the LSS samples. The experimental results indicate that conductivity was increased with solvent assistance for samples of lower silver content (40%), but for a content of 60 wt% Ag, solvent assistance barely helped improve electrical conductivity. As such, we concluded that

since no benefit comes from using solvent for higher silver loadings, the solvent-free method was the best way to prepare that formulation. Furthermore, we found the optimal solvent-free formulation with 60 wt% Ag and 0.75 wt% Gr(s) exhibited the best LSS and electrical conductivity.

Next, we studied how the elastic modulus (from an indentation method) would change as we increased the weight loading of Gr/Gr(s). We learned that Gr(s) peaks at much lower weight concentrations (0.05 wt% to 0.15 wt%) when compared to Gr. On the other hand, Gr peaks at higher weight concentrations (0.5 wt% to 0.8 wt%) and overall reinforces the material more effectively, as using Gr obtains the highest elastic modulus values for the epoxy-based composite.

Our final study used water-based PEDOT:PSS as co-filler for conventional ECAs and successfully improved the electrical conductivity of the composite. It was observed that with a constant Ag weight concentration, an increase in PEDOT:PSS resulted in an increase in conductivity akin to adding more Ag into the system, but with the added benefit of not using as much Ag to achieve the same values. However, since PEDOT:PSS is water-based, we followed up on a suspicion that adding higher concentrations of the co-filler would weaken the mechanical properties of the composite especially because the polymer matrix epoxy is hydrophobic and typically loses cross-linking density upon the presence of residual water molecules during cure. We learned that the LSS showed an apparent drop as the content of PEDOT:PSS increased, concluding that PEDOT:PSS is responsible for weakening the mechanical properties is inaccurate. Instead, it would be more suitable to conclude that introducing higher concentrations of PEDOT:PSS into they system adds higher variability, as each increasing concentration of PEDOT:PSS into the composite exhibited higher standard deviation. This result is reasonable as adding more material into the composite could result in more variability using the same procedure, for example, different mixing results, more inconsistencies with dispersion, gradual ineffectiveness of desiccation, etc. Overall, PEDOT:PSS as a co-filler holds promise as it not only keeps the material low in viscosity, but also exhibits high conductivities at low Ag loadings.

7.2 Future Research

This thesis has explored a variety of different aspects regarding ECAs, however, left room for further investigations, which are recommended to be followed up for a more comprehensive understanding. Topics below will outline questions and ideas that would require further investigation.

In chapter 3, we discussed the idea of using these solvent-free ECA formulations for printer technologies that dispense conductive ink, thereby making the traces and landing spots for the electrical components at an industrial scale. However, although this idea has great traction and in theory should work, it is important to use an actual printer loaded with our hybrid ECA paste to prove that this concept is feasible for further commercialization of ECAs. Needless to say, extra work will be required to find the optimal formulation that fits both the capabilities of the printer's dispensing head as well as the conductivity requirements in order to guarantee the smooth operation of the PCB. With this follow-up, we can fully conclude that the incorporation of Gr(s) is an important component that the ECAs require in order to be usable in an industrial level, and in effect, an important part of commercializing ECAs.

Furthermore, in chapter 4, many questions were formed or left unanswered upon completion. The first question that needs to be addressed is whether or not the cross-linking density was dropping for formulations that used solvent to disperse and mix the fillers, or if it was a combination of solvent and surfactant from Gr(s) that was responsible for this drop. Since thermal studies have already alluded to this phenomenon occurring, it is worth pursuing this question using a different characterization method to confirm that this is indeed happening, as it affects the mechanical properties of the final composite for better or worse. The second question to address is what the LSS surface response plot would look like, had we incorporated more data points in between and possibly above and beyond the ones we used in order to form a comprehensive map of how the addition of either Gr(s) and or Ag affects the system's shear strength for both solvent-free and solvent-assisted formulations. Aside from these questions, it would also be beneficial to conduct the following experiments for a complete understanding of our

hybrid ECA system: a) creating another 3D graph where the second independent variable uses non-decorated Graphene to determine if Graphene is a better reinforcing agent than Gr(s) for both solvent-free and solvent-assisted environments; b) creating another 3D graph where the response surface is electrical conductivity as opposed to LSS; c) setting up a practical test that involves using SMD resistors/capacitors that are attached onto an FR-4 board using our ECAs, which are then tested for adhesion through dye shear testing.

Moreover, in chapter 5, it has to be noted that we were unsuccessful at determining how to incorporate co-solvent methanol into the hybrid ECA and then casting it into the electrical conductivity measurement molds successfully. If future work could solve this problem and do a comparative study in hopes of seeing if the assistance of the co-solvent has a positive effect on the electrical conductivity of the hybrid ECA, we would then be able to fully complete our study in the use of PEDOT:PSS as a co-filler for conventional ECAs.

Other topics that have not been discussed, but would further enhance our general understanding of the physical properties of ECAs include: tensile strength tests, drop tests, and bend tests.

Finally, one topic that the author wished to explore but was not able to complete was the search for an epoxy resin that exhibited reversible crosslinking after cure. This idea was conceived in order to address a practical problem that surrounded the recycling and re-working of PCBs, because when a thermoset such as epoxy is fully cured, further processing, reclaiming and removal is extremely difficult especially without damaging either of the components it is attached to. Because the knowledge of thermally degradable ECAs is already explored, the next step is naturally to determine if there is a way to make the bond between the FR-4 board and the component reversible, similar to the way how traditional Pb/Sn can be reversed and then reclaimed using the solder irons. Works that involve reversible cross-linkers were touched upon in this thesis, but extensive work need to be carried out in order to realize a fully reversible and functioning ECA that has cured. The most important part about this idea is that only the cross-linker is substituted into the

system and as such, will likely not change the function of the other components, meaning the incorporation of the co-fillers like Gr/Gr(s) should not be a problem. With these ideas and potential future works in mind, the understanding of the physical properties of hybrid ECAs utilizing Gr(s) as a co-filler has been outlined in this thesis to provide the field with a greater understanding of a material holding the potential to replace traditional Sn/Pb solders as a fully commercial electronic packaging material.

Bibliography

[1] Y. Li, C.P. Wong, Recent advances of conductive adhesives as a lead-free alternative in electronic packaging: Materials, processing, reliability and applications, Mater. Sci. Eng. R Reports. 51 (2006) 1–35. doi:10.1016/j.mser.2006.01.001.

[2] H. Ma, J.C. Suhling, A review of mechanical properties of lead-free solders for electronic packaging, J. Mater. Sci. 44 (2009) 1141–1158. doi:10.1007/s10853-008-3125-9.

[3] J. Trinidad, B. Amoli, B. Zhao, The Investigation of Physical Properties of Epoxy Nanocomposites Filled with Graphene as Electrically Conductive Adhesives, 2014. (Technical Paper)

[4] H.J. Lewis, A.. Ryan, Using Electrically Conductive Inks and Adhesives as a Means to Satisfy European PCB Manufacturing Directives, J. Adhes. Sci. Technol. 22 (2008) 893–913. doi:10.1163/156856108X305534.

[5] J. Trinidad, W. Zhang, A. Chen, B. Zhao, J. Persic, R. Lyn, IMPLEMENTING PEDOT : PSS AS A CO-FILLER FOR ELECTRICALLY CONDUCTIVE ADHESIVE APPLICATIONS, (2016) (Technical Paper)

[6] H. Jiang, K.S. Moon, Y. Li, C.P. Wong, Surface functionalized silver nanoparticles for ultrahigh conductive polymer composites, Chem. Mater. 18 (2006) 2969–2973. doi:10.1021/cm0527773.

[7] D. Lu, Q.K. Tong, C.P. Wong, Mechanisms underlying the unstable contact resistance of conductive adhesives, IEEE Trans. Electron. Packag. Manuf. 22 (1999) 228–232. doi:10.1109/6104.795858.

[8] N.-W. Pu, Y.-Y. Peng, P.-C. Wang, C.-Y. Chen, J.-N. Shi, Y.-M. Liu, M.-D. Ger, C.-L. Chang, Application of nitrogen-doped graphene nanosheets in electrically conductive adhesives, Carbon N. Y. 67 (2014) 449–456. doi:10.1016/j.carbon.2013.10.017.

[9] S. Xu, D. a Dillard, J.. Dillard, Environmental aging effects on the durability of electrically conductive adhesive joints, Int. J. Adhes. Adhes. 23 (2003) 235–250. doi:10.1016/S0143-7496(03)00027-7.

[10] Y. Li, K.-S. Moon, A. Whitman, C.P. Wong, Enhancement of Electrical Properties of Electrically Conductive Adhesives (ECAs) by Using Novel Aldehydes, IEEE Trans. Components Packag. Technol. 29 (2006) 758–763. doi:10.1109/TCAPT.2006.885940.

[11] B.-S. Yim, J.-M. Kim, S.-H. Jeon, S.H. Lee, J. Kim, J.-G. Han, M. Cho, Hybrid Interconnection Process Using Solderable ICAs (Isotropic Conductive Adhesives) with Low-Melting-Point Alloy Fillers, Mater. Trans. 50 (2009) 2649–2655. doi:10.2320/matertrans.M2009109.

[12] M. Abtew, G. Selvaduray, Lead-free Solders in Microelectronics, Mater. Sci. Eng. R Reports. 27 (2000) 95–141. doi:10.1016/S0927-796X(00)00010-3.

[13] H.J. Lewis, F.M. Coughlan, An Overview of the Use of Electrically Conductive Adhesives (ECAs) as a Solder Replacement, J. Adhes. Sci. Technol. 22 (2008) 801–813. doi:10.1163/156856108X305543.

[14] Y. Rao, D. Lu, C.P. Wong, A study of impact performance of conductive adhesives, Int. J. Adhes. Adhes. 24 (2004) 449–453. doi:10.1016/j.ijadhadh.2003.12.003.

[15] D.A. Shnawah, M.F.M. Sabri, I.A. Badruddin, A review on thermal cycling and drop impact reliability of SAC solder joint in portable electronic products, Microelectron. Reliab. 52 (2012) 90–99. doi:10.1016/j.microrel.2011.07.093.

[16] Shuangyan Xu, D.A. Dillard, Determining the impact resistance of electrically conductive adhesives using a falling wedge test, IEEE Trans. Components Packag. Technol. 26 (2003) 554–562. doi:10.1109/TCAPT.2003.817646.

[17] B. Meschi Amoli, J. Trinidad, A. Hu, Y.N. Zhou, B. Zhao, Highly electrically conductive adhesives using silver nanoparticle (Ag NP)-decorated graphene: the effect of NPs sintering on the electrical conductivity improvement, J. Mater. Sci. Mater. Electron. 26 (2015) 590–600. doi:10.1007/s10854-014-2440-y.

[18] B. Meschi Amoli, J. Trinidad, G. Rivers, S. Sy, P. Russo, A. Yu, N.Y. Zhou, B. Zhao, SDS-stabilized graphene nanosheets for highly electrically conductive adhesives, Carbon N. Y. 91 (2015) 188–199. doi:10.1016/j.carbon.2015.04.039.

[19] B.M. Amoli, E. Marzbanrad, A. Hu, Y.N. Zhou, B. Zhao, Electrical Conductive Adhesives Enhanced with High-Aspect-Ratio Silver Nanobelts, Macromol. Mater. Eng. 299 (2014) 739–747. doi:10.1002/mame.201300295.

[20] H. WU, X. WU, M. GE, G. ZHANG, Y. WANG, J. JIANG, Properties investigation on isotropical conductive adhesives filled with silver coated carbon nanotubes, Compos. Sci. Technol. 67 (2007) 1182–1186. doi:10.1016/j.compscitech.2006.05.010.

[21] J. Trinidad, K. Liew, A. Cholewinski, B. Zhao, The Negative Effect of Residual Solvent on the Lap-Shear Strength of SDS-Decorated Graphene Hybrid ECAs, (In preparation for publishing)

[22] J. Du, H.-M. Cheng, The Fabrication, Properties, and Uses of Graphene/Polymer Composites, Macromol. Chem. Phys. 213 (2012) 1060–1077. doi:10.1002/macp.201200029.

[23] P.Y. Huang, C.S. Ruiz-Vargas, A.M. van der Zande, W.S. Whitney, M.P. Levendorf, J.W. Kevek, S. Garg, J.S. Alden, C.J. Hustedt, Y. Zhu, J. Park, P.L. McEuen, D. a Muller, Grains and grain boundaries in single-layer graphene atomic patchwork quilts., Nature. 469 (2011) 389–92. doi:10.1038/nature09718.

[24] S.G. Prolongo, A. Jimenez-Suarez, R. Moriche, A. Ureña, In situ processing of epoxy composites reinforced with graphene nanoplatelets, Compos. Sci. Technol. 86 (2013) 185–191. doi:10.1016/j.compscitech.2013.06.020.

[25] Y.J. Wan, L.C. Tang, D. Yan, L. Zhao, Y.B. Li, L. Bin Wu, J.X. Jiang, G.Q. Lai, Improved dispersion and interface in the graphene/epoxy composites via a facile surfactant-assisted process, Compos. Sci. Technol. 82 (2013) 60–68. doi:10.1016/j.compscitech.2013.04.009.

[26] D. Galpaya, M. Wang, G. George, N. Motta, E. Waclawik, C. Yan, Preparation of graphene oxide/epoxy nanocomposites with significantly improved mechanical properties, J. Appl. Phys. 116 (2014) 53518. doi:10.1063/1.4892089.

[27] J. Trinidad, B.M. Amoli, W. Zhang, R. Pal, B. Zhao, Effect of SDS decoration of graphene on the rheological and electrical properties of graphene-filled epoxy/Ag composites, J. Mater. Sci. Mater. Electron. (2016). doi:10.1007/s10854-016-5434-0.

[28] P.T. Vianco, Y. Feng, Electronic Packaging: Solder Mounting Technologies, in: Ref. Modul. Mater. Sci. Mater. Eng., Elsevier, 2016: pp. 2705–2715. doi:10.1016/B978-0-12-803581-8.10099-2.

[29] P.T. Vianco, D.R. Frear, Issues in the replacement of lead-bearing solders, JOM. 45 (1993) 14–19. doi:10.1007/BF03222374.

[30] J.F. Bard, R.W. Clayton, T.A. Feo, Machine setup and component placement in printed circuit board assembly, Int. J. Flex. Manuf. Syst. 6 (1994) 5–31. doi:10.1007/BF01324873.

[31] C. Basaran, R. Chandaroy, Mechanics of Pb40/Sn60 near-eutectic solder alloys subjected to vibrations, Appl. Math. Model. 22 (1998) 601–627. doi:10.1016/S0307-904X(98)10059-8.

[32] I. Mir, D. Kumar, Recent advances in isotropic conductive adhesives for electronics packaging applications, Int. J. Adhes. Adhes. 28 (2008) 362–371. doi:10.1016/j.ijadhadh.2007.10.004.

[33] R.H. Tien, G.E. Geiger, A Heat-Transfer Analysis of the Solidification of a Binary Eutectic System, J. Heat Transfer. 89 (1967) 230. doi:10.1115/1.3614365.

[34] W.-L. Jang, T.-S. Wang, Y.-F. Lai, K.-L. Lin, Y.-S. Lai, The performance and fracture mechanism of solder joints under mechanical reliability test, Microelectron. Reliab. 52 (2012) 1428–1434. doi:10.1016/j.microrel.2012.03.011.

[35] H. Li, C.P. Wong, A Reworkable Epoxy Resin for Isotropically Conductive Adhesive, IEEE Trans. Adv. Packag. 27 (2004) 165–172. doi:10.1109/TADVP.2004.824939.

[36] M.A. Uddin, M.O. Alam, Y.C. Chan, H.P. Chan, Adhesion strength and contact resistance of flip chip on flex packages - Effect of curing degree of anisotropic conductive film, Microelectron. Reliab. 44 (2004) 505–514. doi:10.1016/S0026-2714(03)00185-9.

[37] J.E. Morris, J. Lee, Drop Test Performance of Isotropic Electrically Conductive Adhesives, J. Adhes. Sci. Technol. 22 (2008) 1699–1716. doi:10.1163/156856108X320546.

[38] F. Tan, X. Qiao, J. Chen, H. Wang, Effects of coupling agents on the properties of epoxy-based electrically conductive adhesives, Int. J. Adhes. Adhes. 26 (2006) 406–413. doi:10.1016/j.ijadhadh.2005.06.005.

[39] Z. Zhang, X. Chen, H. Yang, H. Fu, F. Xiao, Electrically conductive adhesives with sintered silver nanowires, in: 2009 Int. Conf. Electron. Packag. Technol. High Density Packag., IEEE, 2009: pp. 834–837. doi:10.1109/ICEPT.2009.5270629.

[40] E. Sancaktar, L. Bai, Electrically Conductive Epoxy Adhesives, Polymers (Basel). 3 (2011) 427–466. doi:10.3390/polym3010427.

[41] M.J. Yim, Y. Li, K. Moon, K.W. Paik, C.P. Wong, Review of Recent Advances in Electrically Conductive Adhesive Materials and Technologies in Electronic Packaging, J. Adhes. Sci. Technol. 22 (2008) 1593–1630. doi:10.1163/156856108X320519.

[42] S.-L.F. Huann-Wu Chiang, Cho-Liang Chung, Liu-Chin Chen, Yi Li, C.P. Wong, Processing and shape effects on silver paste, J. Adhes. Sci. Technol. 19 (2005) 565–578. doi:10.1163/1568561054352487.

[43] H. Wolfson, G. Elliot, Electrically Conducting cements containing epoxy resins and silver, US patent 2774, 747, 1957. https://patentimages.storage.googleapis.com/pdfs/US2807013.pdf.

[44] H.-W. Cui, J.-T. Jiu, S. Nagao, T. Sugahara, K. Suganuma, H. Uchida, Using Ozawa method to study the curing kinetics of electrically conductive adhesives, J. Therm. Anal. Calorim. 117 (2014) 1365–1373. doi:10.1007/s10973-014-3902-4.

[45] F. Hussain, Polymer-matrix Nanocomposites, Processing, Manufacturing, and Application: An Overview, J. Compos. Mater. 40 (2006) 1511–1575. doi:10.1177/0021998306067321.

[46] S. Stankovich, D.A. Dikin, G.H.B. Dommett, K.M. Kohlhaas, E.J. Zimney, E.A. Stach, R.D. Piner, S.T. Nguyen, R.S. Ruoff, Graphene-based composite materials, Nature. 442 (2006) 282–286. doi:10.1038/nature04969.

[47] W.-J. Jeong, H. Nishikawa, D. Itou, T. Takemoto, Electrical Characteristics of a New Class of Conductive Adhesive, Mater. Trans. 46 (2005) 2276–2281. doi:10.2320/matertrans.46.2276.

[48] R. Zhang, W. Lin, K.S. Moon, C.P. Wong, Fast preparation of printable highly conductive polymer nanocomposites by thermal decomposition of silver carboxylate and sintering of silver nanoparticles, ACS Appl. Mater. Interfaces. 2 (2010) 2637–2645. doi:10.1021/am100456m.

[49] R. Zhang, K. Moon, W. Lin, C.P. Wong, Preparation of highly conductive polymer nanocomposites by low temperature sintering of silver nanoparticles, J. Mater. Chem. 20 (2010) 2018–2023. doi:10.1039/b921072e.

[50] H. Gao, L. Liu, K. Liu, Y. Luo, D. Jia, J. Lu, Preparation of highly conductive adhesives by in situ generated and sintered silver nanoparticles during curing process, J. Mater. Sci. Mater. Electron. 23 (2011) 22–30. doi:10.1007/s10854-011-0388-8.

[51] B.M. Amoli, S. Gumfekar, A. Hu, Y.N. Zhou, B. Zhao, Thiocarboxylate functionalization of silver nanoparticles: effect of chain length on the electrical conductivity of nanoparticles and their polymer composites, J. Mater. Chem. 22 (2012) 20048. doi:10.1039/c2jm33280a.

[52] B. Meschi Amoli, A. Hu, N.Y. Zhou, B. Zhao, Recent progresses on hybrid micro–nano filler systems for electrically conductive adhesives (ECAs) applications, J. Mater. Sci. Mater. Electron. 26 (2015) 4730–4745. doi:10.1007/s10854-015-3016-1.

[53] Y. Kornyushin, Thermodynamic theory of sintering and swelling, Metallofiz. I Noveishie Tekhnologii. 29 (2007) 949–970.

[54] B. Wiley, Y. Sun, B. Mayers, Y. Xia, Shape-controlled synthesis of metal nanostructures: The case of silver, Chem. - A Eur. J. 11 (2005) 454–463. doi:10.1002/chem.200400927.

[55] Lilei Ye, Zonghe Lai, Johan Liu, A. Tholen, Effect of Ag particle size on electrical conductivity of isotropically conductive adhesives, IEEE Trans. Electron. Packag. Manuf. 22 (1999) 299–302. doi:10.1109/6104.816098.

[56] D. Chen, X. Qiao, X. Qiu, F. Tan, J. Chen, R. Jiang, Effect of silver nanostructures on the resistivity of electrically conductive adhesives composed of silver flakes, J. Mater. Sci. Mater. Electron. 21 (2010) 486–490. doi:10.1007/s10854-009-9943-y.

[57] Z.X. Zhang, X.Y. Chen, F. Xiao, The sintering behavior of electrically conductive adhesives filled with surface modified silver nanowires., J. Adhes. Sci. Technol. 25 (2011) 1465–1480. doi:10.1163/016942410X549924.

[58] D. Lu, C.P. Wong, Q.K. Tong, A fundamental study on silver flakes for conductive adhesives, Adv. Packag. Mater. 1998. Proceedings. 1998 4th Int. Symp. (1998) 256–260. doi:10.1109/ISAPM.1998.664466.

[59] C.P. Wong, D. Lu, Q.K. Tong, Lubricants of silver fillers for conductive adhesive applications, Proc. 3rd Int. Conf. Adhes. Join. Coat. Technol. Electron. Manuf. 1998 (Cat. No.98EX180). (1998) 184–192. doi:10.1109/ADHES.1998.742025.

[60] F. Tan, X. Qiao, J. Chen, Removal of chemisorbed lubricant on the surface of silver flakes by chemicals, Appl. Surf. Sci. 253 (2006) 703–707. doi:10.1016/j.apsusc.2005.12.163.

[61] A.J. Lovinger, Development of Electrical Conduction in Silver-filled Epoxy Adhesives, J. Adhes. 10 (1979) 1–15. doi:10.1080/00218467908544607.

[62] I. Balberg, A comprehensive picture of the electrical phenomena in carbon black-polymer composites, Carbon N. Y. 40 (2002) 139–143. doi:10.1016/S0008-6223(01)00164-6.

[63] L. Flandin, T. Prasse, R. Schueler, K. Schulte, W. Bauhofer, J.-Y. Cavaille, Anomalous percolation transition in carbon-black–epoxy composite materials, Phys. Rev. B. 59 (1999) 14349–14355. doi:10.1103/PhysRevB.59.14349.

[64] F. Gubbels, S. Blacher, E. Vanlathem, R. Jérôme, R. Deltour, F. Brouers, P. Teyssié, Design of electrical conductive composites: key role of the morphology on the electrical properties of carbon black filled polymer blends, Macromolecules. 28 (1995) 1559–1566. doi:10.1021/ma00109a030.

[65] K. Dai, X. Bin Xu, Z.M. Li, Electrically conductive carbon black (CB) filled in situ microfibrillar poly(ethylene terephthalate) (PET)/polyethylene (PE) composite with a selective CB distribution, Polymer (Guildf). 48 (2007) 849–859. doi:10.1016/j.polymer.2006.12.026.

[66] I. Novák, I. Krupa, I. Janigová, Hybrid electro-conductive composites with improved toughness, filled by carbon black, Carbon N. Y. 43 (2005) 841–848. doi:10.1016/j.carbon.2004.11.019.

[67] F. El-Tantawy, K. Kamada, H. Ohnabe, In situ network structure, electrical and thermal properties of conductive epoxy resin-carbon black composites for electrical heater applications, Mater. Lett. 56 (2002) 112–126. doi:10.1016/S0167-577X(02)00401-9.

[68] J. Sumfleth, X.C. Adroher, K. Schulte, Synergistic effects in network formation and electrical properties of hybrid epoxy nanocomposites containing multi-wall carbon nanotubes and carbon black, J. Mater. Sci. 44 (2009) 3241–3247. doi:10.1007/s10853-009-3434-7.

[69] C.K. Leong, D.D.L. Chung, Improving the electrical and mechanical behavior of electrically conductive paint by partial replacement of silver by carbon black, J. Electron. Mater. 35 (2006) 118–122. doi:10.1007/s11664-006-0193-y.

[70] R. Schueler, R. Schueler, J. Petermann, J. Petermann, K. Schulte, K. Schulte, H. Wentzel, H. Wentzel, Agglomeration and electrical percolation behavior of carbon black dispersed in epoxy resin, J. Appl. Polym. Sci. 63 (1997) 1741–1746. doi:10.1002/(SICI)1097-4628(19970328)63:13<1741::AID-APP5>3.3.CO;2-S.

[71] P.-C. Ma, M.-Y. Liu, H. Zhang, S.-Q. Wang, R. Wang, K. Wang, Y.-K. Wong, B.-Z. Tang, S.-H. Hong, K.-W. Paik, J.-K. Kim, Enhanced Electrical Conductivity of Nanocomposites Containing Hybrid Fillers of Carbon Nanotubes and Carbon Black, ACS Appl. Mater. Interfaces. 1 (2009) 1090–1096. doi:10.1021/am9000503.

[72] S.P. Bao, S.C. Tjong, Mechanical behaviors of polypropylene/carbon nanotube nanocomposites: The effects of loading rate and temperature, Mater. Sci. Eng. A. 485 (2008) 508–516. doi:10.1016/j.msea.2007.08.050.

[73] F. Marcq, P. Demont, P. Monfraix, A. Peigney, C. Laurent, T. Falat, F. Courtade, T. Jamin, Carbon nanotubes and silver flakes filled epoxy resin for new hybrid conductive adhesives, Microelectron. Reliab. 51 (2011) 1230–1234. doi:10.1016/j.microrel.2011.03.020.

[74] C. Schilde, M. Schlömann, A. Overbeck, S. Linke, A. Kwade, Thermal, mechanical and electrical properties of highly loaded CNT-epoxy composites - A model for the electric conductivity, Compos. Sci. Technol. 117 (2015) 183–190. doi:10.1016/j.compscitech.2015.06.013.

[75] S.A. Sydlik, J.H. Lee, J.J. Walish, E.L. Thomas, T.M. Swager, Epoxy functionalized multi-walled carbon nanotubes for improved adhesives, Carbon N. Y. 59 (2013) 109–120. doi:10.1016/j.carbon.2013.02.061.

[76] M.L. Gupta, S.A. Sydlik, J.M. Schnorr, D.J. Woo, S. Osswald, T.M. Swager, D. Raghavan, The effect of mixing methods on the dispersion of carbon nanotubes during the solvent-free processing of multiwalled carbon nanotube/epoxy composites, J. Polym. Sci. Part B Polym. Phys. 51 (2013) 410–420. doi:10.1002/polb.23225.

[77] K. Liu, S. Chen, Y. Luo, D. Jia, H. Gao, G. Hu, L. Liu, Edge-functionalized graphene as reinforcement of epoxy-based conductive composite for electrical interconnects, Compos. Sci. Technol. 88 (2013) 84–91. doi:10.1016/j.compscitech.2013.08.032.

[78] C. Mette, E. Stammen, K. Dilger, Challenges in joining conductive adhesives in structural application-Effects of tolerances and temperature, Int. J. Adhes. Adhes. 67 (2016) 49–53. doi:10.1016/j.ijadhadh.2015.12.025.

[79] X. Peng, F. Tan, W. Wang, X. Qiu, F. Sun, X. Qiao, J. Chen, Conductivity improvement of silver flakes filled electrical conductive adhesives via introducing silver-graphene nanocomposites, J. Mater. Sci. Mater. Electron. 25 (2014) 1149–1155. doi:10.1007/s10854-013-1671-7.

[80] R. Verdejo, M.M. Bernal, L.J. Romasanta, M. a. Lopez-Manchado, Graphene filled polymer nanocomposites, J. Mater. Chem. 21 (2011) 3301–3310. doi:10.1039/c0jm02708a.

[81] R.J. Young, I.A. Kinloch, L. Gong, K.S. Novoselov, The mechanics of graphene nanocomposites: A review, Compos. Sci. Technol. 72 (2012) 1459–1476. doi:10.1016/j.compscitech.2012.05.005.

[82] M. a. Rafiee, W. Lu, A. V. Thomas, A. Zandiatashbar, J. Rafiee, J.M. Tour, N. a. Koratkar, Graphene nanoribbon composites, ACS Nano. 4 (2010) 7415–7420. doi:10.1021/nn102529n.

[83] C. Jin, H. Lan, L. Peng, K. Suenaga, S. Iijima, Deriving carbon atomic chains from graphene, Phys. Rev. Lett. 102 (2009) 1–4. doi:10.1103/PhysRevLett.102.205501.

[84] S. Chatterjee, F. a Nüesch, B.T.T. Chu, Comparing carbon nanotubes and graphene nanoplatelets as reinforcements in polyamide 12 composites., Nanotechnology. 22 (2011) 275714. doi:10.1088/0957-4484/22/27/275714.

[85] M. Fang, K. Wang, H. Lu, Y. Yang, S. Nutt, Covalent polymer functionalization of graphene nanosheets and mechanical properties of composites, J. Mater. Chem. 19 (2009) 7098. doi:10.1039/b908220d.

[86] M. Kotaki, K. Wang, M.L. Toh, L. Chen, Electrically Conductive Epoxy / Clay / Vapor Grown Carbon Fiber Hybrids, Communications. (2006) 908–911.

[87] K.-S. Kim, I.-Y. Jeon, S.-N. Ahn, Y.-D. Kwon, J.-B. Baek, Edge-functionalized graphene-like platelets as a co-curing agent and a nanoscale additive to epoxy resin, J. Mater. Chem. 21 (2011) 7337. doi:10.1039/c0jm03504a.

[88] S.P. Gumfekar, A. Chen, B. Zhao, Silver-polyaniline-epoxy electrical conductive adhesives - A percolation threshold analysis, 2011 IEEE 13th Electron. Packag. Technol. Conf. EPTC 2011. (2011) 180–184. doi:10.1109/EPTC.2011.6184411.

[89] S. Desvergne, A. Gasse, A. Pron, Electrical characterization of polyaniline-based adhesive blends, J. Appl. Polym. Sci. 120 (2011) 1965–1973. doi:10.1002/app.33292.

[90] I.A. Mir, D. Kumar, Development of Polyaniline / Epoxy Composite as a Prospective Solder Replacement Material, Int. J. Polym. Mater. Polym. Biomater. 59 (2010) 994–1007. doi:10.1080/00914037.2010.504150.

[91] I.A. Mir, D. Kumar, Development of Polypyrrole/Epoxy Composites as Isotropically Conductive Adhesives, J. Adhes. 86 (2010) 447–462. doi:10.1080/00218461003704519.

[92] W. Zhang, Y. Zhou, K. Feng, J. Trinidad, A. Yu, B. Zhao, Morphologically Controlled Bioinspired Dopamine-Polypyrrole Nanostructures with Tunable Electrical Properties, Adv. Electron. Mater. 1 (2015) 1500205. doi:10.1002/aelm.201500205.

[93] F. Kuechenmeister, E. Meusel, Polypyrrole as an interlayer for bonding conductive adhesives to activated aluminum bond pads, IEEE Trans. Components, Packag. Manuf. Technol. Part A. 20 (1997) 9–14. doi:10.1109/95.558538.

[94] L. Groenendaal, F. Jonas, D. Freitag, H. Pielartzik, J.R. Reynolds, Poly(3,4-ethylenedioxythiophene) and Its Derivatives: Past, Present, and Future, Adv. Mater. 12 (2000) 481–494. doi:10.1002/(SICI)1521-4095(200004)12:7<481::AID-ADMA481>3.0.CO;2-C.

[95] W. Zhang, F.K. Yang, Z. Pan, J. Zhang, B. Zhao, Bio-inspired dopamine functionalization of polypyrrole for improved adhesion and conductivity, Macromol. Rapid Commun. 35 (2014) 350–354. doi:10.1002/marc.201300761.

[96] S.R. Broadbent, J.M. Hammersley, Percolation processes, Math. Proc. Cambridge Philos. Soc. 53 (1957) 629. doi:10.1017/S0305004100032680.

[97] A. Mikrajuddin, F.G. Shi, S. Chungpaiboonpatana, K. Okuyama, C. Davidson, J.M. Adams, Onset of electrical conduction in isotropic conductive adhesives: A general theory, Mater. Sci. Semicond. Process. 2 (1999) 309–319. doi:10.1016/S1369-8001(99)00035-9.

[98] N. Lebovka, M. Lisunova, Y.P. Mamunya, N. Vygornitskii, Scaling in percolation behaviour in conductive–insulating composites with particles of different size, J. Phys. D. Appl. Phys. 39 (2006) 2264–2271. doi:10.1088/0022-3727/39/10/040.

[99] B.E. Kilbride, J.N. Coleman, J. Fraysse, P. Fournet, M. Cadek, A. Drury, S. Hutzler, S. Roth, W.J. Blau, Experimental observation of scaling laws for alternating current and direct current conductivity in polymer-carbon nanotube composite thin films, J. Appl. Phys. 92 (2002) 4024–4030. doi:10.1063/1.1506397.

[100] J.K.W. Sandler, J.E. Kirk, I.A. Kinloch, M.S.P. Shaffer, A.H. Windle, Ultra-low electrical percolation threshold in carbon-nanotube-epoxy composites, Polymer (Guildf). 44 (2003) 5893–5899. doi:10.1016/S0032-3861(03)00539-1.

[101] L. Li, J.E. Morris, S. Member, Electrical Conduction Models for Isotropically Conductive Adhesive Joints, 20 (1997) 3–8.

[102] J.-S. Chen, C.K. Ober, M.D. Poliks, Characterization of thermally reworkable thermosets: materials for environmentally friendly processing and reuse, Polymer (Guildf). 43 (2002) 131–139. doi:10.1016/S0032-3861(01)00605-X.

[103] S.L. Buchwalter, L.L. Kosbar, Cleavable epoxy resins: design for disassembly of a thermoset., J. Polym. Sci. Part A Polym. Chem. 34 (1996) 249–260. doi:10.1002/(SICI)1099-0518(19960130)34:2<249::AID-POLA11>3.0.CO;2-Q.

[104] N.I. Khan, S. Halder, M.S. Goyat, Effect of epoxy resin and hardener containing microcapsules on healing efficiency of epoxy adhesive based metal joints, Mater. Chem. Phys. 171 (2016) 267–275. doi:10.1016/j.matchemphys.2016.01.017.

[105] B. Bilyeu, W. Brostow, K.P. Menard, Epoxy Thermosets and Their Applications I: Chemical Structures and Applications, J. Mater. Educ. 22 (1999) 107–129.

[106] J.R. Fried, Polymer Science and Technology 3rd Edition, Pearson Education, Cambridge, 2012. http://ebooks.cambridge.org/ref/id/CBO9781107415324A009.

[107] C.J. Kloxin, T.F. Scott, B.J. Adzima, C.N. Bowman, Covalent Adaptable Networks (CANs): A Unique Paradigm in Cross-Linked Polymers, Macromolecules. 43 (2010) 2643–2653. doi:10.1021/ma902596s.

[108] J.S. Chen, C.K. Ober, M.D. Poliks, Y. Zhang, U. Wiesner, C. Cohen, Controlled degradation of epoxy networks: Analysis of crosslink density and glass transition temperature changes in thermally reworkable thermosets, Polymer (Guildf). 45 (2004) 1939–1950. doi:10.1016/j.polymer.2004.01.011.

[109] P.I. Engelberg, G.C. Tesoro, Mechanical and thermal properties of epoxy resins with reversible crosslinks, Polym. Eng. Sci. 30 (1990) 303–307. doi:10.1002/pen.760300507.

[110] L. González, X. Ramis, J.M. Salla, A. Mantecón, A. Serra, The degradation of new thermally degradable thermosets obtained by cationic curing of mixtures of DGEBA and 6,6-dimethyl (4,8-dioxaspiro[2.5]octane-5,7-dione), Polym. Degrad. Stab. 92 (2007) 596–604. doi:10.1016/j.polymdegradstab.2007.01.007.

[111] M.M. Cross, Rheology of non-Newtonian fluids: A new flow equation for pseudoplastic systems, J. Colloid Sci. 20 (1965) 417–437. doi:10.1016/0095-8522(65)90022-X.

[112] J. Singh, M. Rudman, H.M. Blackburn, A. Chryss, L. Pullum, L.J.W. Graham, The importance of rheology characterization in predicting turbulent pipe flow of generalized Newtonian fluids, J. Nonnewton. Fluid Mech. 232 (2016) 11–21. doi:10.1016/j.jnnfm.2016.03.013.

[113] S.M. Richardson, NON-NEWTONIAN FLUIDS, in: A-to-Z Guid. to Thermodyn. Heat Mass Transf. Fluids Eng., Begell House, 2014: pp. 1–6. doi:10.1615/AtoZ.n.non-newtonian_fluids.

[114] P. Lugt, Grease Lubrication Mechanisms in Rolling Bearing Systems, Evol. Bus. Technol. Mag. SKF. (2013) 36–39. http://evolution.skf.com/grease-lubrication-mechanisms-in-rolling-bearing-systems/.

[115] R. Krishnamoorti, R.A. Vaia, E.P. Giannelis, Structure and Dynamics of Polymer-Layered Silicate Nanocomposites, Chem. Mater. 8 (1996) 1728–1734. doi:10.1021/cm960127g.

[116] J. Zhu, S. Wei, A. Yadav, Z. Guo, Rheological behaviors and electrical conductivity of epoxy resin nanocomposites suspended with in-situ stabilized carbon nanofibers, Polymer (Guildf). 51 (2010) 2643–2651. doi:10.1016/j.polymer.2010.04.019.

[117] R. Kotsilkova, D. Nesheva, I. Nedkov, E. Krusteva, S. Stavrev, Rheological, electrical, and microwave properties of polymers with nanosized carbon particles, J. Appl. Polym. Sci. 92 (2004) 2220–2227. doi:10.1002/app.20240.

[118] K.L. White, S. Hawkins, M. Miyamoto, A. Takahara, H.-J. Sue, Effects of aspect ratio and concentration on rheology of epoxy suspensions containing model plate-like nanoparticles, Phys. Fluids. 27 (2015) 123306. doi:10.1063/1.4937145.

[119] T. Hattori, A stress-singularity-parameter approach for evaluating the adhesive strength of single-lap joints, JSME Int. J. 34 (1991) 326–331. doi:10.1299/kikaia.56.618.

[120] H.S. da Costa Mattos, E.M. Sampaio, A.H. Monteiro, Static failure analysis of axially loaded aluminium–epoxy butt joints, Int. J. Adhes. Adhes. 30 (2010) 774–780. doi:10.1016/j.ijadhadh.2010.08.004.

[121] R. Quispe Rodríguez, W.P. de Paiva, P. Sollero, M.R. Bertoni Rodrigues, É.L. de Albuquerque, Failure criteria for adhesively bonded joints, Int. J. Adhes. Adhes. 37 (2012) 26–36. doi:10.1016/j.ijadhadh.2012.01.009.

[122] S.C. Her, Stress analysis of adhesively-bonded lap joints, Compos. Struct. 47 (1999) 673–678. doi:10.1016/S0263-8223(00)00052-0.

[123] ASTM, ASTM D1002: Standard Test Method for Apparent Shear Strength of Single-Lap-Joint Adhesively Bonded Metal Specimens by Tension Loading (Metal-to-Metal), Standards. (2005) 1–5.

[124] R.B. Thompson, K.O. Rasmussen, T. Lookman, Elastic moduli of multiblock copolymers in the lamellar phase, J. Chem. Phys. 120 (2004) 3990. doi:10.1063/1.1643899.

[125] S. Karthiyayini, G. Amaranath, Debye Temperature and the Structure of Nanocrystalline materials, Int. J. Emerg. Trends Electr. Electron. xx (2015) 142–144.

[126] A.J. Owen, I. Koller, A note on the young's modulus of isotropic two-component materials, Polymer (Guildf). 37 (1996) 527–530. doi:10.1016/0032-3861(96)82926-0.

[127] W.C. Oliver, G.M. Pharr, An improved technique for determining hardness and elastic modulus using load and displacement sensing indentation experiments, J. Mater. Res. 7 (1992) 1564–1583. doi:10.1557/JMR.1992.1564.

[128] K.R. Shull, Contact mechanics and the adhesion of soft solids, Elsevier B.V., 2002.

[129] K. Zeng, K. Breder, D.J. Rowcliffe, C. Herrstrom, Elastic modulus determined by Hertzian indentation, J. Mater. Sci. 27 (1992) 3789–3792. doi:10.1007/BF00545457.

[130] T. Filleter, J.L. McChesney, A. Bostwick, E. Rotenberg, K. V. Emtsev, T. Seyller, K. Horn, R. Bennewitz, Friction and dissipation in epitaxial graphene films, Phys. Rev. Lett. 102 (2009) 1–4. doi:10.1103/PhysRevLett.102.086102.

[131] J. Lin, L. Wang, G. Chen, Modification of Graphene Platelets and their Tribological Properties as a Lubricant Additive, Tribol. Lett. 41 (2011) 209–215. doi:10.1007/s11249-010-9702-5.

[132] J. Koo, C. Kleinstreuer, Viscous dissipation effects in microtubes and microchannels, Int. J. Heat Mass Transf. 47 (2004) 3159–3169. doi:10.1016/j.ijheatmasstransfer.2004.02.017.

[133] R.M. Bowman, K.B. Eisenthal, The role of translational friction in isomerization reactions, Chem. Phys. Lett. 155 (1989) 99–101. doi:10.1016/S0009-2614(89)87367-1.

[134] M. Pudas, N. Halonen, P. Granat, J. Vähäkangas, Gravure printing of conductive particulate polymer inks on flexible substrates, Prog. Org. Coatings. 54 (2005) 310–316. doi:10.1016/j.porgcoat.2005.07.008.

[135] K. LAU, M. LU, H. CHEUNG, F. SHENG, H. LI, Thermal and mechanical properties of single-walled carbon nanotube bundle-reinforced epoxy nanocomposites: the role of solvent for nanotube dispersion, Compos. Sci. Technol. 65 (2005) 719–725. doi:10.1016/j.compscitech.2004.10.005.

[136] F.H. Quina, P.M. Nassar, J.B.S. Bonilha, B.L. Bales, Growth of sodium dodecyl sulfate micelles with detergent concentration, J. Phys. Chem. 99 (1995) 17028–17031. doi:10.1021/j100046a031.

[137] P. Muller, Glossary of terms used in physical organic chemistry (IUPAC Recommendations 1994), Pure Appl. Chem. 66 (1994) 2014. doi:10.1351/pac199466051077.

[138] R. McKennell, Cone-Plate Viscometer, Anal. Chem. 28 (1956) 1710–1714. doi:10.1021/ac60119a021.

[139] S. Biggs, J. Selb, F. Candau, Effect of surfactant on the solution properties of hydrophobically modified polyacrylamide, Langmuir. 8 (1992) 838–847. doi:10.1021/la00039a018.

[140] S. Nilsson, K. Thuresson, P. Hansson, B. Lindman, Mixed Solutions of Surfactant and Hydrophobically Modified Polymer. Controlling Viscosity with Micellar Size, J. Phys. Chem. B. 102 (1998) 7099–7105. doi:10.1021/jp9812379.

[141] A. Zupančič, R. Lapasin, M. Sumer, Rheological characterisation of shear thickening TiO2 suspensions in low molecular polymer solution, Prog. Org. Coatings. 30 (1997) 67–78. doi:10.1016/S0300-9440(96)00670-4.

[142] a. Srivastava, A. Majumdar, B.S. Butola, Improving the Impact Resistance of Textile Structures by using Shear Thickening Fluids: A Review, Crit. Rev. Solid State Mater. Sci. 37 (2012) 115–129. doi:10.1080/10408436.2011.613493.

[143] J. Bender, Reversible shear thickening in monodisperse and bidisperse colloidal dispersions, J. Rheol. (N. Y. N. Y). 40 (1996) 899. doi:10.1122/1.550767.

[144] M. Wang, X. Fan, W. Thitsartarn, C. He, Rheological and mechanical properties of epoxy/clay nanocomposites with enhanced tensile and fracture toughnesses, Polymer (Guildf). 58 (2015) 43–52. doi:10.1016/j.polymer.2014.12.042.

[145] D.E. Smith, H.P. Babcock, S. Chu, Single-polymer dynamics in steady shear flow., Science. 283 (1999) 1724–7. doi:10.1126/science.283.5408.1724.

[146] D. Wu, Y. Cheng, S. Feng, Z. Yao, M. Zhang, Crystallization Behavior of Polylactide/Graphene Composites, Ind. Eng. Chem. Res. 52 (2013) 6731–6739. doi:10.1021/ie4004199.

[147] B. Briscoe, P. Luckham, S. Zhu, The effects of hydrogen bonding upon the viscosity of aqueous poly(vinyl alcohol) solutions, Polymer (Guildf). 41 (2000) 3851–3860. doi:10.1016/S0032-3861(99)00550-9.

[148] W.J. Frith, P. Haene, R. Buscall, J. Mewis, Shear thickening in model suspensions of sterically stabilized particles Shear thickening in model suspensions of sterically stabilized particles, J. Rheol. (N. Y. N. Y). 40 (1996) 531–547. doi:10.1122/1.550791.

[149] J. Noh, D. Yeom, C. Lim, H. Cha, J. Han, J. Kim, Y. Park, V. Subramanian, G. Cho, Scalability of roll-to-roll gravure-printed electrodes on plastic foils, IEEE Trans. Electron. Packag. Manuf. 33 (2010) 275–283. doi:10.1109/TEPM.2010.2057512.

[150] H.-V. Nguyen, E. Andreassen, H. Kristiansen, K.E. Aasmundtveit, Die Shear Testing of a Novel Isotropic Conductive Adhesive—Epoxy Filled With Metal-Coated Polymer Spheres, IEEE Trans. Components, Packag. Manuf. Technol. 3 (2013) 1084–1093. doi:10.1109/TCPMT.2013.2259166.

[151] H. Jiang, K.-S. Moon, J. Lu, C.P. Wong, Conductivity enhancement of nano silver-filled conductive adhesives by particle surface functionalization, J. Electron. Mater. 34 (2005) 1432–1439. doi:10.1007/s11664-005-0202-6.

[152] U. Khan, K. Ryan, W.J. Blau, J.N. Coleman, The effect of solvent choice on the mechanical properties of carbon nanotube-polymer composites, Compos. Sci. Technol. 67 (2007) 3158–3167. doi:10.1016/j.compscitech.2007.04.015.

[153] J.N. Coleman, U. Khan, W.J. Blau, Y.K. Gun'ko, Small but strong: A review of the mechanical properties of carbon nanotube-polymer composites, Carbon N. Y. 44 (2006) 1624–1652. doi:10.1016/j.carbon.2006.02.038.

[154] M. Zwolinski, J. Hickman, H. Rubin, Y. Zaks, S. McCarthy, T. Hanlon, P. Arrowsmith, A. Chaudhuri, R. Hermansen, S. Lan, D. Napp, Electrically conductive adhesives for surface mount solder replacement, IEEE Trans. Components, Packag. Manuf. Technol. Part C. 19 (1996) 241–250. doi:10.1109/3476.558550.

[155] G. Rivers, A. Rogalsky, P. Lee-Sullivan, B. Zhao, Thermal analysis of epoxy-based nanocomposites: Have solvent effects been overlooked?, J. Therm. Anal. Calorim. 119 (2015) 797–805. doi:10.1007/s10973-013-3613-2.

[156] ASTM, ASTM D638: Standard test method for tensile properties of plastics, Standards. (2013) 1–16.

[157] L. Jin, T. Wang, Z.-Q. Feng, M.K. Leach, J. Wu, S. Mo, Q. Jiang, A facile approach for the fabrication of core–shell PEDOT nanofiber mats with superior mechanical properties and biocompatibility, J. Mater. Chem. B. 1 (2013) 1818. doi:10.1039/c3tb00448a.

[158] R. Balint, N.J. Cassidy, S.H. Cartmell, Conductive polymers: Towards a smart biomaterial for tissue engineering, Acta Biomater. 10 (2014) 2341–2353. doi:10.1016/j.actbio.2014.02.015.

[159] R. Yue, J. Xu, Poly(3,4-ethylenedioxythiophene) as promising organic thermoelectric materials: A mini-review, Synth. Met. 162 (2012) 912–917. doi:10.1016/j.synthmet.2012.04.005.

[160] K. Sun, S. Zhang, P. Li, Y. Xia, X. Zhang, D. Du, F.H. Isikgor, J. Ouyang, Review on application of PEDOTs and PEDOT:PSS in energy conversion and storage devices, J. Mater. Sci. Mater. Electron. 26 (2015) 4438–4462. doi:10.1007/s10854-015-2895-5.

[161] X. Crispin, F.L.E. Jakobsson, A. Crispin, P.C.M. Grim, P. Andersson, A. Volodin, C. van Haesendonck, M. Van der Auweraer, W.R. Salaneck, M. Berggren, The origin of the high conductivity of poly(3,4-ethylenedioxythiophene)-poly(styrenesulfonate) (PEDOT- PSS) plastic electrodes, Chem. Mater. 18 (2006) 4354–4360. doi:10.1021/cm061032+.

[162] J.E. McCarthy, C.A. Hanley, L.J. Brennan, V.G. Lambertini, Y.K. Gun'ko, Fabrication of highly transparent and conducting PEDOT:PSS films using a formic acid treatment, J. Mater. Chem. C. 2 (2014) 764–770. doi:10.1039/C3TC31951B.

[163] M. Döbbelin, R. Marcilla, M. Salsamendi, C. Pozo-Gonzalo, P.M. Carrasco, J. a Pomposo, D. Mecerreyes, Influence of Ionic Liquids on the Electrical Conductivity and Morphology of PEDOT:PSS Films, Chem. Mater. 19 (2007) 2147–2149. doi:10.1021/cm070398z.

[164] S.K.. Jönsson, J. Birgerson, X. Crispin, G. Greczynski, W. Osikowicz, A.. Denier van der Gon, W.. Salaneck, M. Fahlman, The effects of solvents on the morphology and sheet resistance in poly(3,4-ethylenedioxythiophene)–polystyrenesulfonic acid (PEDOT–PSS) films, Synth. Met. 139 (2003) 1–10. doi:10.1016/S0379-6779(02)01259-6.

[165] H. Spanggaard, F.C. Krebs, A brief history of the development of organic and polymeric photovoltaics, Sol. Energy Mater. Sol. Cells. 83 (2004) 125–146. doi:10.1016/j.solmat.2004.02.021.

[166] G. Greczynski, T. Kugler, M. Keil, W. Osikowicz, M. Fahlman, W.R. Salaneck, Photoelectron spectroscopy of thin films of PEDOT – PSS conjugated polymer blend : a mini-review and some new results, J. Electron Spectros. Relat. Phenomena. 121 (2001) 1–17. doi:10.1016/S0368-2048(01)00323-1.

[167] J. Bredas, G. Street, Polarons, bipolarons, and solitons in conducting polymers, Acc. Chem. Res. 1305 (1985) 309–315. doi:10.1021/ar00118a005.

[168] J.B. Enns, J.K. Gillham, Effect of the Extent of Cure on the Modulus, Glass Transition, Water Absorption, and Density of an Amine-Cured Epoxy., J. Appl. Polym. Sci. 28 (1983) 2831–2846. doi:10.1002/app.1983.070280914.

[169] P. Nogueira, C. Ramirez, A. Torres, M.J. Abad, J. Cano, J. Lopez, I. Lopez-Bueno, L. Barral, Effect of water sorption on the structure and mechanical properties of an epoxy resin system, J. Appl. Polym. Sci. 80 (2001) 71–80. doi:10.1002/1097-4628(20010404)80:1<71::AID-APP1077>3.0.CO;2-H.